DESIGN AND SYNTHESIS OF NOVEL DONOR-ACCEPTOR TYPE
MONOMERS AND INVESTIGATION OF OPTOELECTRONIC
PROPERTIES OF THEIR POLYMERS

A THESIS SUBMITTED TO
THE GRADUATE SCHOOL OF NATURAL AND APPLIED SCIENCES
OF
MIDDLE EAST TECHNICAL UNIVERSITY

BY

ELİF KÖSE ÜNVER

IN PARTIAL FULFILLMENT OF THE REQUIREMENTS
FOR
THE DEGREE OF DOCTOR OF PHILOSOPHY
IN
CHEMISTRY

JANUARY 2010

Approval of the thesis:

DESIGN AND SYNTHESIS OF NOVEL DONOR-ACCEPTOR TYPE MONOMERS AND INVESTIGATION OF OPTOELECTRONIC PROPERTIES OF THEIR POLYMERS

submitted by **ELİF KÖSE ÜNVER** in partial fulfillment of the requirements for the degree of **Doctor of Philosophy in Chemistry Department, Middle East Technical University** by,

Prof. Dr. Canan Özgen
Dean, Graduate School of **Natural and Applied Sciences**

Prof. Dr. İlker Özkan
Head of Department, **Chemistry**

Prof. Dr. Cihangir Tanyeli
Supervisor, **Chemistry Dept., METU**

Prof. Dr. Levent Toppare
Co-Supervisor, **Chemistry Dept., METU**

Examining Committee Members:

Prof. Dr. Savaş Küçükyavuz
Chemistry Dept., METU

Prof. Dr. Cihangir Tanyeli
Chemistry Dept., METU

Prof. Dr. Özdemir Doğan
Chemistry Dept., METU

Prof. Dr. Mustafa Güllü
Chemistry Dept., Ankara University

Assist. Prof. Dr. Yasemin Arslan Udum
Institute of Science and Technology
Dept. of Adv. Tech., Gazi University

Date: February 24, 2010

I hereby declare that all information in this document has been obtained and presented in accordance with academic rules and ethical conduct. I also declare that, as required by these rules and conduct, I have fully cited and referenced all material and results that are not original to this work.

Name, Last Name   : Elif Köse Ünver

Signature   :

ABSTRACT

DESIGN AND SYNTHESIS OF NOVEL DONOR-ACCEPTOR TYPE MONOMERS AND INVESTIGATION OF OPTOELECTRONIC PROPERTIES OF THEIR POLYMERS

Ünver, Elif Köse

Ph.D., Department of Chemistry

Supervisor : Prof. Dr. Cihangir Tanyeli

Co-supervisor : Prof. Dr. Levent Toppare

January 2010, 158 pages

A proven strategy, donor-acceptor approach, to reduce the band gap of conjugated materials and possibly improve the photocurrent is to incorporate electron-rich and electron-deficient units in an alternating fashion in a polymer chain. For this purpose, a wise selection of donor and acceptor moieties in a monomer structure results in desired finishing properties of polymeric materials.

In this study, fourteen novel monomers were synthesized to explore the acceptor and donor effects on the electronic and optoelectronic properties. Dibenzophenazine, dibenzopyrido]quinoxaline, tetrahydro- dibenzophenazine, thiadiazoloquinoxaline, pyrazinoquinoxaline, thienopyrazine, benzoselenadiazole, thienoselenadiazole were used as acceptor moieties, while thiophene, 3-hexylthiophene and 2,3-dihydrothienodioxine (EDOT) were used as the donor components in these donor-acceptor molecules.

To synthesize desired monomers, well-known synthetic methods were performed, including bromination, nitration, reduction and condensation. Bromination was achieved by two different ways depends on the aim, NBS and Br_2/HBr medium. For the nitration, HNO_2 and H_2SO_4 were used together. Fe metal in refluxing acetic acid was used as the reducing agent in case of nitro group reductions. On the other hand, Zn metal/AcOH system was chosen for the reduction of both nitro groups and thiadiazole structure to amine, simultaneously. Finally, the Stille Coupling was used to obtain resulting acceptor-donor-acceptor monomers.

These synthesized monomers were polymerized by electrochemically and investigated their properties by methods such as spectroelectrochemistry, kinetic and colorimetry studies. Spectroelectrochemistry experiments were performed in order to investigate key properties of conducting polymers such as band gap, maximum absorption wavelength, the intergap states that upon doping and evolution of polaron and bipolaron bands. Switching time and optical contrast of the polymers were evaluated via kinetic studies.

Keywords: Donor-acceptor approach, Stille Coupling, Electrochromism, Conducting Polymer.

ÖZ

YENİ DONOR-AKSEPTÖR TİPTE MONOMERLERİN DİZAYN VE SENTEZİ VE POLİMERLERİNİN OPTOELEKTRONİK ÖZELLİKLERİNİN ARAŞTIRILMASI

Ünver, Elif Köse

Doktora, Kimya Bölümü

Tez Yöneticisi   : Prof. Dr. Cihangir Tanyeli

Ortak Tez Yöneticisi : Prof Dr. Levent Toppare

Şubat 2010, 158 sayfa

Konjuge malzemelerin bant aralığını düşürmek ve fotoakımı geliştirmek için kullanılan ispatlanmış bir strateji olan donor-akseptör yaklaşımı, elektronca zengin ve fakir birimlerin polimer zincirinde sıralı bir şekilde birbirlerini izlemesidir. Bu amaçla, monomerdeki donor-akseptör içeriğin doğru seçimi, polimerik malzemede son özelliklerin istenildiği şekilde olmasını sağlar.

Bu çalışmada, elektronik ve optoelektronik özellikler üzerine akseptör ve donor etkilerinin araştırılması için ondört yeni monomer sentezlendi. Bu donor-akseptör moleküllerde, dibenzofenazin, dibenzopiridokinokzalin, tetrahidrodibenzofenazin, tiadiazolokinokzalin, pirazinokinokzalin, tiyenopirazin, benzoselenadiazol, tiyenoselenadiazol akseptör olarak kullanılırken, tiyofen, 3-hekziltiyofen and 2,3-dihidrotiyenodioksin (EDOT) donör bileşenler olarak kullanıldı.

Bromlama, nitrolama, indirgeme ve kondenzasyon gibi genel sentez metotları, istenilen monomerlerin sentezlenmesi için kullanıldı. Bromlama için duruma bağlı

olarak, NBS ve Br$_2$/HBr yöntemlerinden biri tercih edildi. Nitrolamada HNO$_3$ ve H$_2$SO$_4$ birlikte kullanıldı. Nitro grup indirgemelerinde indirgeyici ajan olarak, asetik asitte demir riflaksı kullanıldı. Diğer taraftan Zn/AcOH sistemi nitro guruplarının ve tiadiazol yapısının amine indirgenmesinde kullanılmıştır. Son olarak, Stille eşleşme reaksiyonu, sonuç donor-akseptör monomerlerinin eldesinde kullanıldı.

Sentezlenen bu monomerler elektrokimyasal olarak polimerleştirilmiştir. Elde edilen polimerin özellikleri, spektroelektrokimya, kinetik ve kolorimetrik çalışmalar gibi yöntemlerle araştırılmıştır. Spektroelektrokimya deneyleri bant aralığı, maksimum dalga boyu, katkılama sonucu ortaya çıkan arabant halleri ve polaron, bipolaron bantları gibi iletken polimerlerin özelliklerini ortaya çıkarmak için yapılmıştır. Polymerlerin tepki zamanı ve optik kontrast özellikleri kinetik çalışmalarla incelenmiştir.

Anahtar Kelimeler: Donör-akseptör yaklaşımı, Stille Coupling, Elektrokromizm, İletken Polimer.

To My Parents

ACKNOWLEDGEMENTS

TABLE OF CONTENTS

xiii

LIST OF TABLES

TABLES

LIST OF FIGURES

FIGURES

CHAPTER 1

INTRODUCTION

1.1 Electroactive Polymers

Electroactive polymers have been the object of increasing academic and industrial interest and in the past 30 years. Substantial progress has been achieved in the development and the characterization of this important new class of conducting materials. These materials are usually classified in two main groups according to their mode of their electric transport. One group includes polymers having transport properties almost exclusively of the ionic type and they are often called 'polymer electrolytes' or, in a broader way, 'polymer ionics'. The other group includes polymeric materials where the transport mechanism is mainly electronic in nature and hence, commonly termed as 'conducting polymers' [1].

Ionically conducting polymers or polymer ionics may be typically described as polar macromolecular solids. The most classic example is the combination of poly(ethylene oxide), PEO, and lithium salts, LiX. The various type of polymer ionic can be easily fabricated into flexible thin films with large surface areas where the ions are free to move and can conduct electricity as in conventional liquid electrolytes. Thus, polymer ionics are key importance for the fabrication and development of exciting devices, such as laminated optical displays and sensors.

1.1.1 Conducting Polymers

The other group of electroactive polymers, mentioned in the previous section, covers the electronic conductors, including conjugated polymers. The electronic structure of

conjugated polymers may be significantly modified by electrochemical processes, sometimes designated as doping processes, which involve the oxidation (removal of π electrons) or the reduction (addition of π electrons) of the polymer chain. Typical examples are the heterocyclic polymers, such as polypyrrole, polythiophene and their derivatives, and the polyanilines.

The history of conjugated conducting polymers or 'synthetic metals' can be dated back to 1862, when Letheby reported the electrochemical synthesis of a 'thick layer of dirty bluish-green pigment' by the oxidation of aniline in sulfuric acid at a platinum electrode [2].   With the discovery of the metallic properties of poly(acetylene),which led to the award of the 2000 Nobel Prize in Chemistry to Shirakawa, Heeger and MacDiarmid, a great deal of interest in conjugated conducting polymers has grown up until now.

Poly(acetylene), the simplest form of conjugated conducting polymers, has few applications because of its intractability and air sensitivity. The most research on conjugated conductive polymers has been carried out with materials derived from aromatic and heterocyclic aromatic structures. Consequently, chemical or electrochemical oxidation of many resonance-stabilized aromatic molecules, such as pyrrole, thiophene, 3,4-(ethylenedioxy)thiophene (EDOT), aniline, furan, carbazole, azulene, indole, and others, results in electroactive conducting polymers (Figure 1).
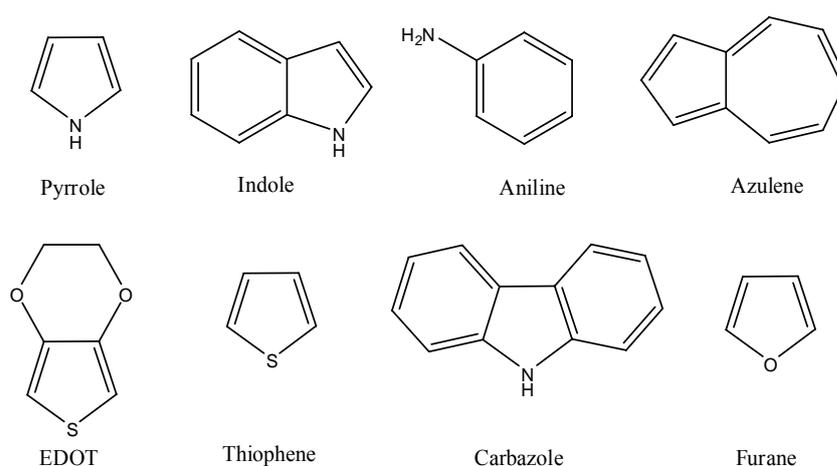
Figure 1 Some aromatic molecules, using in electroactive conducting polymer synthesis.

The poly(thiophene)s, poly(pyrrole)s and poly(aniline)s have received relatively more attention due to their electrochromic properties.

Since 1977, electroactive conducting polymers have been intensively investigated for their conducting, semiconducting and electrochemical properties [3]. Numerous electronic applications have been proposed and some realized, including electrochromic devices (ECDs), electroluminescent organic light-emitting diodes (OLEDs) [4,5], photovoltaic elements for solar-energy conversion [6] sensors [7] and thin-film field-effect transistors [8].

1.2   Conduction in Polymers

Electronic conductivity in electroactive polymers results from the extended conjugation within the polymer, longer chains promoting high conductivity. The average number of linked monomer units within a conducting polymer is often termed the 'conjugation length'. Due to their electronic configuration, conjugated polymers are different from saturated polymers, in which all of the four valence electrons of carbon are used up in covalent bond. Conjugated polymers can more efficiently lower its energy by bond alteration (alternating short and long bonds), which, introduces a band width of 1.5 eV making it a moderate energy gap semiconductor.

In a polymer, just as in a crystal, the interaction of a polymer unit cell with all its neighbors leads to the formation of electronic bands. The highest occupied electronic levels constitute the valence band (VB) and the lowest unoccupied levels, the conduction band (CB). The width of the forbidden band, or band gap (E_g), between the VB and CB determines the intrinsic optical properties of these materials.

1.2.1 Doping up Conductivity

The conduction process is described with two important mechanisms, doping and hopping. Conjugated polymers become highly conductive upon doping. Thus, they

are similar to semiconductors in this respect. Doping a polymer provide electrons or create holes and generate defects in polymers structure without destroying the chain. These defects, solitons, polarons and bipolarons, in the polymer are the charge carriers and can be radicals, anions, cations or combination of these.

A key discovery in the development of conducting polymers was the finding in 1973 that an inorganic polymer polysulfur nitride, $(SN)_x$ is a metal. The room-temperature conductivity of $(SN)_x$ is of the order of 10^3 $(\Omega\text{-cm})^{-1}$, compare to $6x10^5$ $(\Omega\text{-cm})^{-1}$ for copper and 10^{-14} $(\Omega\text{-cm})^{-1}$ for polyethylene. Below a critical temperature of about 0.3 K, $(SN)_x$ becomes a superconductor. These discoveries were of particular importance because they proved the existence of highly conducting polymers and stimulated the enormous amount of work necessary to synthesize other polymeric conductors. It must be stressed that the metallic character of (SN), is an intrinsic property of the material, related with the presence of one unpaired electron for each S-N unit. As a result, the highest occupied electronic levels (i.e., valence band) are only half-occupied. Since there is no forbidden gap between the highest occupied and the lowest unoccupied levels, the unpaired electrons can readily move under the application of an electrical field giving rise to electrical conductivity. In 1976-1977, it was observed that the room-temperature conductivity of $(SN)_x$ can be enhanced by an order of magnitude following exposure to bromine and similar oxidizing agents [9].

The major breakthrough in the area of conducting plastics occurred later in 1977 when the same redox chemistry was applied to an intrinsically insulating organic polymer, polyacetylene. It was discovered that polyacetylene, which has an intrinsic conductivity lower than 10^{-5} $(\Omega\text{-cm})^{-1}$, could be made highly conducting, approximately 10^3 $(\Omega\text{-cm})^{-1}$, by exposing it to oxidizing or reducing agents [10]. This process is often referred to as "doping" by analogy with the doping of inorganic semiconductors.

The halogen doping that transforms polyacetylene to a good conductor of electricity is oxidation (or *p*-doping). Reductive doping (called *n*-doping) is also possible using,

e.g., an alkali metal. Figure 2 shows illustrative conductivity ranges for poly(acetylene), poly(thiophene) and poly(pyrrole).

$$[CH]n + 3x/2\ I_2 \longrightarrow [CH]n^{x+} + xI_3^- \qquad \text{oxidative doping} \qquad \text{Eq. 1}$$

$$[CH]n + xNa \longrightarrow [CH]n^{x-} + xNa^+ \qquad \text{reductive doping} \qquad \text{Eq. 2}$$
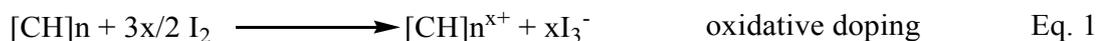
The doped polymer is thus a salt. However, it is not the counter ions, I_3^- or Na^+, but the charges on the polymer that are mobile. By applying an electric field perpendicular to the film, the counter ions can be made to diffuse from or into the structure, causing the doping reaction to proceed backwards or forwards. In this way the conductivity can be switched off or on.
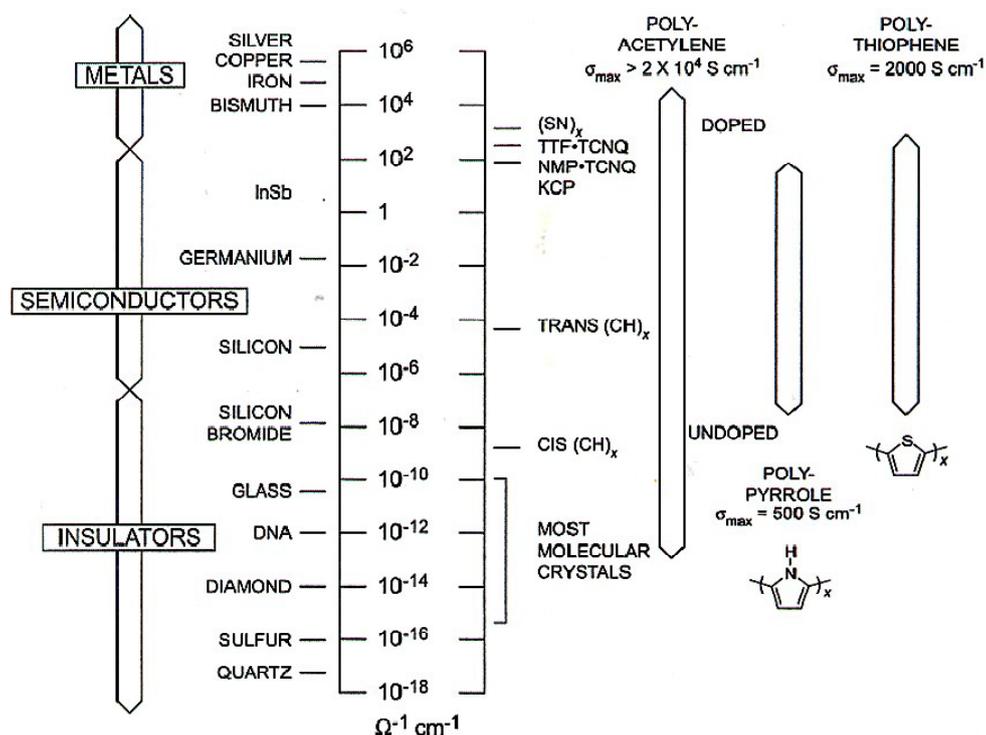
Figure 2 The conductivity ranges of some conducting polymers [11].

In some cases, oxidation or reduction of the polymer can be achieved electrochemically by subjecting the neutral polymer to the appropriate oxidizing or reducing voltage in an electrochemical cell. The charge appearing on the polymer chain is then neutralized by a counterion from the electrolyte solution. An interesting

5

group of conducting polymers consists of those prepared by the electrochemical oxidation and simultaneous polymerization of the monomer on the anode in an electrochemical cell. This group includes polypyrrole, polythiophene, and their derivatives [9].

Initially, the high conductivity increase observed upon doping organic polymers was thought to result from the formation of unfilled electronic bands. It was simply assumed that upon p-type or n-type doping, electrons were respectively, removed from the top of the VB or added to the bottom of the CB, in analogy to the mechanism of generation of charge carriers in doped inorganic semiconductors. This assumption was however quickly challenged by the discovery that polyacetylene (PA) [12] polyparaphenylene (PPP) [13], and polypyrrole (PPY) [14-16] can display conductivity which does not seem to be associated with unpaired electrons but rather with spinless charge carriers.

1.2.2 Polaron and Bipolaron

A polymer may store charge in two ways. In an oxidation process it could either lose an electron from one of the bands or it could localize the charge over a small section of the chain. Localizing the charge causes a local distortion due a change in geometry. However, the generation of this local geometry decreases the ionization energy of the polymer chain and increases its electron affinity making it more able to accommodate the newly formed charges. This method increases the energy of the polymer less than it would if the charge was delocalized and, hence, takes place in preference of charge delocalization. This is consistent with an increase in disorder detected after doping by Raman spectroscopy. A similar scenario occurs for a reductive process.

The doping phenomenon of polymers can be clarified by the help of several examples. In case of polypyrrole the oxidative doping proceeds as given in Figure 3. An electron is removed from the system of the backbone producing free radical and a spinless positive charge. The radical and cation are coupled to each other via local

resonance of the charge and the radical. In this case, a sequence of quinoid-like rings is used. The distortion produced by this is of higher energy than the remaining portion of the chain. The creation and separation of these defects costs a considerable amount of energy. This limits the number of quinoid-like rings that can link these two bound species together. For polypyrrole, it is believed that the lattice distortion extends over four pyrrole rings. This combination of a charge site and a radical is called a polaron. This could be either a radical cation or radical anion. This creates new localized electronic states in the gap, with the lower energy states being occupied by single unpaired electrons.
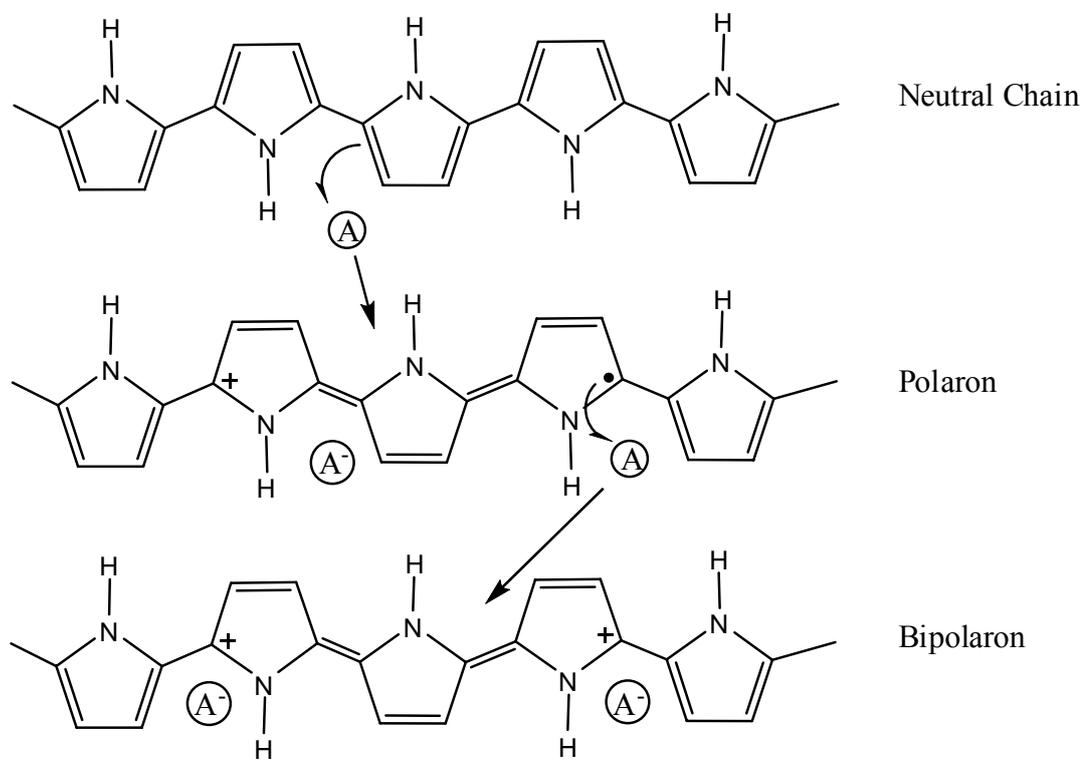
Figure 3 Polaron, bipolaron formation for polypyrrole.

Upon further oxidation the free radical of the polaron is removed, creating a new spinless defect called a bipolaron. This is of lower energy than the creation of two distinct polarons. At higher doping levels it becomes possible that two polarons combine to form a bipolaron. Thus at higher doping levels the polarons are replaced with bipolarons. This eventually, with continued doping, forms into a continuous

bipolaron bands. Their band gap also increases as newly formed bipolarons are made at the expense of the band edges. As presented in Figure 4, for a very heavily doped polymer it is conceivable that the upper and the lower bipolaron bands will merge with the conduction and the valence bands respectively to produce partially filled bands and metallic like conductivity.
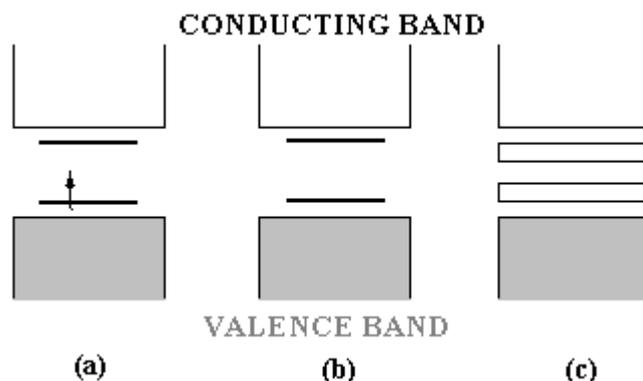
Figure 4 Band structure evolution upon doping: (a) low doping level, polaron formation; (b) moderate doping level, bipolaron formation; (c) high doping level, formation of bipolaron bands.

1.3 Synthesis of Conducting Polymers

Besides electrochemical and chemical polymerization, conducting polymers can be synthesized using specific techniques which include Grignard reaction, ring-opening metathesis, plasma, solid state polymerization and transition metal-catalyzed polymerization. While chemical procedures afford insulating polymers, which can be doped to their conducting form by chemically and electrochemically, electrochemical operations give conducting polymers, in oxidized state. It is possible to control the thickness and morphology of the polymer film during the electrolytic process.

1.3.1 Electrochemical Polymerization

In addition to the oxidative anodic electropolymerization of the monomer, which is the most convenient and most widely used method, cathodic route is also used for the

conducting polymer synthesis. The major drawback of this method is that the polymer is produced in its neutral insulating form which leads rapidly to a passivation of the electrode and limits attainable film thickness to ca. 100 nm. On the other hand, this technique presents the advantage to be applicable to electrode materials subject to anodic corrosion such as small band gap semiconductors [17].

Compared to other chemical and electrochemical syntheses of conducting poly(heterocycles), the anodic electropolymerization of the monomer presents several distinct advantages such as absence of catalyst, direct grafting of the doped conducting polymer onto the electrode surface (which is of particular interest for electrochemical applications), easy control of the film thickness by the deposition charge, and possibility to perform a first in situ characterization of the growing process or of the polymer by electrochemical and/or spectroscopic techniques. Figure 8 represents the mechanism proposed for the electropolymerization of heterocylics, analogy to the already known coupling reactions of aromatic compound.

The first electrochemical step (E) consists the oxidation of the monomer to its radical cation. Since the electron-transfer reaction is much faster than the diffusion of the monomer from the bulk solution, it follows that a high concentration of radicals is continuously maintained near the electrode surface. The second step involves the coupling of two radicals to produce a dihydro dimer dication which leads to a dimer after loss of two protons and rearomatization. This rearomatization constitutes the driving force of the chemical step (C). Due to the applied potential, the dimer, which is more easily oxidized than the monomer, occurs in its radical form and undergoes a further coupling with a monomeric radical. Electropolymerization proceeds then through successive electrochemical and chemical steps according to a general (ECE), scheme, until the oligomer becomes insoluble in the electrolytic medium and precipitates onto the electrode surface [18].
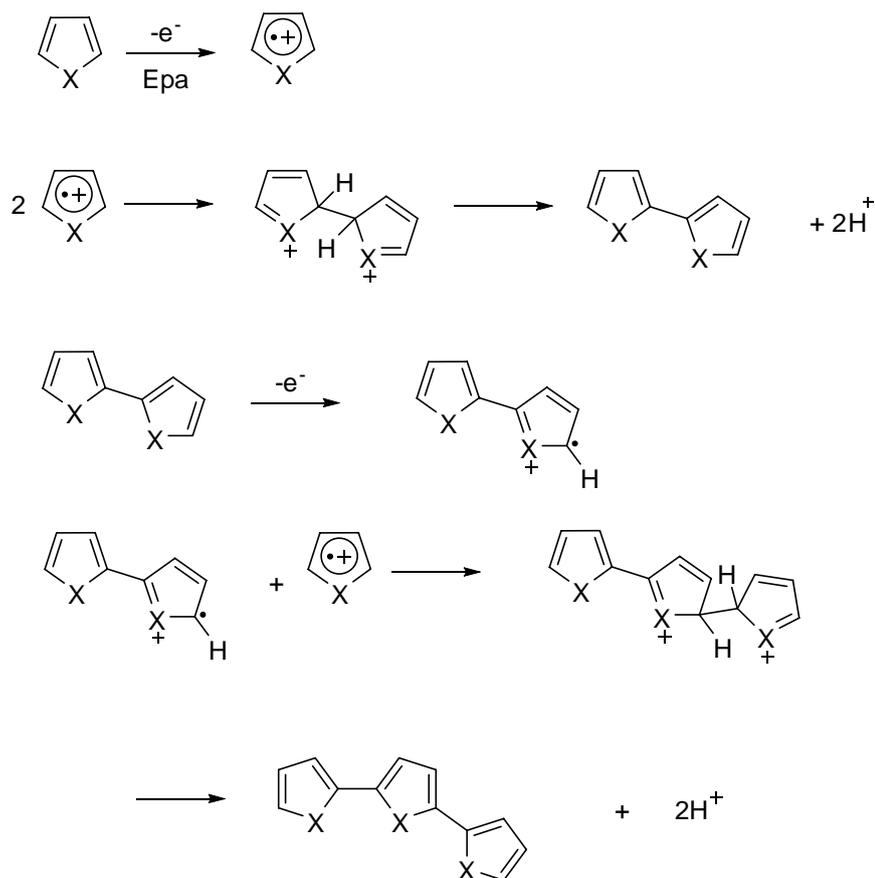
Figure 5 Mechanism of electropolymerization of five-membered heterocycles.

1.3.2 Effect of Electrosynthesis Conditions

The electropolymerization of five-membered heterocycles involves many experimental variables such as the solvent, concentration of reagents, temperature, cell geometry, nature and shape of the electrodes, and applied electrical conditions. Electropolymerization is carried out at moderate potentials to prevent the oxidative decomposition of the solvent, electrolyte and polymer film. The polymerization potential determines the stability of intermediate species.

The electropolymerization reaction may be sensitive to nucleophilic nature of the solvent and electrolyte. For this reason, many of the films are prepared in aprotic solvents, such as acetonitrile, which are poor nucleophiles [19]. If the solvent is nucleophilic, it will react with the free radical intermediates, easily. Solvent must

have a high dielectric constant in order to allow for ionic conductivity and be stable over a broad potential range such that solvent redox processes do not interfere with electrochemical processes occurring during polymerization [1].

The anode material selection is a critical consideration since the physicochemical properties of its surface determine the nature and the strength of the bond between the polymer and the electrode, which can affect both the polymerization process and the properties of the resulting polymer.

1.4   Electrochromism and Electrochromic Materials

Theoretical considerations suggest that the absorption and emission spectra of certain dyes may be shifted by hundreds of angstroms upon application of a strong electric field. This effect is called "electrochromism", in analogy to "thermochromism" and "photochromism" which describe changes of color produced by heat and light. This definition of electrochromism does not, however, fit within the modern sense of the world. An electrochromic material is the one that changes color in a persistent but reversible manner by an electrochemical reaction and the phenomenon is called *electrochromism*.

Electrochromism is the reversible and visible change in transmittance and/or reflectance that is associated with an electrochemically induced oxidation–reduction reaction. It results from the generation of different visible region electronic absorption bands on switching between redox states. The color change is commonly between a transparent "bleached" state and a colored state, or between two colored states [20].

Transition metal oxides [21-26], prussian blue, phthalocyanines, violegens, buckminsterfullerene [27,28] and conducting polymers can be given as the most important examples from the major classes of electrochromic materials.

In case more than two redox states are electrochemically available, the electrochromic material may exhibit several colors and may be termed as multielectrochromic or can be said to possess multicolor-electrochromism. This optical change is affected by a small electric current at low dc potentials of the order of a fraction of volts to a few volts. A suitable example is methyl viologen (MV), which is colorless as a dication, MV^{2+} (II), blue as a radical cation, and red–brown as a di-reduced neutral species. Electrochromic viologens with as many as six colors have been synthesized (Figure 6) [29].
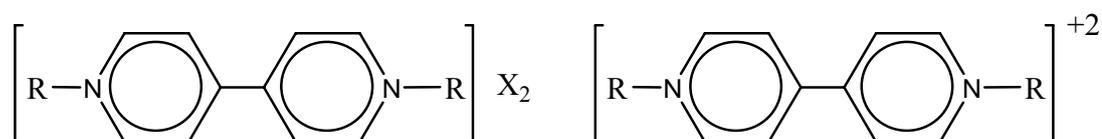
Figure 6 (a) General chemical formulae of viologen; (b) viologen ion.

1.4.1 Conducting Polymers

Conducting polymers have attached significant interest in the field of electrochromism, since they offer additional advantages, such as, low processing cost, enhanced mechanical properties, no dependence with angle of vision, good UV stability high coloration efficiency, fast switching ability and fine-tuning of the band gap through the modification of polymer's chemical structure. By adjusting the electronic character of the π system along the neutral polymer backbone, the π - π * transition can be adjusted across the electromagnetic spectrum from the UV, through the visible and into the near-infrared [30].

Chemical or electrochemical oxidation of numerous resonance stabilized aromatic molecules including pyrrole, thiophene, aniline, furan, carbazole, azulene and indole produces novel electronically conducting polymers [31]. In their oxidized forms, such conducting polymers are 'doped' with counter anions (p-doping) and possess a delocalized π-electron band structure, the energy gap between HOMO and LUMO determining the intrinsic optical properties of these materials. The doping process (oxidation) introduces polarons which are the major charge carriers. Reduction of

conducting polymers with concurrent counter anion exit removes the electronic conjugation, to give the 'undoped' (neutral) electrically insulating form. Conducting polymers can also, in principle, undergo cathodic doping with cation insertion (n-doping) to balance the injected charge. However, n-doped forms are less stable than p-doped forms and few reports are available concerning the electrochromism of the n-doping process [32].

The electrochemical p-doping-undoping process, which switches conjugated polymers between insulating and conductive states and causes the color changes, can be rendered as shown below with polypyrrole as the conjugated polymer. Doped (oxidized) polypyrrole is blue-violet (λ_{max} 670 nm) and electrochemical reduction yielding the yellow-green (λ_{max} 420nm) 'undoped' form, Eq. 3.

Insulating
(yellow-green)

Conductive
(blue-violet)

$$+ \quad nyX^- \quad \underset{\text{undoping}}{\overset{\text{p-doping}}{\rightleftharpoons}} \quad + \quad nye^- \qquad \text{Eq. 3}$$
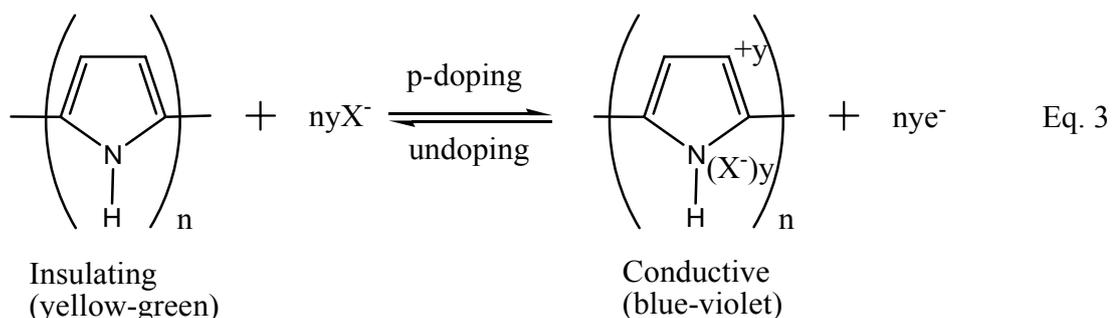
In other words, the color changes elicited by doping are due to the modification of the polymer's band electronic structure. Doping generates defects, polarons, bipolarons, solitons, in the polymer's structural chain. These defects produce new electronic states in the gap that cause the color changes.

Figure 10 shows the expected transitions in a conjugated polymer according to literature [33]. In the neutral state the polymer exhibits single broad transition from the valence band to the conduction band (π-π*) upon oxidation, removal of an electron from the valence band, leads to the formation of polaron. This results in state with an unpaired electron whose energy state is higher than the valence band. Accordingly, there occurs the lowering of the corresponding antibonding level in the conduction band; leading to formation of new two intragap states. This should lead to

possible four new transitions. However, since the oscillator strength of transitions *a* and *b* (Figure 7) are much greater than transitions *c* or *d*, two low energy transitions are expected as the signature for a polaron. Upon oxidation, the absorbance of the main inter-band peak (π to $\pi*$) decreases along with a formation of new peak at lower energy region of the spectrum. Further oxidation of the polymer will create more polarons by the removal of electrons from the valence band. The unpaired electron of the polaron will be removed to form a dication. Thus, bipolaron will be formed. Since the bipolaron levels are unoccupied, only transitions from valence band are possible. The signature of a bipolaron is one broad low energy transition. This is because of the stronger nature of the transition *e* with respect to transition *f*. Yet, basically conducting polymers change color by the creation and destruction of polarons and bipolarons [34].
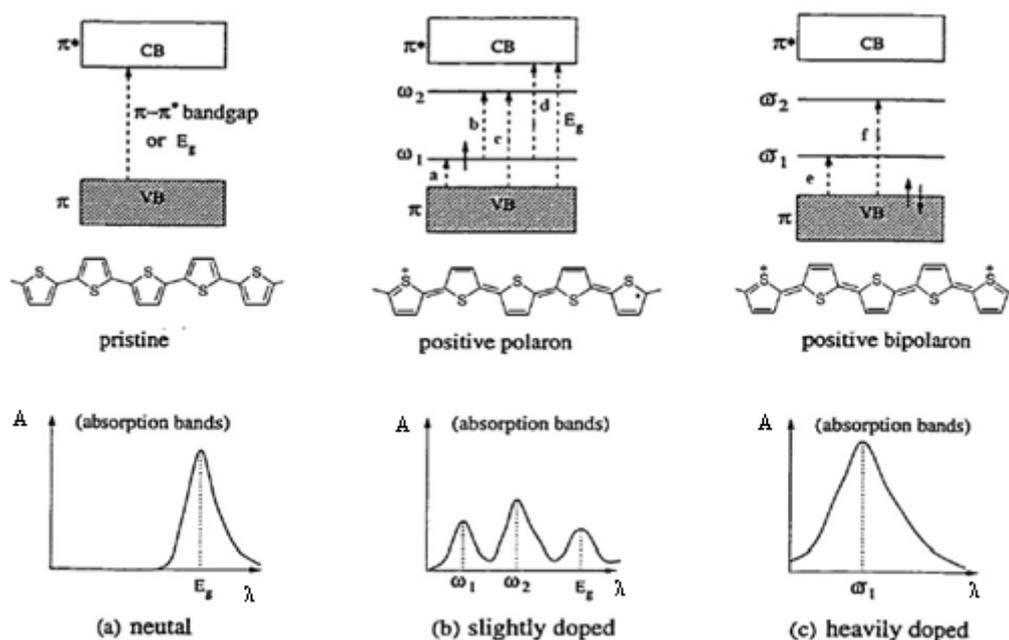
Figure 7 Polaron and bipolarons in non-degenerate ground state polymers: Band diagrams for neutral, positive polaron and positive bipolaron; absorption bands for neutral, slightly doped and heavily doped.

Doping shifts the absorption towards the lower energies, and the color contrast between doped and undoped forms of the polymer depends on the magnitude of the energy gap of the undoped polymer. Polymers with E_g greater than 3 eV are

transparent or slightly colored in the undoped form and in the doped form are generally highly absorbant in the visible region, whereas those with small E_g (1,5-2 eV) are highly absorbant in the undoped form but, after doping, the free carrier absorption is relatively weak in the visible region. For example, poly(methylthiophene) with E_g=2.34 eV in neutral form is highly absorbant in the visible region and purple in color, whereas after doping the free carrier absorption is weak in the visible region and the polymer is transparent pale blue [35].

Three major strategies of color control are used with electrochromic properties. The polymer's band gap (defined as the onset of the π-π^* transition) is directly related to the relative energies of the HOMO and the LUMO. By judiciously substituting the polymer's repeat unit, the electrochromic properties can be controlled by the induced steric and electronic effects. These substituents determine the effective conjugation length and the electron density of the polymer backbone [20]. With this respect electrochromic properties of polythiophene and of several substituted thiophenes are given in Table 1.

Table 1 Electrochromic properties of polythiophene and of several substituted thiophenes.

Monomer	Polymer λ_{max} / nm and color	
	Oxidized	Reduced
Thiophene	730 / Blue	470 / Red
3-Methylthiophene	750 / Deep blue	480 / Red
3,4-Dimethylthiophene	750 / Dark blue	620 / Pale brown
2,2'-Bithiophene	680 / Blue-grey	460 / Red-orange

Copolymers offer a second means of controlling the electrochromic properties of the CPs. Copolymerization of distinct monomers or homo polymerization of hybrid monomers containing several distinct units can lead to an interesting combination of

the properties observed in the corresponding homopolymers. Indeed, it has been observed that the color of copolymers based on carbazole, thiophene and pyrrole derivatives can be controlled by altering the ratio of the respective monomers. Blends, laminates and composites offer a third method, similar to copolymers, for combining the electrochromic properties of several systems. The use of two polymers covering different color regions is a simplest way to achieve multicolor electrochromism [1, 35, 36, 37].

1.5   Electrochromic Devices

Conjugated polymers that can be repeatedly driven from insulating to conductive states electrochemically with high contrast in color are promising materials for electrochromic device technology.

An electrochromic device is essentially a rechargeable battery in which the electrochromic electrode is separated by a suitable solid or liquid electrolyte from a charge-balancing counter electrode, and the color changes occur by charging and discharging the electrochemical cell with applied potential of a few volts. After the resulting pulse of current has decayed and the color change has been effected, the new redox state persists, with little or no input of power, in the so called "memory effect". Figure 8 illustrates an electrochromic device configuration [20].
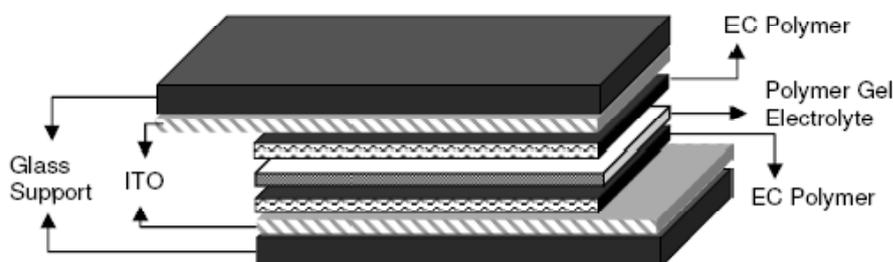
Figure 8 Schematic illustrations of dual type electrochromic device.

The electrochromic electrode, which can work in the reflective or transmissive mode, is generally glass coated with an electrically conducting film such as tin-doped indium oxide (ITO), onto which is deposited the electrochromic material. Alternatively, if one or both redox states are soluble, the electrochromic material may be present in the electrolyte solution. In variable light transmissive devices the counter electrode substrate also has to be transparent ITO glass, with the counter electrode chemical species being either colorless in either its redox forms or electrochromic in a complementary mode to the primary electrochromic material. For applications that are designed to operate in the reflective mode, such as displays, the counter electrode can be of any material with a suitable reversible redox reaction [32].

1.5.1 Criteria and Terminology for Electrochromic Device Application

Many types of chemical species exhibit electrochromism, only those with favorable electrochromic performance parameters are potentially useful in commercial applications. Thus most applications require electrochromic materials with a high contrast ratio, coloration efficiency, cycle life, write-erase efficiency and response time.

The *contrast ratio* CR is a commonly employed measure denoting the intensity of color formed electrochemically, as seen by eye, and given in Eq. 4

$$CR = \left(\frac{R_0}{R_x} \right) \qquad \text{Eq. 4}$$

where R_x is the intensity of light reflected diffusely though the colored state of a display, and R_0 is the intensity reflected similarly but from a non-shiny white card. The ratio CR is best quoted at a specific wavelength – usually at λ_{max} of the colored state. As in practice, a CR of less than about 3 is almost impossible to see by eye. As high a value as possible is desirable [3].

The time required for an ECD to color from its bleached state (or vice versa) is termed its *response time* or switching time (τ). For most devices, τ values are of the order of a few seconds. While most applications do not require a rapid color change, some such as for electrochromic office windows actually require a very slow response, as workers can feel ill when the color changes too rapidly [38]. However, applications such as display devices require a more rapid response.

The *write-erase efficiency* is the percentage of the originally formed coloration that may be subsequently electro-bleached. It can conveniently be expressed as a ratio of absorbance changes. The efficiency should closely approach 100 % for a successful display which is a major test of ECD design and construction.

An adjunct to the write-erase efficiency is the electrochromic device's cycle life which represents the number of write-erase cycles to be performed by the ECD before any significant extent of degradation has occurred. (Such a write-erase cycle is also termed as "double potential step".) When an ECD is continually cycled between its colored and bleached states, device failure will eventually occur resulting from physical changes in solid phases or from chemical side reactions. The *cycle life* is a measure of its stability, being the number of cycles possible before such failure. A major aim of device fabrication is obviously to maximize the cycle life [39].

Coloration efficiency, defined as the relationship between the injected/ejected charge as a function of electrode area and the change in optical density units. Electrochromic materials could be employed for the fabrication of very rapid, efficient displays and light modulators if they could exhibit sufficiently high coloration efficiency. The ideal device should exhibit a large change in transmittance with a small increase in charge, giving rise to large coloration efficiency values [40]. The coloration efficiency η is defined according to Eq. 5

$$Abs = \eta\, Q \qquad\qquad\qquad Eq.\ 5$$

where Abs is the absorbance formed by passing a charge density of Q. A graph of Abs against Q accurately gives η as the gradient.

The reported values of coloration efficiency for inorganic materials and conducting polymers were in the ranges of 10–50 cm^2 C^{-1} and 30–700 cm^2 C^{-1}, respectively [41].

1.6 Applications of Conducting Polymers

Conducting polymers are the materials that contain conjugated double bonds or band gaps that allow them to become conductive when doped. A doped conducting polymer may be used for many applications. Good processibility, high stability and low cost manufacturing of polymers make the field of conductive polymers an expanding industry.

Conducting polymers find applications especially in electronics and surface practices. In the near future conductive polymeric coatings will be the most economical way to fight corrosion. [42-44] Moreover, these polymers have found their way into many other areas including the photovoltaics that gather light and emit electricity. [45] These materials continue to find uses in consumer electronics and antistatic textiles. [46] Among the most exciting applications is the use of conducting polymers in light-emitting devices (LEDs), replacing silicon as the traditional substrate material for clock radios, audio equipment, televisions, cellular telephones, automotive dashboard displays, aircraft cockpit displays, and some other electroluminescent displays [47] Conducting polymers provide benefits to industries such as electronics by shielding against electromagnetic interference (EMI). [48] Conductive polymers are also already used in devices that detect environmentally hazardous chemicals, factory emissions, and flavors or aromas in food products. [49] Conducting polymers can also be used to directly convert electrical energy into mechanical energy. This utilizes large changes in size undergone during the doping and dedoping of many conducting polymers, which can be as large as 10 %. The applications of this include microtweezers, microvalves, micropositioners for microscopic optical elements, and actuators for micromechanical sorting (such as the sorting of biological cells) [50, 51] One of the most futuristic applications for conducting polymers are 'smart' structures. [51] Another publicized and promising

current application of conductive polymers is light weight rechargeable batteries. [48] At last but not the least their electrochromic properties can be used to produce, e.g. "smart windows" that absorb sunlight in summer.

1.7   Characterization of Electrochromic Materials

Electrochromic materials are generally first studied at a single working electrode, under potentiostatic or galvanostatic control, using three-electrode circuitry. Traditional techniques such as cyclic voltammetry, coulometry, chronoamperometry, all with, as appropriate, *in situ* spectroscopic measurements are employed for characterization.

1.7.1 Cyclic Voltammetry (CV)

The most common electrochemical method employed for characterization is cyclic voltammetry. CV is the triangular sweep voltammetry (LSV), which measures the electric response with sampling at a constant scan rate from initial to final electric potential. In cyclic voltammetry, the electrode potential ramps linearly versus time as presented in Figure 9. This ramping is known as the experiment's scan rate (V/s).
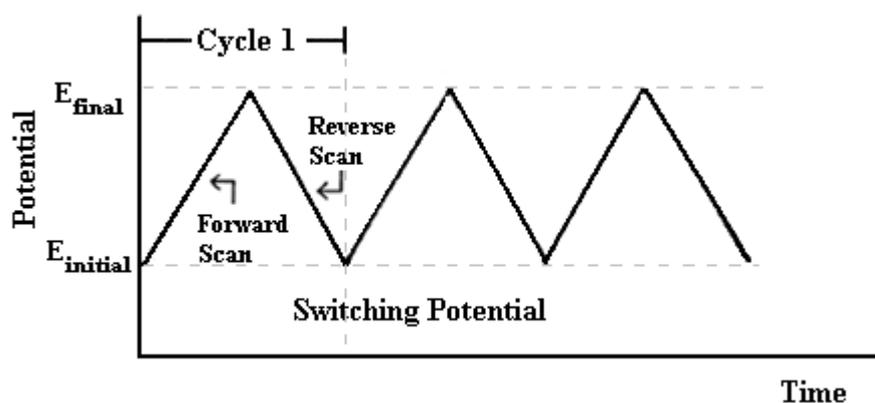
Figure 9 Cyclic voltammetry wave form.

Figure 10 depicts a schematic circuit for cyclic voltammetric analyses, indicating the nature of the connections between the three electrodes and a typical cyclic voltammogram (CV).
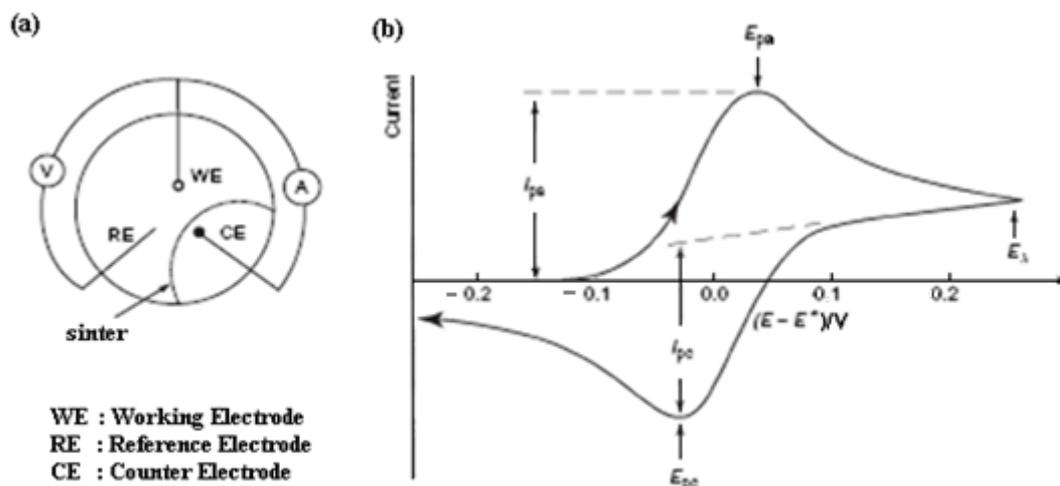
Figure 10 Schematic descriptions of CV circuit and cyclic voltammogram **[3]**.

The potential is measured between the reference electrode and the working electrode and the current is measured between the working electrode and the counter electrodes. This data is then plotted as current (i) vs. potential (E). As the waveform shows, the forward scan produces a current peak for any analyte that can be reduced (or oxidized depending on the initial scan direction) through the range of the potential scanned. The current will increase as the potential reaches the reduction potential of the analyte, but then falls off as the concentration of the analyte is depleted close to the electrode surface. If the redox couple is reversible then when the applied potential is reversed, it will reach the potential that will reoxidize the product formed in the first reduction reaction, and produce a current of reverse polarity from the forward scan. This oxidation peak will usually have a similar shape to the reduction peak. As a result, information about the redox potential and electrochemical reaction rates of the compounds is obtained.

The peak current for a reversible couple is given by Randles & Sevcik equation:

$$i_p = (2.69 \times 10^5) \, n^{3/2} \, A \, D^{1/2} \, C \, v^{1/2} \qquad\qquad \text{Eq. 6}$$

where n is the number of electrons, A is the electrode area (in cm^2), C is the concentration (in mol cm^{-3}), D is the diffusion coefficient (in $cm^2 \, s^{-1}$), and v is the scan rate (in Vs^{-1}). This equation is applicable to 'reversible' all-solution systems, those undergoing rapid electron transfer at the electrode, where slower electron transfer results in a different i_p formulation and shape of CV. Furthermore, if reactant or product, or both, are adsorbed or deposited on the electrode, different current-potential curves, following alternative equations, are found. Commonly iP_c refers to the peak for a cathodic (reduction) process, while iP_a refers to an anodic (oxidative) process [39]. According to the equation, the current is directly proportional to concentration and increases with the square root of the scan rate.

1.7.2 Spectroelectrochemistry

Spectroelectrochemistry is the combination of electrochemical and spectroscopic techniques that can be operated at the same time. It can provide information on both electrochemical response and accompanying optical characteristics of all states of the electrochemical reaction.

The electronic transitions of conjugated polymers have been the subject of many articles. UV-Vis spectroscopy can be used to investigate these electronic transitions. Spectra are recorded while the polymer is oxidized by increasing the potential stepwise. This experiment is commonly referred as spectroelectrochemistry. Spectroelectrochemistry experiments reveal key properties of conjugated polymers such as band gap (E_g), λ_{max}, the intergap states that appear upon doping and evolution of polaron and bipolaron bands. Similar studies were accomplished for electrochromic devices in order to investigate the spectral variations [34].

1.7.3   Colorimetry

Color is a very subjective phenomenon, causing its description or, for example, the comparison of two colors, to be quite difficult. However, a new developed method of color analysis, in situ colorimetric analysis, is based on the CIE (Commission Internationale de l'Eclairage (the 'International Commission on Illumination') system of colorimetry. The CIE method has been applied to the quantitative color measurement of conducting electroactive polymer and other electrochromic films on optically transparent electrodes under electrochemical potential control in a spectroelectrochemical cell. To describe color, there is a set of color cordinates, CIE Lab color space Figure 11.

According to the color coordinate, color is described by three attributes. The first identifies the color by its location in the spectral sequence, i.e. the wavelength associated with the color. This is known as the *hue (a),* dominant wavelength or chromatic color, and is the wavelength where maximum contrast occurs. The second attribute relates to the relative levels of white and/or black, and is known as *saturation (b)*, chroma, tone, intensity or purity. The third attribute is the brightness of the color, and is also referred to as *brightness (L)* or luminance. Luminance provides information about the perceived transparency of a sample over the entire visible range. Using the three attributes of hue, saturation and luminance, any color can be both described and actually quantified [3,52].
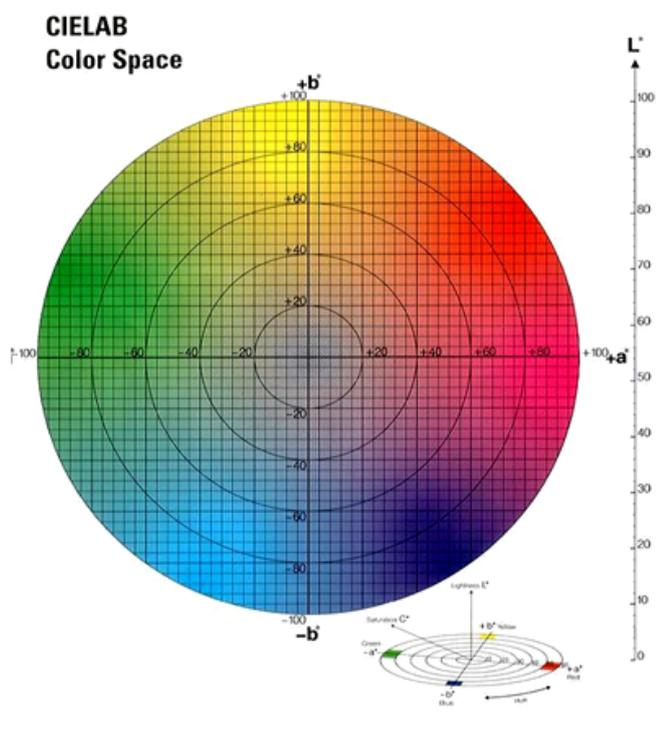
Figure 11 CIE Lab color space.

1.8 Donor-Acceptor Theory

The search for stable organic polymers with low band gaps has been progressing steadily over the past 25 years [53]. Among their many potential advantages [54-61] such materials will be intrinsic conductors, eliminating the need for doping. A significant number of stable conducting polymers with band gaps below 1 eV are known today [62].

To produce low-bandgap conjugated polymers, the most successful approach involves the incorporation of alternating electron-rich and electron-deficient aromatic units into the polymer chain [63-66]. The resulting polymers are so-called donor (D)-acceptor (A) conjugated polymers [67]. Intramolecular charge transfer (ICT) interaction between the electron donor (D) and electron acceptor (A) units within D-A polymers can facilitate ready manipulation of their electronic structures (HOMO/LUMO levels) and thus electronic and optoelectronic properties. Through the careful design and selection of the donor (*p-type*) and acceptor (*n-type*) building

24

blocks, the strength of ICT can be tuned, allowing such D-A polymer semiconductors to exhibit small band gaps, broad absorption bands that extend into near-infrared spectral range, high electron affinity and low ionization potential, efficient photo induced charge transfer and separation, and ambipolar charge transport with high mobilities.

Conjugated D-A polymers with strong intramolecular charge transfer between the D and A moieties are of special interest for photovoltaic applications because their small band gaps, broad absorption spectra, and ambipolar charge transport could facilitate efficient harvesting of the solar spectrum and improve charge photogeneration and collection [68].

Furthermore, among the organic recording materials being extensively studied, D-A type charge-transfer complex and compounds are considered to be very promising materials for future information storage due to their electronic switching property induced by reversible intermolecular charge transfer [69-71].

Donor–acceptor systems lead to a narrower bandgap due to resonances that enable a stronger double bond character between the donor and acceptor units. This results in a decreased bond length alternation. This is attributed to hybridization between the energy levels, especially the HOMO of the donor and the LUMO of the acceptor [72]. The idea is to combine the high lying HOMO level of the donor and low lying level of LUMO of the acceptor in the same polymer to induce a lower band gap. Figure 12 illustrates this concept for PEDOT [73], poly(cyanoacetylene) (PCA) [74] and PBEDOT-CNV.
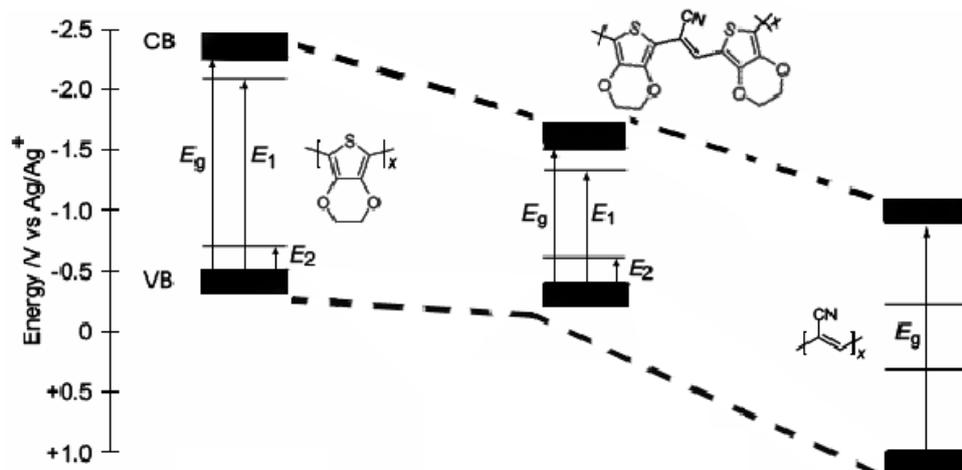
Figure 12 The Donor-Acceptor approach, alternating donor and acceptor moieties results in a polymer that has the combined optical properties of the parent donor or acceptor monomers [75].

All the HOMO and LUMO levels were anticipated from the spectroelectrochemical series, potentials for the electrochemical doping /undoping processes or from the known band gaps of the materials. This figure clearly illustrates that the resulting donor-acceptor type polymers has very similar valence band energy of the donor moiety and has a very close conduction band energy value of the acceptor moiety. This resulted in a tremendously decreased band gap compared to both PEDOT and PCA [76].

There are three types of the reactions used mostly to synthesize donor-acceptor-donor type monomers, which are Suzuki Coupling, Neigishi Coupling and Stille Coupling.

1.9 Metal-Catalyzed Cross-Coupling Reactions

1.9.1 The Stille Coupling

Stille reaction is just one member of a large family of transition metal-catalyzed cross-coupling reactions. Although cross-coupling involving organotin derivatives are today linked indivisibility with the name of the late J. K. Stille, it is known that he was not in fact the true "inventor" of this type of chemistry. Examples of the palladium-catalyzed coupling of organotin compounds with carbon electrophiles were first reported in 1977 by Kosugi, Shimizu, and Migita [77-79]. In 1978, the first study by Stille appeared [80]. Beletskaya, using "ligandless" catalysts in cross-coupling reactions, also often studied with organostannes in early work [81]. This coupling is now referred to as Stille reaction due to his comprehensive synthetic and mechanistic studies [82]. Many reviews on what is now known either as "Stille coupling" or "Stille cross-coupling" have been written.

One obvious reason for such popularity is the reaction's versatility. As opposed to most cross-coupling reactions which operate in more or less strongly basic media, the Stille reaction works under neutral conditions, and is therefore compatible with virtually all functional groups without requiring protection. It is one of very few reactions that can form carbon-carbon bonds under such mild conditions, and it does so often with complete stereospecificity. Therefore, it is often used in the total syntheses of complex molecules as a way of coupling together complex subunits. It is an excellent tool for medicinal chemists, allowing the rapid and systematic modification of lead structures, again simply because it can be predictably performed regardless of other functional groups present in the molecule [83].

One of the major limitations usually associated with the Stille reaction is the presence of toxic and hard-to-remove tin-containing by products. This has indeed limited the industrial applications of the reaction, because, in such setting, the tolerance for tin-containing impurities is low (in the ppm range). For the academic

lab, however, this limitation is not a serious one because there are some methods that can be used for the removal of tin.

1.9.2 Mechanism

The Stille reaction can be formulated as follows:

$$R_3Sn\text{-}R' \quad + \quad R''\text{-}X \quad \xrightarrow[\text{environment}]{\text{catalyst system}} \quad R'\text{-}R'' \quad + \quad R_3SnX$$
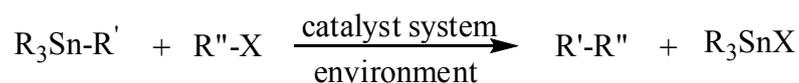
where R'-R" is the target molecule, and R_3SnX is the unwanted byproduct. The term "environment" is used in a broad sense. Normally it can be replaced by the word "solvent", but as we shall see it now encompasses more. The term "catalyst system" comprises the catalyst precursor and any additives used (such as phosphines or copper salts) [84] R' is a typically an unsaturated moiety (e.g., vinyl, aryl, heteroaryl, alkynyl, allyl) or less often an alkyl group, and R, nontransferable ligand, is almost always butyl or methyl. The range of functionalities which are available as R' is very broad, but in some cases (e.g., bulky organotins) there have been-or still are-problems to overcome.

Organotin reagents are air- and moisture-stable organometallics, and can be conveniently purified and stored. Since they do not react with most common functional groups, the use of protecting groups is almost always unnecessary in conjunction with the Stille reaction. This is a very unusual and attractive feature for an organometallic process. Also, the reaction is often neither air nor moisture sensitive. In some cases, water and oxygen have actually been shown to promote the coupling.

The three step catalytic cycle proposed for the Stille reaction follows the general principles of transition metal mediated cross-coupling reactions and is shown in Scheme 1 [82].
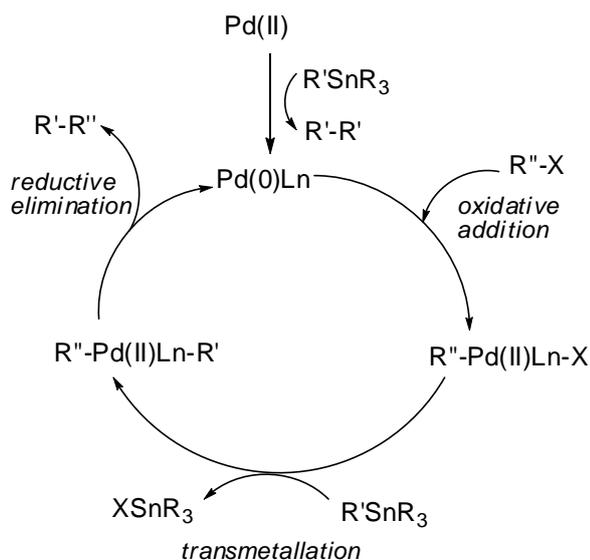
Scheme 1 Catalytic cycle of the Stille reaction

When the catalyst is introduced as Pd(II), fast reduction by the stannane to a Pd(0) species enters the cycle. Alternatively, the catalyst can be introduced directly as Pd(0). The first step of the catalytic cycle is oxidative addition of R"-X to the active catalyst to give R"-Pd(II)Ln-X, followed by transmetallation to give R"-Pd(II)Ln-R' and finally reductive elimination to give R'-R".

1.9.3 Stille Reaction in Polymer Chemistry

The construction of conjugated polymers lies essentially in the efficient carbon-carbon single bond formation between two unsaturated carbons in the aromatic units. In addition to electrochemical [85-87] or chemical [88] oxidative polymerizations, transition-metal-catalyzed cross-coupling reactions provide a particularly powerful arsenal for Csp^2–Csp^2 and Csp–Csp^2 bond formation [89]. The reaction, in general, involves a transition-metal-catalyzed oxidative addition reaction across the C-X bond of an electrophile and then transmetalation with a main group organometallic nucleophile, followed by a reductive elimination step leading to the carbon–carbon bond formation. The most commonly employed transition-metal catalysts are nickel- or palladium based complexes, although other metals have also been used. The organometallic nucleophiles can be Grignard reagents (Kumada-Corriu), [90] stannyl

(Stille), [91] boron reagents (Suzuki-Miyaura), [92] or copper (Sonogashira) [93]. Thus, conjugation lengths can be extended through consecutive transformations in the catalytic cycle. When the electrophilic and nucleophilic centers of the monomeric substrates are readily accessible, regioregularity of the polymers can be easily achieved. Another advantage is that these reaction conditions are generally mild and can tolerate many functional groups. This is particularly important for synthesizing advanced functional conjugated polymers.

As mentioned before, Stille and Suzuki coupling reactions are the most efficient and widely used methods for preparing donor-acceptor type monomers, copolymers and polymers. It is noteworthy that stannyl groups substituted on the benzene ring of substrate always give poor reactivity with aryl halides under Stille coupling conditions [94]. Therefore, Stille coupling is more suitable for thiophene-containing polymers using substrate with stannyl groups on the thiophene ring, whereas Suzuki coupling is more widely used for preparing benzene-containing polymers with boronic groups on the benzene ring [95].

An alternative design strategy to intensify the absorption ability of p-type polymers is to introduce additional absorptive chromophores directly and conjugatively attached to the main chain backbone [96,97]. Li et al. designed and synthesized, by Stille coupling, a series of polythiophene derivatives **P4** having conjugated bi(thienylenevinylene) side chains (Scheme 2). It has been shown that extension of a conjugated side chain to the polythiophene main chain leads to strong and broad absorption covering both the UV and visible regions from 350 to 650 nm.
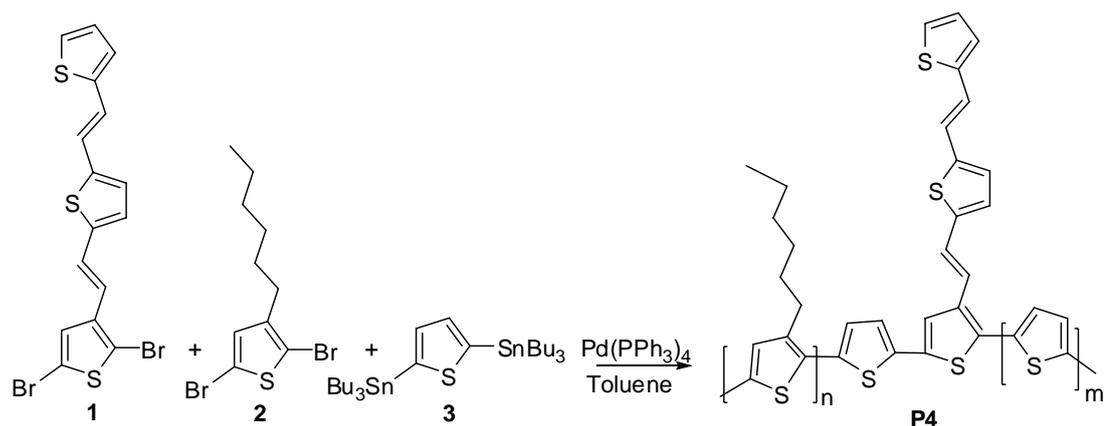
Scheme 2

To decrease the band gap and improve the absorption coverage, poly[2,6-(4,4-bis(2-ethylhexyl)-4*H*-cyclopenta[2,1-*b*;3,4-*b*']dithiophene)-*alt*-4,7-(2,1,3-enzothiadiazole)] (**P7**) containing alternating cyclopentadithiophene units as the donor and benzothiadiazole units as the acceptor was developed and synthesized by Zhu and co-workers via a Stille coupling (Scheme 3) [98]. With two ethylhexyl groups, **P7** is very soluble in organic solvents and has high processability for solar cell application.
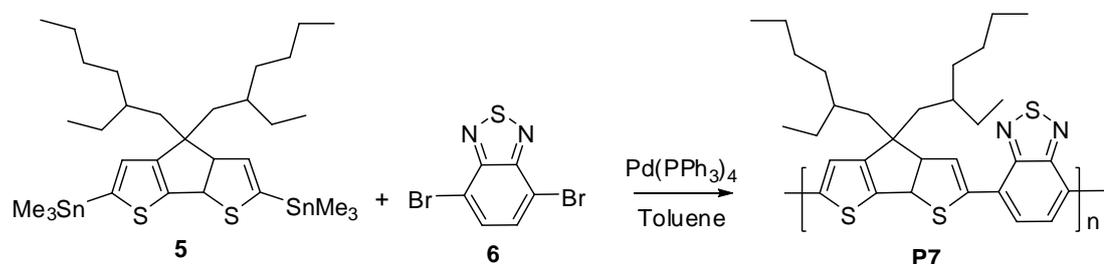
Scheme 3

Müllen and co-workers reported a polymer (**P10**) analogous to (**P7**) but with 4,4-dihexyldecyl substituents instead of the ethylhexyl groups (Scheme 4). **P10** shows a markedly high hole mobility of 0.17 cm2/(V s) in field effect transistor. This can be attributed to the enhanced packing order as a result of the introduction of the straight side chains [99].
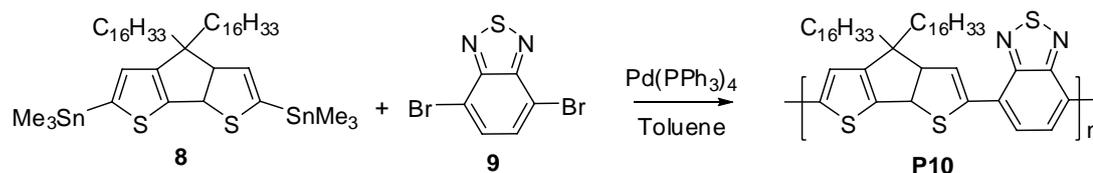
Scheme 4

Compared with many heterocyclic arenes such as thiophene furan, or pyrrole, the silole (silacyclopentadiene) ring has the smallest HOMO-LUMO band gap and the lowest lying LUMO level due to the σ*-π* conjugation between the π-symmetrical σ* orbital of two σ exocyclic bonds on silicon and the π* orbital of the butadiene moiety [100]. As a result a variety of conjugated small molecules and polymers consisting of silole derivatives exhibit extraordinarily unique properties such as high fluorescence efficiency and electron affinity and excellent electron mobility [101-104]. Recently, Yang and co-workers reported dithienosilole-containing copolymer (**P13**) (Scheme 5). Here benzothiadiazole is the acceptor and 2-ethylhexyls are the solubilizing groups, [105] The HOMO and LUMO of the polymer were estimated to be -5.05 and -3.27 eV, respectively. Although the optical band gap of 1.45 eV is very close to the **P7**, the substitution of the silicon atom significantly improved the hole-transport properties. The hole mobility of **P13** ($3 \times 10\text{-}3$ cm^2/(V s)), determined by a field-effect transistor, is 3 times higher than that for **P7**.
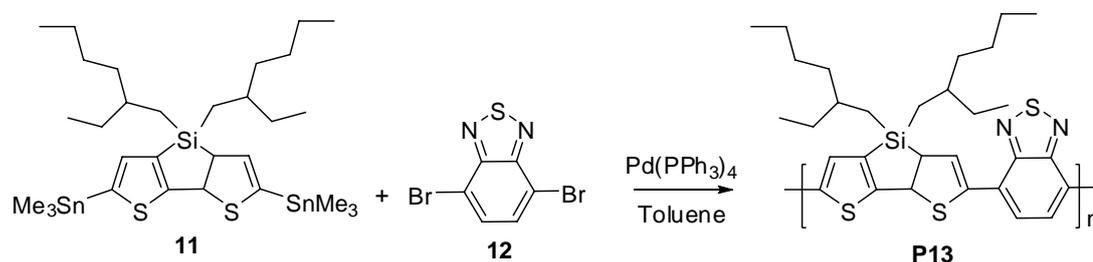
Scheme 5

Benzobis(thiadiazole), derived from benzothiadiazole fused with another thiadiazole ring, is an extremely electron deficient unit due to its high tendency for the formation of quinoid structures and the hypervalent sulfur atom (Figure 13) [106,107].
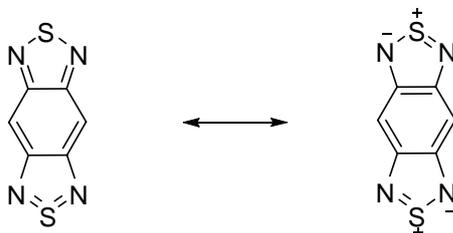
Figure 13 Resonance structure of benzobis(thiadiazole)

A polymer (**P17**) containing quaterthiophene as the donor and benzobis(thiadiazole) as the acceptor was synthesized by Stille coupling (Scheme 6) [108]. An analogous polymer (**P18**) using benzothiadiazole as the acceptor was also prepared for comparison.

Scheme 6

33
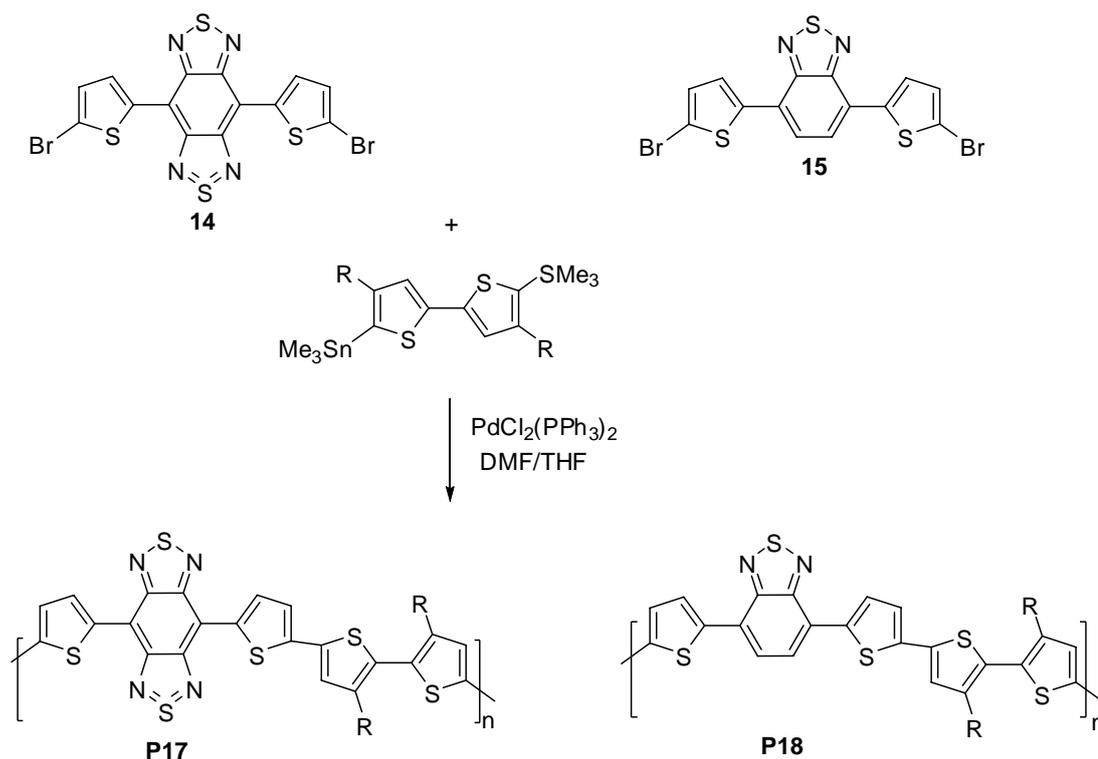
From the absorption spectra, **P17** shows an extremely low band gap of 0.67 eV, which is 1 eV lower than 1.65 eV for **P18** and even lower than that of polyisothianaphthene (1 eV). This result further demonstrates the exceptional electron-accepting power of the benzobis(thiadiazole) subunit. **P18** gave better results than **P17** in solar cell applications which is ascribed to the mismatch of LUMO energy levels between **P17** and [6,6]-phenyl-C_{61}-butyric acid methyl ester (PCBM), the most ubiquitously used acceptor for current BHJ solar cell research. This result again emphasizes the importance of controlling the band gap and corresponding energy levels of the polymer with respect to PCBM when the band gap starts to decrease.

To reflect red or blue color in neutral state, the materials have to absorb at only one dominant wavelength. On the contrary, to have a green color, there should exist at least two simultaneous absorption bands in the red and blue regions of the visible spectrum where these bands should be controlled with the same applied potential. Toppare and co-workers reported the synthesis of 4,7-di(2,3-dihydro-thieno[3,4-b][1,4]dioxin-5-yl)benzo [1,2,5]thiadiazole **21** [109] (Scheme 7).

P21 is the first green electrochromic material, with a highly transmissive sky blue oxidized state. It reveals nearly 40 % optical contrast in the visible and 70 % in the NIR region with exceptional switching properties and remarkable stability.
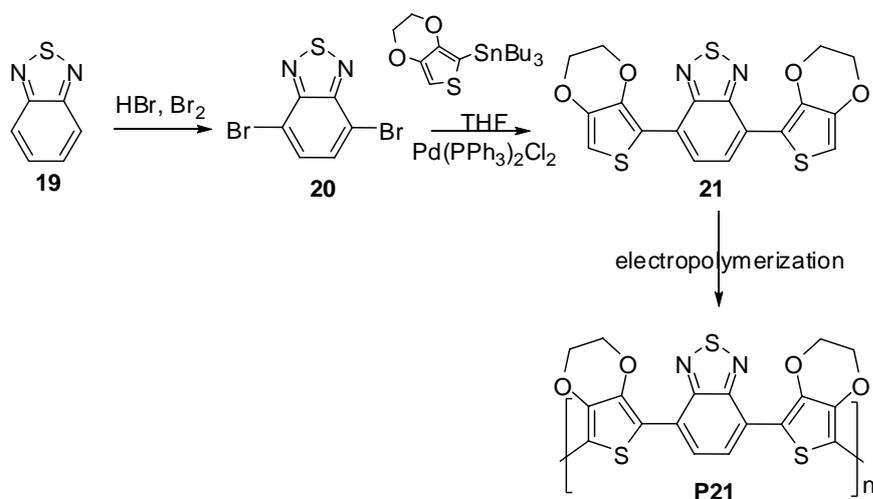
Scheme 7

Toppare and co-workers reported that a polymer containing thiophene as the donor and benzotriazole as the acceptor was synthesized by Stille coupling [110]. **P24** switches between all RGB colors, black and transmissive states. The polymer is soluble, processable, both p- and n-dopable, fluorescent and its properties in entire spectrum offer potential uses in NIR devices, LEDs and solar cells. **P24** possesses almost all properties in a single polymer for optoelectronic applications (Scheme 8).
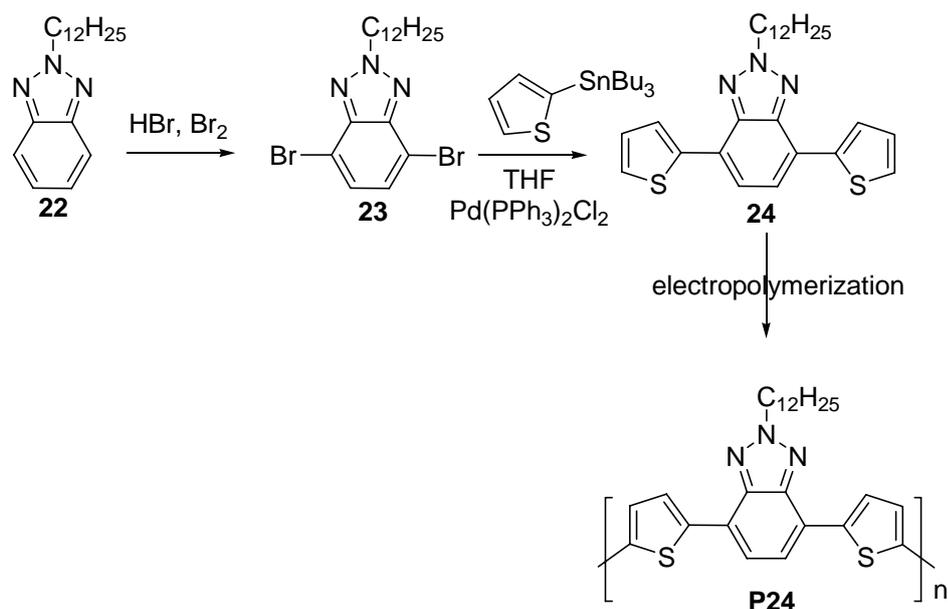
Scheme 8

1.10 Aim of The Work

There are number of methodologies for the synthesis of narrow band gap polymers, namely reduction of bond-length alternation, synthesis of highly planar systems, and alteration of interchain and resonance effects. Besides these methods, donor-acceptor approach was commonly applied for reducing the band gap and avoiding solubility problems.

Since the optoelectronic properties of a donor-acceptor polymer depend on the interaction between HOMO of the donor and LUMO of the acceptor unit, the

selection of suitable donor-acceptor couple is important issue in the synthesis of conducting polymers.

In this study, our aim is to synthesize novel donor-acceptor type monomers and to investigate the optical and electronic properties of their polymers. For this reason, the synthesis of the polymers bearing dibenzophenazine, dibenzopyridoquinoxaline, tetrahydrodibenzo phenazine, thiadiazoloquinoxaline, pyrazinoquinoxaline, thienopyrazine, benzoselenadiazole, thienoselenadiazole as the acceptor units and 3-hexylthiophene, thiophene and ethylendioxythiophene (EDOT) as the donor units is aimed.

Scheme 9, 10, 11 and 12 show the retrosynthetic route for selected donor-acceptor type monomer synthesis.

X: 29, 30, 31

X: 32, 33, 34

X: 35, 36, 37

Cross coupling

26

27

28

Condensation reaction

25

Bromination
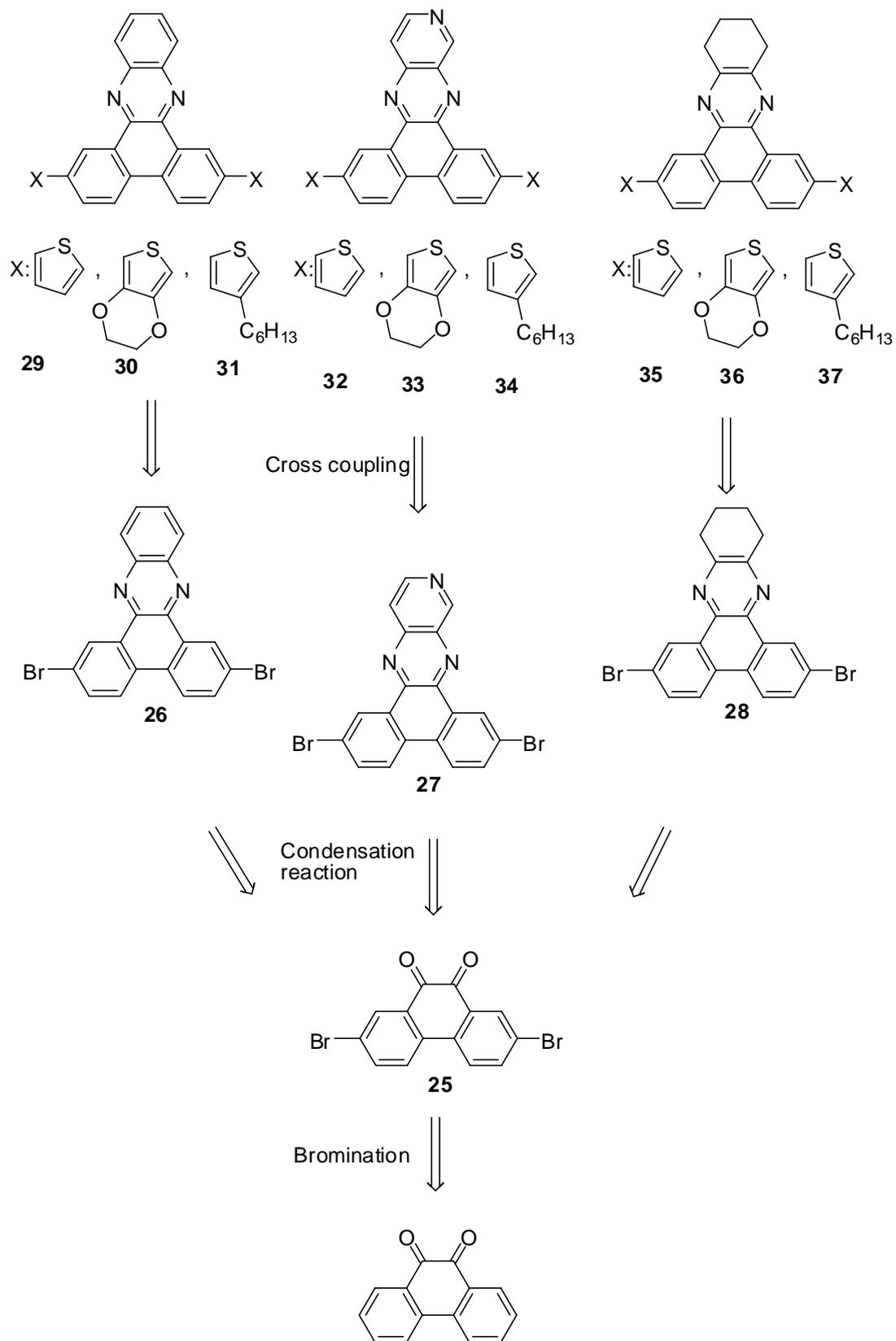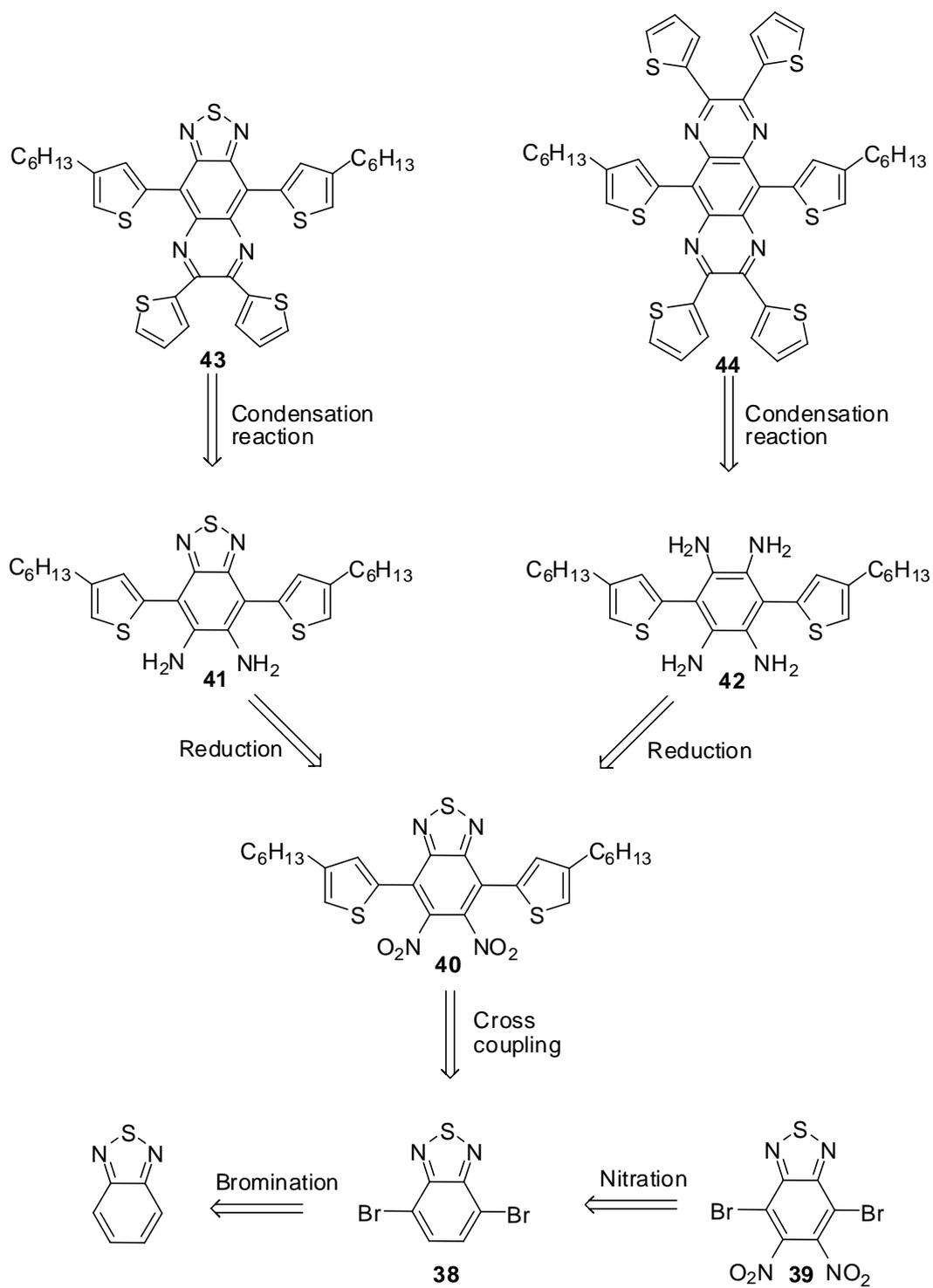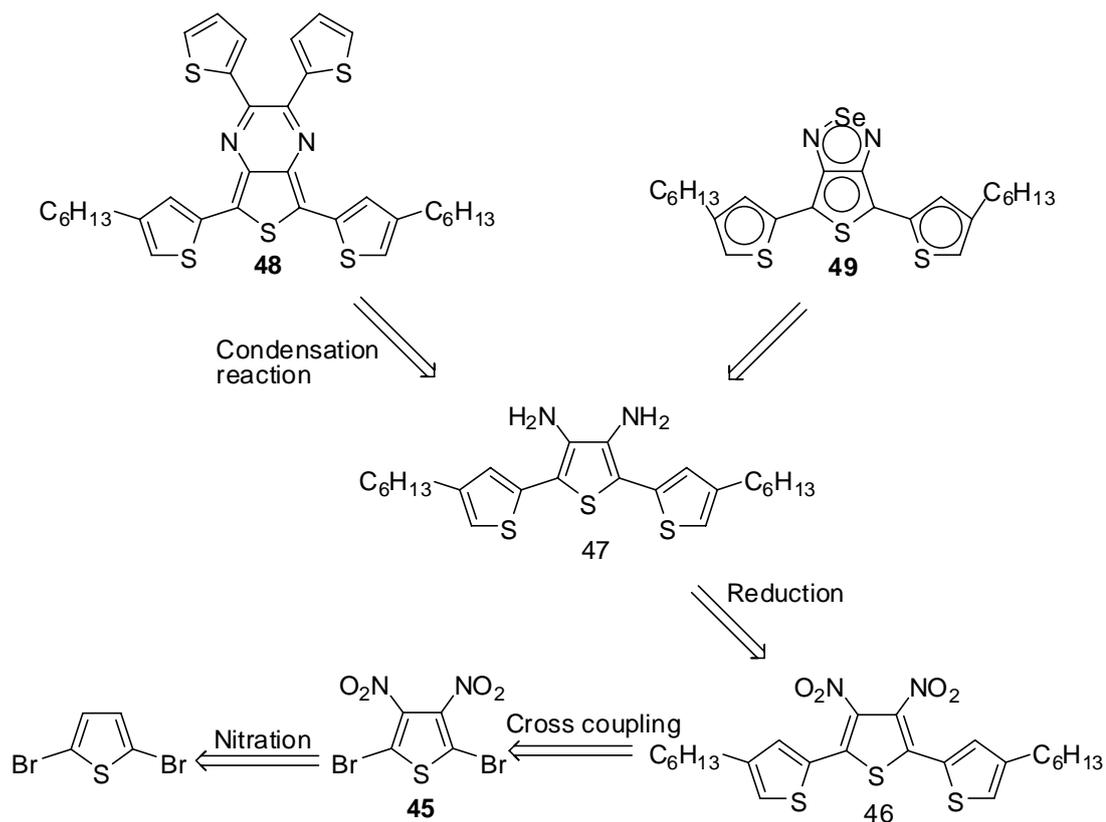
Scheme 9

Scheme 10

Scheme 11
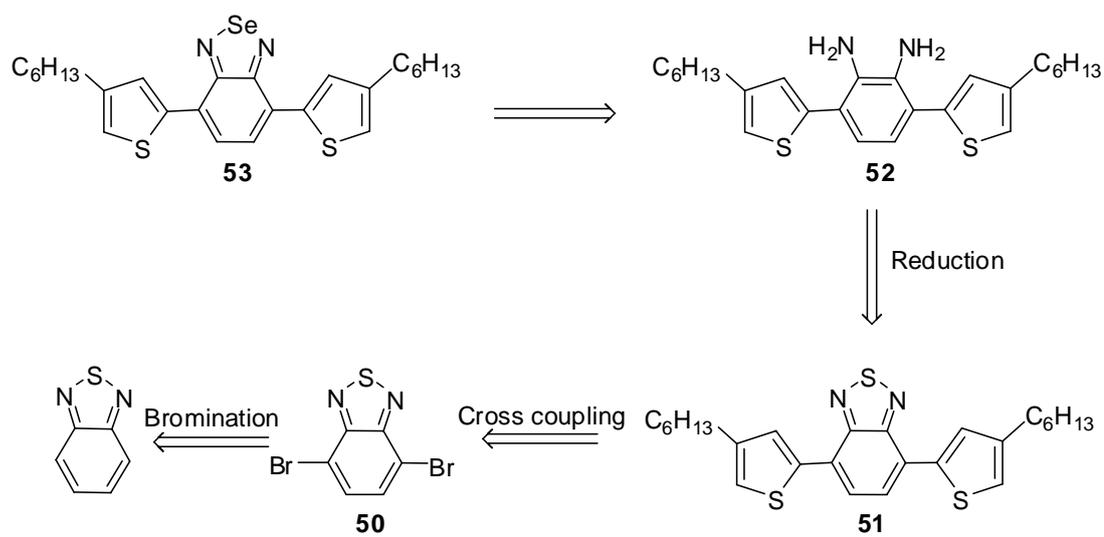
Scheme 12

CHAPTER 2

RESULTS AND DISCUSSION

2.1 Synthesis and Characterization of Monomers

2.1.1 Perspective of the work

Conjugated fused organic molecules, bearing polymerizing units in their structure, are candidates for versatile monomers which can give conducting polymers. These conducting polymers, among organic molecules, have attracted significant interest in the field of electrochromism, since they offer additional advantages, such as low processing cost, enhanced mechanical properties, no dependence with angle of vision, good UV stability high coloration efficiency, fast switching ability and fine-tuning of the band gap through the modification of polymer's chemical structure.

Also, they have been mainly investigated for their conducting, semiconducting and electrochemical properties in the last three decades [42-51]. Some of these materials have practical and potential applications including rechargeable batteries, sensors, light emitting diodes, microwave absorbing materials, smart windows, solar cells and field effect transistors.

As mentioned before, donor-acceptor type monomers are very important for the synthesis of small band gap semiconductor polymers. Moreover, these materials have also enhanced third-order nonlinear optical properties.

In this study, well-known synthetic methods were used for the synthesis of desired monomers, designed based on donor-acceptor approach, such as bromination, nitration, condensation, reduction and Stille coupling.

Two different methods were performed to obtain brominated compounds, from the starting materials. One of them is HBr/Br_2 mediated bromination method. The other one is the method in which *N*-bromo succinimide (NBS) was used as brominating agent. The nitration reactions were carried out in the presence of HNO_3 and H_2SO_4. The reduction procedure was changed depending on the purpose. Fe metal in refluxing acetic acid was used as the reducing agent in case of nitro group reductions. On the other hand, Zn metal/AcOH system was chosen for the reduction of both nitro groups and thiadiazole structure to amine, simultaneously. The use of the condensation reaction between amines and diketones yielded fused monomeric structures.

Based on preliminary information available to us from previous work in the literature [109,110], we were able to synthesize donor-acceptor-donor type monomers by use of Stille coupling. In this reaction, $Pd(PPh_3)_2Cl_2$ was used as catalyst and tetrahydrofuran (THF) as solvent.

2.1.2 Synthesis of Dibenzo[*a,c*]phenazine, Dibenzo[*f,h*]pyrido[3,4-*b*]quinoxaline Derivatives and Tetrahydrodibenzo[*a,c*]phenazine Derivatives

Some polymers based on phenazine moieties linked via 2,7-linkages have already been reported in the literature, but they were found to be highly insoluble [111-113]. Very recently, Jenekhe and co-workers reported the synthesis and photophysical properties of some soluble poly(dibenzo[*a,c*]phenazine- 3,6-diyl)/dioctylfluorene) co-polymers [114] and used them in blue-light-emitting diodes. Linking through the 3- and 6-positions is, however, not expected to give polymers with a p-electron system conjugated along the backbone. In the expectation of obtaining polymers with a more conjugated backbone, we chose 2,7-dibromodibenzo[*a,c*]phenazines as the acceptor group. The rationale behind this choice of approach is the following (i) a

fully conjugated phenanthrene backbone allows intramolecular electron (and more generally energy) transfers to occur, (ii) alkyl chain and alkoxy substituents attached to thiophene may allow fine tuning of the solubility and/or electrochemical properties of the materials.

The synthesis of all dibenzo[*a,c*]phenazine, dibenzo[*f,h*]pyrido[3,4-*b*]quinoxaline and tetrahydrodibenzo[*a,c*]phenazine derivatives was achieved using the same synthetic route. During this study, firstly phenanthrene-9,10-dione was brominated with NBS in concentrated H_2SO_4 and then condensation reaction was performed with diamino compounds and 2,7-dibromophenatroquinone to obtain dibenzophenazines, dibenzopyridoquinoxalines and tetrahydrodibenzophenazines. Finally, it was subjected to Stille coupling with stannanes to get final products. (Scheme 13)

a) NBS, conc. H_2SO_4, rt, 3h b) benzene-1,2-diamine, PTSA, EtOH, reflux, 5 h c) pyridine-3,4-diamine, PTSA, EtOH, overnight reflux d) cyclohexane-1,2-diamine, PTSA, EtOH, reflux, 5 h e) Pd(PPh$_3$)$_2$Cl$_2$, stannanes, dry THF, overnight reflux

Scheme 13 General synthetic route for dibenzo[*a,c*]phenazine, dibenzo[*f,h*]pyrido[3,4-*b*]quinoxaline and 10,11,12,12-tetrahydrodibenzo[*a,c*] phenazine derivatives.

43
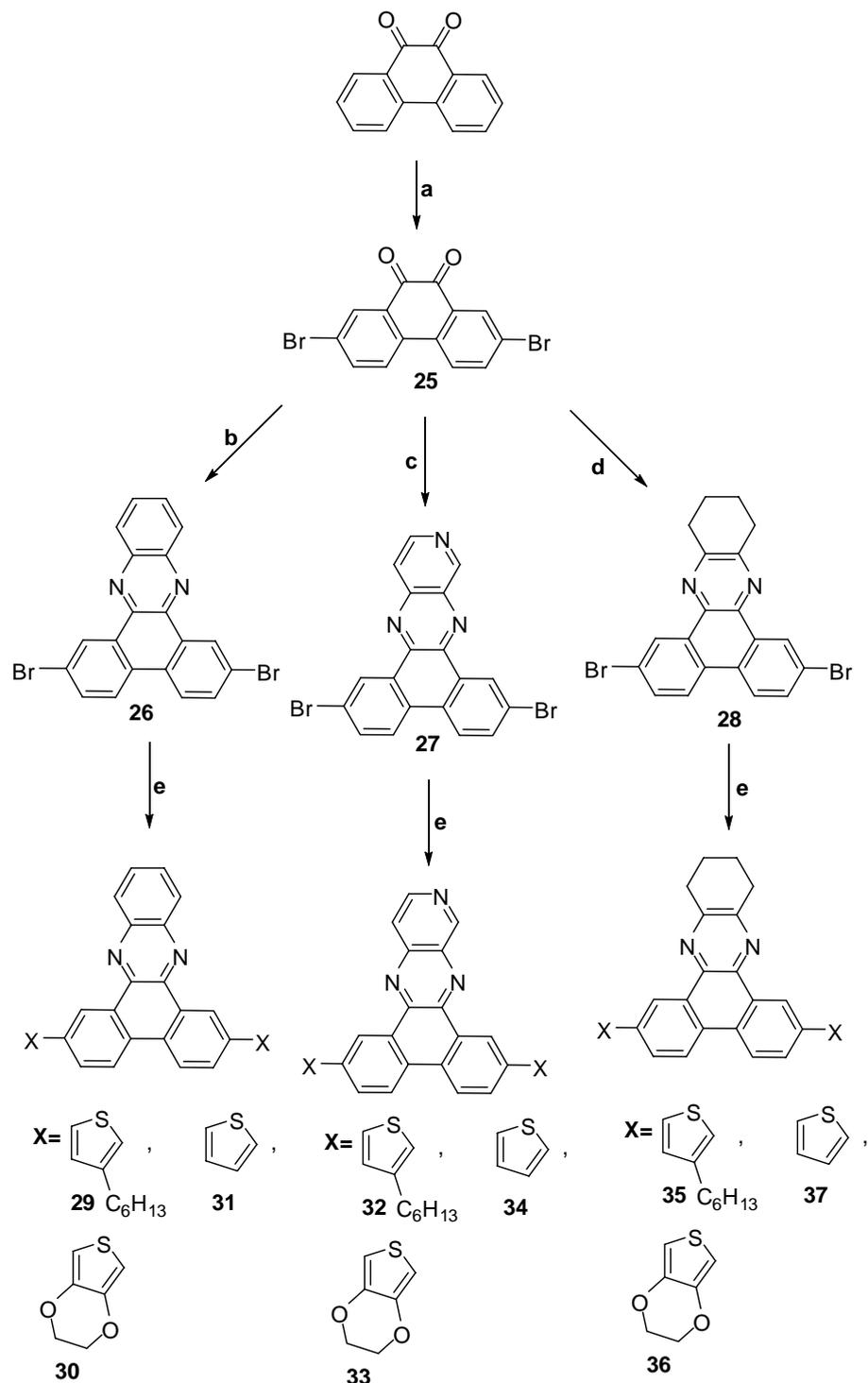
In the literature, there are a number of methods [115-118] for the synthesis of 2,7-dibromophenanthrene-9,10-dione **25** starting from phenanthrene-9,10-dione or 2,7-dibromophenantherene. By help of one of them [116], it was synthesized starting from phenanthrene-9,10-dione in the presence of NBS and concentrated H_2SO_4. The concentration of sulfuric acid plays an important role as diluted sulfuric acid can lead to a mixture of products that are difficult to separate. At the end of the reaction, the mixture poured on the crushed ice with stirring for an hour destroyed succinimide (a byproduct) by converting it to water-soluble succinic acid which was washed away during filtration. DMSO was used as the recrystallization solvent for purification (75% yield).

The product 2,7-dibromophenanthrene-9,10-dione **25** was identified by use of NMR spectroscopy in d_6-DMSO. From the ^{1}H-NMR spectrum of **25**, we observed a doublet at 8.09 ppm with 1.9 Hz as coupling constant for nearest proton to carbonyl unit. ^{13}C-NMR data could not been obtained because of the solubility problem. Melting point was monitored by DSC at 326.8 ℃.

 In the present work the required dibenzo[*a,c*]phenazine, dibenzo[*f,h*]pyrido[3,4-*b*]quinoxaline and tetrahydrodibenzo[*a,c*]phenazine derivatives were prepared by condensing 2,7-dibromophenanthrene-9,10-quinone **25** with the appropriate diamino compounds. Benzene-1,2-diamine was used for the preparation 2,7 dibromodibenzo[*a,c*]phenazine **26**. Similarly, pyridine-3,4-diamine and cyclohexane-1,2-diamine were used for the preparation of 2,7-dibromodibenzo[*f,h*]pyrido[3,4-*b*]quinoxaline **27** and 2,7 dibromo-10,11,12,13-tetrahydrodibenzo[*a,c*]phenazine **28**, respectively. Due to the fact that a catalyst was needed for the increment of the reaction yields, *p*-toluenesulfonic acid (PTSA) was utilized. The reaction mixture was refluxed for 5 hours in EtOH. The condensation reactions proceeded in good yields (49-86%).
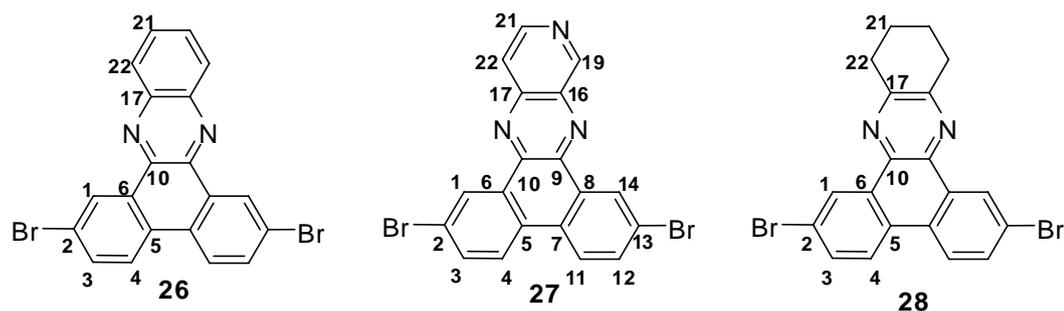
Figure 14 The backbone numbering for **26**, **27** and **28** derivatives.

The structure elucidation of the condensation products **26**, **27** and **28** were done using NMR spectroscopy. It was observed that the characteristic aromatic proton, H-1, in compound **26** resonates at 9.46 ppm as doublet with 2.2 Hz coupling constant. On the other hand the same proton (H-1) in compound **27** resonated at 9.28 ppm as doublet with 1.7 Hz coupling constant. Moreover, another proton (H-3), closer to the Br connected carbon, in compound **27** resonated at 8.07 ppm as triplet of doublet instead of doublet of doublet because of asymmetry in the structure.

2,7-Dibromo-10,11,12,13-tetrahydrodibenzo[*a,c*]phenazine **28** was synthesized by refluxing in EtOH as the same with **26** and **27.** If the reaction medium is kept at room temperature without catalyst, there is no aromatization in the phenazine ring. But this product is highly unstable and undergoes rearrangement with heat or light [119]. From ^{1}H-NMR data we observed the characteristic aromatic proton, H-1, as a doublet at 9.04 ppm (*J*=2.2 Hz) and the methylene protons of cyclohexyl moiety (H-22 and H-21) at 3.10 and 2.00 ppm as multiplet. ^{13}C-NMR spectrum shows the characteristic signals of methylene carbons at 32.7 ppm and 22.8 ppm.

Finally, the desired monomers, **29, 30, 31, 32, 33, 34, 35, 36, 37** were prepared by Stille coupling of the bromo-compounds **26, 27** and **28** with stannanes, tributyl(thiophen-2-yl)stannane, tributyl(4-hexylthiophen-2-yl)stannane and tributyl(2,3-dihydrothieno[3,4-*b*][1,4]dioxin-5-yl)stannane, in the presence of the palladium catalyst. The general reaction mechanism is illustrated on the example of compound **26** and tributyl(thiophen-2-yl)stannane (Scheme 14).
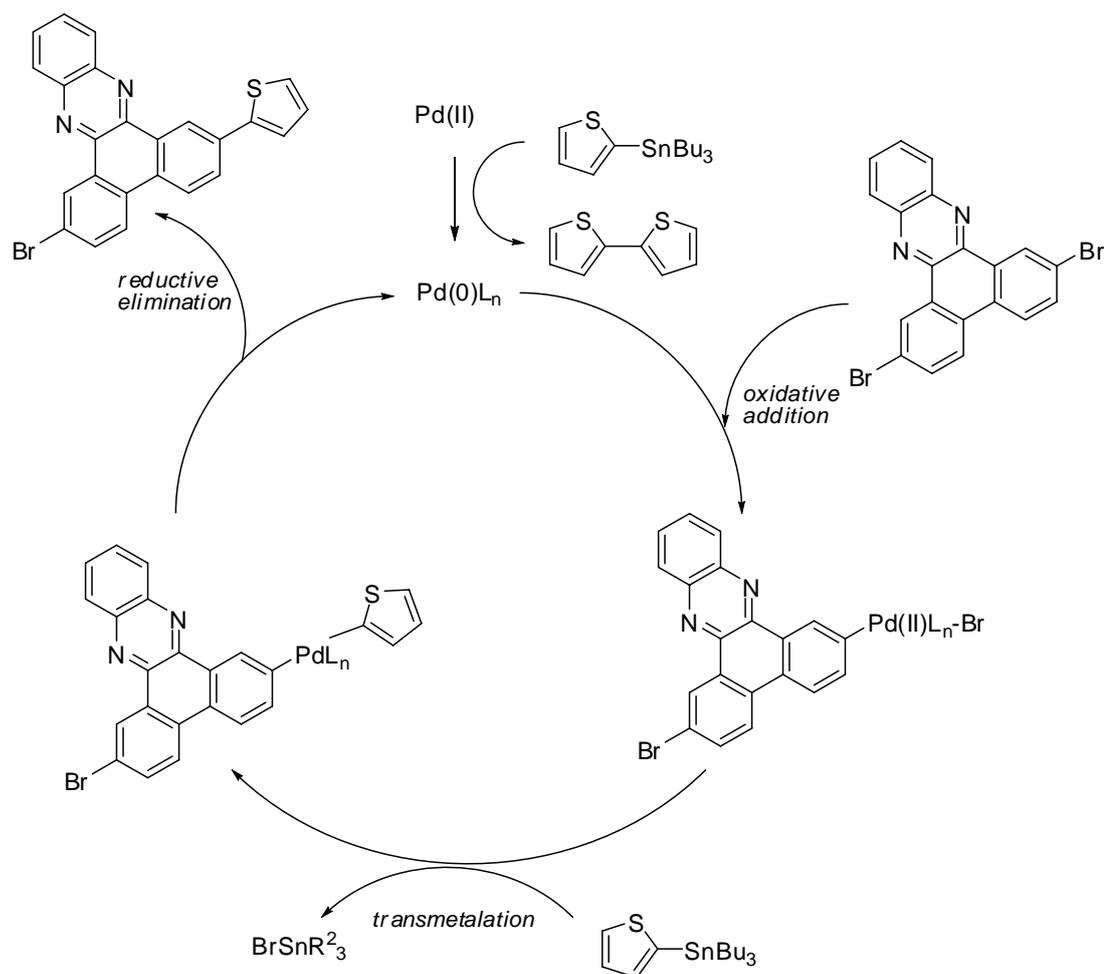
Scheme 14

In this mechanism proposed by Stille [82], firstly Pd-(II) reduces to Pd-(0) by stannane. The oxidative addition of the 2,7-dibromophenazine (R-Br) to the active palladium(0)-complex forms a palladium(II)-ligand2-Br-R-complex. Secondly tributyltinstanne (R'SnBu$_3$) attacks the complex causing transmetalation of the complex forming R-palladium-(II)-ligand2-R' and tributyltin bromide. Finally, reductive elimination of the complex results in the R-R' product and regenerating of the active palladium-(0) complex.

Tributylstannane compounds were synthesized according to previously described methods [120-122]. In the presence of Pd(PPh$_3$)$_2$Cl$_2$ catalyst, Stille coupling

reactions were performed in dry tetrahydrofurane (THF). Overnight reflux provided the final products with reasonable yields (64-71%). The backbone numbering of dibenzophenazine derivatives is given in Figure 15 to follow their structure elucidation.

29- R^1=hexyl, R^2=H
30- R^1,R^2= -OCH$_2$CH$_2$O-
31- R^1, R^2=H
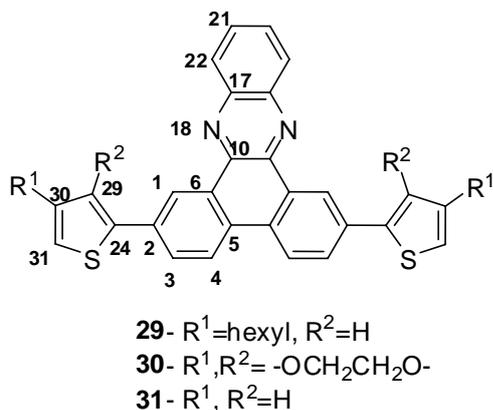
Figure 15 The backbone numbering for dibenzo[*a,c*]phenazine derivatives.

2,7-Bis(4-hexylthiophen-2-yl)dibenzo[*a,c*]phenazine **29** was obtained from the reaction between 2,7-dibromodibenzo[*a,c*]phenazine **26** and tributyl(4-hexylthiophen-2-yl)stannane in good yields (64%). After the purification of the crude product by column chromatography (chloroform/hexane 1:2), the desired product, 2,7-bis(4-hexylthiophen-2-yl)dibenzo[*a,c*]phenazine **29**, was isolated as lemon yellow solid. Identification of 2,7-bis(4-hexylthiophen-2-yl)dibenzo[*a,c*]phenazine **29** was accomplished by NMR spectroscopy. Some characteristic signals were observed as a singlet at 9.48 ppm for H-1, two singlets at 7.40 ppm and 6.92 ppm for H-31 and H-29, respectively (belongs to 3-hexylthiophene) and a triplet (*J*=7.6 Hz) at 2.63 ppm for methylene protons of hexyl chain. In the ^{13}C-NMR spectrum of **29**, it was observed that hexyl carbons resonate between 32.0 ppm and 14.4 ppm.

2,7-Bis(2,3-dihydrothieno[3,4-*b*][1,4]dioxin-5-yl)dibenzo[*a,c*]phenazine **30** was obtained as a result of the reaction between 2,7 dibromodibenzo[*a,c*]phenazine **26** and tributyl(2,3-dihydrothieno[3,4-*b*][1,4]dioxin-5-yl)stannane. At the end of the reaction, the crude product was purified by column chromatograpy

(Chloroform/Hexane 3:1). The structure elucidation of 2,7-bis(2,3-dihydrothieno [3,4-*b*][1,4]dioxin-5-yl)dibenzo[*a,c*]phenazine **30** was done with spectroscopic techniques, NMR and HRMS. From the ^{1}H-NMR, we observed a doublet at 9.59 ppm (*J*=2.0 Hz) for H-1 and two multiplets at 4.39 ppm and at 4.27 ppm for – OCH$_2$CH$_2$O-. From ^{13}C-NMR we observed two signals at 63.8 ppm and 63.4 ppm for –OCH$_2$**C**H$_2$O- and a signal at 97.3 ppm for C-31 of ethylenedioxythiophene (EDOT) unit. HRMS result is in accordance with the calculated result for (C$_{32}$H$_{20}$N$_2$O$_4$S$_2$) as 561.0943[M+H]+ and measured as 561.0961[M+H]+.

The product of the reaction of 2,7 dibromodibenzo[*a,c*]phenazine **26** and tributyl(thiophen-2-yl)stannane was 2,7-di(thiophen-2-yl)dibenzo[*a,c*]phenazine **31**. At the end of the reaction, the filtration of the precipitate gave us the goldish yellow solid (71% yield). The sharp decreasing in the solubility prevented the further purification of the product. Identification of the product was achieved by using ^{1}H-NMR and HRMS data. ^{13}C-NMR could not be obtained due to low solubility. From ^{1}H-NMR spectrum we observed a doublet at 9.83 ppm (*J*=1.6 Hz) for H-1 and a triplet at 7.50 ppm for –CH (H-30) of thiophene. HRMS *m/z* calculated value for (C$_{28}$H$_{16}$N$_2$S$_2$) is 445.0833[M+H]$^+$ and the observed value is 445.0814[M+H]$^+$.

Figure 16 illustrates the backbone numbering of dibenzo[*f,h*]pyrido[3,4-*b*]quinoxaline derivatives for their structure elucidation.
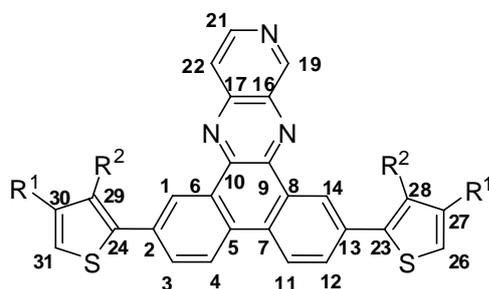
32- R^1=hexyl, R^2=H
33- R^1,R^2= -OCH$_2$CH$_2$O-
34- R^1, R^2=H

Figure 16 The backbone numbering for dibenzo[*f,h*]pyrido[3,4-*b*]quinoxaline.

2,7-Dibromodibenzo[*f,h*]pyrido[3,4-*b*]quinoxaline **27** reacts with tributyl(4-hexylthiophen-2-yl)stannane to give 2,7-bis(4-hexylthiophen-2-yl)dibenzo[*f,h*]pyrido[3,4-*b*]quinoxaline **32**. Reaction mixture was refluxed 14 h and the crude product was purified by column chromatography (2:1 Chloroform:Hexane). In ^{1}H-NMR spectrum, it was determined that H-19 resonates at 9.57 ppm as singlet and H-1 and H-14 protons resonate at 9.11 ppm as triplet (*J*=1.9 Hz), respectively. It is expected that H-1 and H-14 resonate as doublet. However they have different chemical shift due to the asymmetry in the structure. For this reason these doublets belonging to the H-1 and H-14 overlap to form triplet. Some characteristic signals at 153.96 ppm for C-19 and signals between at 30.7 ppm and 13.1 ppm for hexyl group were observed in ^{13}C-NMR. Also HRMS data was taken for compound **32**, calculated and measured values are closer to each other. HRMS *m/z* calculated value is 614.2642[M+H]+ for ($C_{39}H_{39}N_3S_2$) and the measured value is 614.2444[M+H]+.

2,7-Bis(2,3-dihydrothieno [3,4-*b*] [1,4] dioxin-5-yl) dibenzo [*f,h*] pyrido [3,4-*b*] quinoxaline **33** was obtained as the product of **27** and tributyl(2,3-dihydrothieno[3,4-*b*][1,4]dioxin-5-yl)stannane. The low solubility prevented to get ^{13}C-NMR spectrum. H-19 resonated as singlet at 9.77 ppm and $-OCH_2CH_2O-$ protons resonated as multiplet at 4.40 and 4.28 ppm in ^{1}H-NMR. In contrast with compound **33** H-3 and H-12 have different chemical shift so we observed two doublets for these protons. HRMS calculated value is in conformity with observed value for ($C_{31}H_{19}N_3O_4S_2$). HRMS *m/z* calculated value is 562.0872[M+H]+, observed value is 562.0749[M+H]+.

2,7-di(thiophen-2-yl)dibenzo[*f,h*]pyrido[3,4-*b*]quinoxaline **34** was the final product of the Stille coupling reaction of **27** and tributyl(thiophen-2-yl)stannane. Because of the low solubility, only ^{1}H-NMR was obtained. From ^{1}H-NMR spectrum, we observed two characteristic aromatic protons resonating at 9.77 ppm as singlet for H-19 and at 9.53 ppm as doublet (*J*=1.9 Hz) for H-1 and H-14. HRMS result is in accordance with the calculated result for ($C_{27}H_{15}N_3S_2$) as 446.0764[M+H]+ and measured as 446.0627[M+H]+.

Figure 17 shows the backbone numbering of 10,11,12,13-tetrahydrodibenzo [a,c]phenazine derivatives for their structure elucidation.
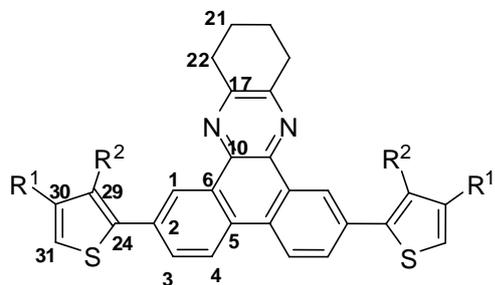
35- R[1]=hexyl, R[2]=H
36- R[1],R[2]= -OCH₂CH₂O-
37- R[1,] R[2]=H

Figure 17 The backbone numbering for dibromodibenzo[f,h]pyrido[3,4-b]quinoxaline.

The product of the reaction between 2,7-dibromo-10,11,12,13-tetrahydrodibenzo [a,c]phenazine **28** and tributyl(4-hexylthiophen-2-yl)stannane is 2,7-bis(4-hexylthiophen-2-yl)-10,11,12,13-tetrahydrodibenzo[a,c]phenazine **35**. At the end of the reaction, the crude product was purified by column chromatography (Dichloromethane/Hexane 1:3) to obtain the desired product, 2,7-bis(4-hexylthiophen-2-yl)-10,11,12,13-tetrahydrodibenzo[a,c]phenazine **35**. Identification of the product was achieved by using NMR spectroscopy. From ^{1}H-NMR spectrum, some characteristic signals were observed, such as multiplet at 3.15 ppm and 1.99 ppm for H-22 and H-21, respectively and a triplet (J=7.6 Hz) at 2.60 ppm for –CH₂-(connected to thiophene) and a triplet (J=7.0 Hz) at 0.84 ppm for –CH₃. The ^{13}C-NMR spectra illustrated that there are two signals at 33.0 ppm and 32.0 ppm for C-22 and C-21 and signals between 31.0 ppm and 14.4 ppm for hexyl carbons.

The reaction between 2,7-dibromo-10,11,12,13-tetrahydrodibenzo[a,c]phenazine **36** and tributyl(2,3-dihydrothieno[3,4-b][1,4]dioxin-5-yl)stannane allocated us 2,7-bis(2,3-dihydrothieno[3,4-b][1,4]dioxin-5-yl)-10,11,12,13- tetrahydrodibenzo[a,c] phenazine **32** as a yellow solid with 66 % yield. After the reaction was completed,

the crude product was purified by column chromatography (Dichloromethane/Hexane 1:3). In ^{1}H-NMR spectrum the peaks at 3.15 ppm and 1.98 ppm correspond to H-22 and H-21, respectively and a singlet at 6.30 ppm, belonging to EDOT aromatic proton (H-31), were observed. Additionally, multiplets at 4.32 ppm and 4.22 ppm were resulted from –OCH$_2$CH$_2$O-. The ^{13}C-NMR revealed two peaks at 31.8 ppm and 21.9 ppm for C-22 and C-21, two peaks at 63.8 ppm and 63.4 ppm for –OCH$_2$CH$_2$O- carbons and a singlet at 97.0 ppm for C-31.

2,7-Dibromo-10,11,12,13-tetrahydrodibenzo[*a,c*]phenazine **28** reacted with tributyl(thiophen-2-yl)stannane to give 2,7-di(thiophen-2-yl)-10,11,12,13-tetrahydrodibenzo[*a,c*]phenazine **37**. The product was purified by column chromatograpy (chloroform/hexane 5:1). In ^{1}H-NMR spectrum, we observed two multiplets at 3.19 ppm and 2.03 ppm for H-22 and H-21 and also a dd with J=5.1, 3.5 Hz at 7.10 ppm for H-30 (belongs to thiophene). ^{13}C-NMR could not be obtained presumably due to the solubility problem of the product.

Among the synthesized monomers, the 3-hexyl-thiophene bearing ones show no solubility problem due to the alkyl chain. Tetrahydrodibenzophenazine groups have better solubility than the others because of alkyl group on the top of the structure. Solubility of **31, 33, 34,** and **37** against organic solvents (even chloroform and tetrahydrofuran) was low so ^{13}C-NMR could not be taken for these monomers.

2.1.3 The Synthesis of Quinoxaline Derivatives 43, 44

As shown in Scheme 15, the synthesis of 4,9-bis(4-hexylthiophen-2-yl)-6,7-di(thiophen-3-yl)-[1,2,5]thiadiazolo[3,4-*g*]quinoxaline **43** and 5,10-bis(4-hexylthiophen-2-yl)-2,3,7,8-tetra(thiophen-2-yl)pyrazino[2,3-*g*]quinoxaline **44** started with the bromination of 2,1,3-benzothiadiazole followed by nitration to give 4,7-dibromo-5,6-dinitrobenzo[*c*][1,2,5]thiadiazole **39.** A Stille coupling between **39** and tributyl(4-hexylthiophen-2-yl)stannane gave 4,7-bis(4-hexylthiophen-2-yl)-5,6-dinitrobenzo[*c*][1,2,5] thiadiazole **40**. Reduction of **40** with iron in acetic acid and zinc in acetic acid gave 4,7-bis(4-hexylthiophen-2-yl)benzo[*c*][1,2,5]thiadiazole-5,6-

diamine **41** and 3,6-bis(4-hexylthiophen-2-yl)benzene-1,2,4,5-tetraamine **42**, respectively. The final step is the condensation reaction of **41** and **42** with 2,2'-thenil to gain the desired monomers **43** and **44.**
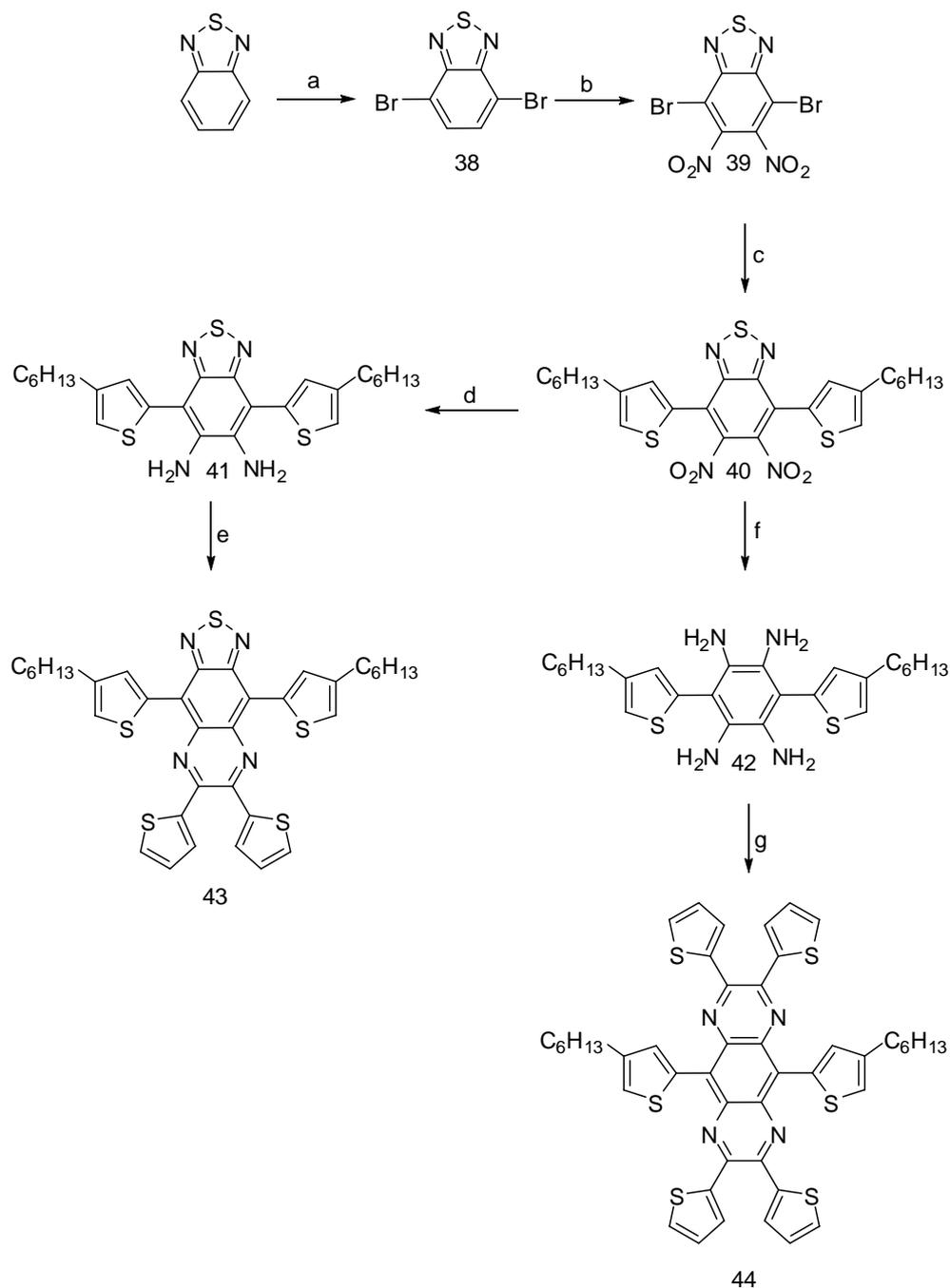
a) HBr, Br$_2$, reflux, 6 h b) conc. H$_2$SO$_4$, fuming HNO$_3$, 0- 5 °C 30 min, 3 h c) PdCl$_2$(PPh$_3$)$_2$, tributyl (4-hexylthiophen-2-yl)stannane, dry THF, overnight reflux d) Fe, AcOH, 30 0C, 4 h e) PTSA, EtOH, 2,2'-thenil, 6 h f) Zn, AcOH, 60 0C, 1 h g) PTSA, EtOH, 2,2'-thenil, 1 h.

Scheme 15 Synthetic route for quinoxaline derivatives.

According to the literature [123], bromination of benzothiadiazole with HBr/Br$_2$ solution, gave as pale yellow needles after purification (88% yield). It was essential that HBr/Br$_2$ solution was added by dropwise to benzothiadiazole very slowly to control the bromination.

A mixture of concentrated sulfuric acid and fuming nitric acid was used for the nitration of 4,7-dibromobenzo[c][1,2,5]thiadiazole **38**. It was added to the mixture in small portions because of heat control. Thus, reaction temperature was kept under 5 °C to prevent over nitration. At the end of the addition, reaction mixture was stirred at room temperature for 3 hours and then mixture was poured into ice-bath. The precipitate was collected by filtration and recyrstallization of the product was performed from acetone-water to yield 4,7-dibromo-5,6-dinitrobenzo[c][1,2,5]thiadiazole **39**, as pale yellow solid. It was used without further purification.

The Stille coupling reaction was done with 4,7-dibromo-5,6-dinitrobenzo[c][1,2,5]thiadiazole **39** and tributyl(4-hexylthiophen-2-yl)stannane, which was chosen to prevent solubility problem, in the presence of Pd(PPh$_3$)$_2$Cl$_2$ catalyst and dry THF to yield 4,7-bis(4-hexylthiophen-2-yl)-5,6-dinitrobenzo[c][1,2,5] thiadiazole **40**. Solvent was evaporated and the residue was purified by column chromatograpy (1:2 dichloromethane/hexane). The product was isolated as orange crystals in 68% yield. ^{1}H and ^{13}C-NMR were used for structure identification. 3-Hexylthiophene ring protons resonated at 7.23 ppm as broad singlet due to the overlapping of these protons and -CH$_2$, connected to the thiophene resonated at 2.57 ppm as triplet. In ^{13}C-NMR spectrum, hexyl carbons resonate in the range of 11.7 ppm and 29.2 ppm.
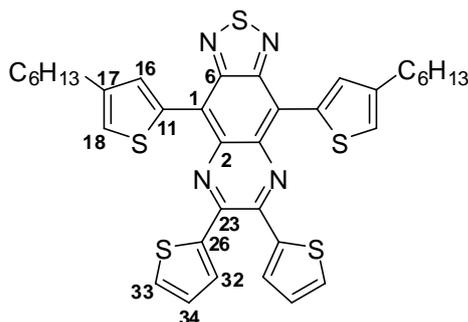
Figure 18 The backbone numbering for 4,9-bis(4-hexylthiophen-2-yl)-6,7-di(thiophen-3-yl)-[1,2,5]thiadiazolo[3,4-*g*]quinoxaline **43.**

Subsequent reduction of **40** was done by iron dust in acetic acid at 30˚C for 4 hours. At the end of the reaction, the mixture were poured into cold NaOH solution to neutralize the medium and then extracted with ether. The product **41** was used without any purification. Then, the condensation reaction between **41** and 2,2'-thenil was carried out in the presence of catalytic amount of PTSA and ethanol. At the end of the reaction, ethanol was evaporated and residue was purified by column chromatograpy (1:1 dichloromethane/hexane). The final product was isolated as green solid **43** in good yield (54%). The structure elucidation was done by the help of NMR Spectroscopy. ^{1}H-NMR spectrum revealed that H-34 resonates at 6.97 ppm as dd with *J*=5.0, 3.7 Hz, H-18 and H-16 resonated at 8.62 ppm as doublet (*J*=1.1 Hz) and 7.19 ppm as broad singlet, respectively.
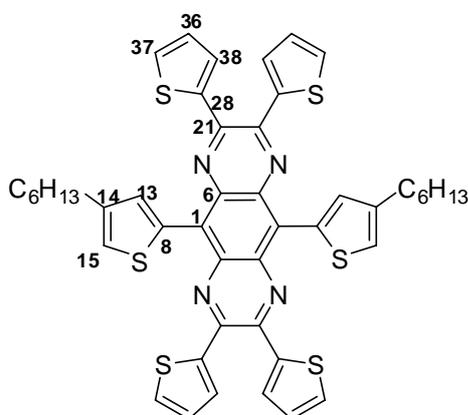
Figure 19 The backbone numbering for 5,10-bis(4-hexylthiophen-2-yl)-2,3,7,8-tetra(thiophen-2-yl)pyrazino[2,3-*g*]quinoxaline **44.**

54

In preparation of 5,10-bis(4-hexylthiophen-2-yl)-2,3,7,8-tetra(thiophen-2-yl)pyrazino[2,3-*g*]quinoxaline **44**, 4,7-bis(4-hexylthiophen-2-yl)-5,6-dinitrobenzo[*c*][1,2,5]thiadiazole **40** reduced with zinc dust, stirred at 60 ºC for 1 hour. Then, the reaction mixture was cooled to room temperature and 2,2'-thenil was added to the solution. After 1 hour, the solvent removed under reduced atmosphere and the residue was purified by column chromatography on silica gel (1:1 dichloromethane/hexane). In the ^{1}H-NMR spectrum, it was observed some characteristic peaks such as H-15 and H-13 resonate at 8.16 ppm and 7.27 ppm as singlet and H-36 resonates at 6.94 ppm as dd with *J*= 5.0, 3.7 Hz.

2.1.4 Synthesis of 5,7-Bis(4-hexylthiophen-2-yl)-2,3-di(thiophen-2-yl)thieno[3,4-*b*]pyrazine 48

Thienopyrazine, as acceptor, and 3-hexylthiophene, preferred as donor group to enhance the solubility of the monomer, were chosen to design a new donor-acceptor type monomer. Therefore, the donor monomer was synthesized in four main steps as shown in Scheme 16.
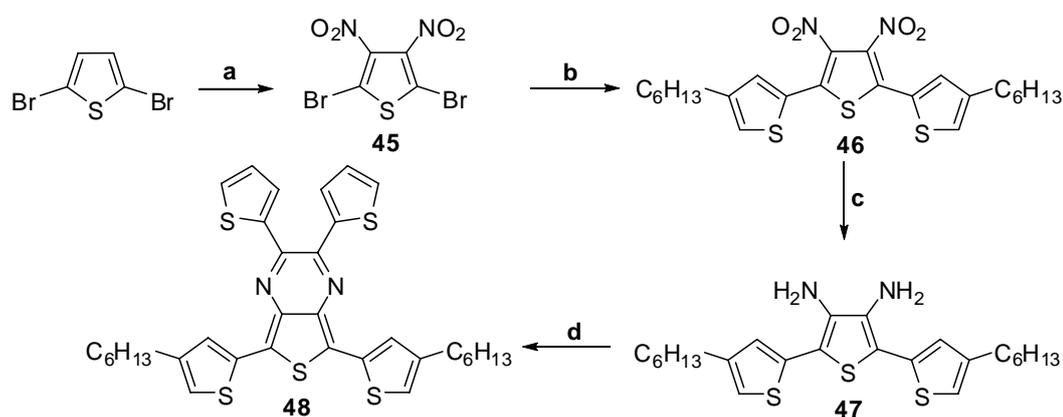
a) conc. and fuming H_2SO_4, conc. HNO_3, 3 h **b)** Pd(PPh$_3$)$_2$Cl$_2$, tributyl(4-hexyltiophen-2-yl)stannane, dry THF **c)** SnCl$_2$, EtOAC, 2 h **d)** EtOH, PTSA, 2,2'-thenil, 6 h

Scheme 16

55

According to a method [124] in the literature, 2,5-dibromo-3,4-dinitrothiophene **45** was obtained by nitration of 2,5-dibromothiophene. Nitration of 2,5-dibromo thiophene was performed by dropwise addition of nitric acid to the solution of 2,5-dibromothiophene and concentrated sulfuric acid, fuming sulfuric acid. During the addition, temperature was kept under 30ºC to prevent explosion. After addition was completed, the mixture was allowed to react for an additional 3 hours. The mixture was poured over ice and the solid residue was recovered by filtration. Recrystallization with methanol gave a light yellow solid. The structure elucidation was achived by ^{13}C-NMR in which it was observed that C-Br resonates at 112.4 ppm and C-NO$_2$ resonates at 139.6 ppm.   Melting point was determined as 136.2ºC (lit. 135.8-136.7 ºC).

5-5'-Bis(4-hexylthiophen-2-yl)-3,4-dinitrothiophene **46** was prepared by Stille coupling of tributyl(4-hexylthiophen-2-yl)stannane and 2,5-dibromo-3,4-dinitrothiophene **45** in the presence of a palladium catalyst. THF was used as solvent and the reaction was monitored by TLC. Overnight reflux was needed for the completion of the reaction. NMR spectroscopy was used for the product structure elucidation. ^{1}H-NMR showed that 3-hexylthiophene ring protons resonate at 7.26 ppm as doublet (*J*=1.3 Hz) and 7.07 ppm as broad singlet and -CH$_2$-protons (belongs to hexyl chain) resonate at 2.51 ppm as triplet.

Corresponding to a method [125], the reduction of **46** to **47** was performed in the presence of tinchloride as reducing agent and ethylacetate as solvent. The nitrogen atom is reduced from an oxidation state of +V to –III and the tin atom is oxidized from +II to +IV hence four equivalents of tin is needed per nitro group. The obtained product was filtrated over celite to remove inorganic compounds from the medium. The mixture was extracted with dichloromethane. The solvent was evaporated and the residue was purified by column chromatography. The final product was isolated as yellow oil. In the ^{1}H-NMR, the characteristic aromatic protons of 3-hexylthiophene ring resonated at 6.85 ppm and 6.77 ppm as singlet and –NH$_2$ protons resonated at 3.25 ppm as broad singlet.
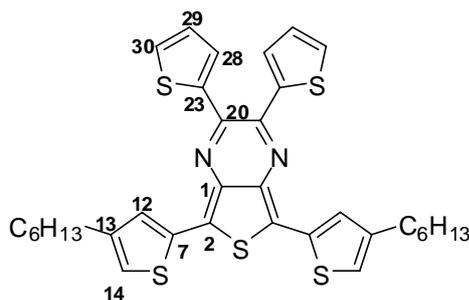
Figure 20 The backbone numbering for 5,7-bis(4-hexylthiophen-2-yl)-2,3-di(thiophen-2-yl)thieno[3,4-*b*]pyrazine **48.**

The condensation reaction between **47** and 2,2'-thenil afforded 5,7-bis(4-hexylthiophen-2-yl)-2,3-di(thiophen-2-yl)thieno[3,4-*b*]pyrazine **48** in EtOH. The reaction was stirred 6 hours at room temperature. PTSA was added catalytic amount into the mixture to complete the reaction. At the end of the reaction, the color changes to dark green. The solvent was evaporated and column chromatography (1:2 Chloroform/Hexane) was used for purification. The product elucidation executed by NMR spectroscopy. Some characteristic signals were observed as doublet and broad singlet at 7.36 ppm and 6.85 ppm for 3-hexylthiophene ring protons and as doublet with *J*=4.5, 3.5 Hz for thiophene ring proton (H-29).

2.1.5 Synthesis of Selenadiazole Derivatives

2.1.5.1 4,6-Bis(4-hexylthiophen-2-yl)-4,6-dihydrothieno[3,4-*c*][1,2,5] selenadiazole 49

Scheme 18

57
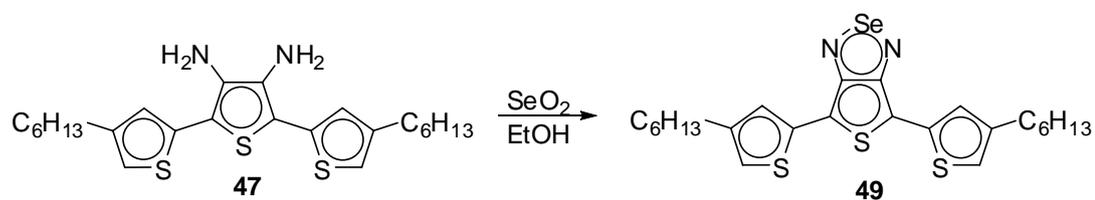
In preparation of 4,6-bis(4-hexylthiophen-2-yl)-4,6-dihydrothieno[3,4-*c*][1,2,5] selenadiazole **49**, a modified method [126] was applied (Scheme 18). Treatment of **47** with SeO$_2$ was successful in giving desired product. Ethanol was used as solvent and no heat was applied during the reaction to prevent the polymerization of product. After the addition of SeO$_2$, the color changed to green immediately. The obtained product was filtered over AlO$_2$ eluting with hexane. The identification was accomplished by NMR spectroscopy. In contrast with diamino compound **47**, 3-hexylthiophene ring protons of the product **48** resonated at 7.34 ppm and 6.82 ppm as doublet (*J*=0.8 Hz) in ^{1}H-NMR spectrum.

2.1.5.2 Synthesis of 4,7-Bis(4-hexylthiophen-2-yl)benzo[*c*][1,2,5]selenadiazole 53

As shown in Scheme 19 the target monomer was synthesized starting from 2,1,3-benzothiadiazole. The bromination of benzothiadizole was mentioned in 2.1.3.
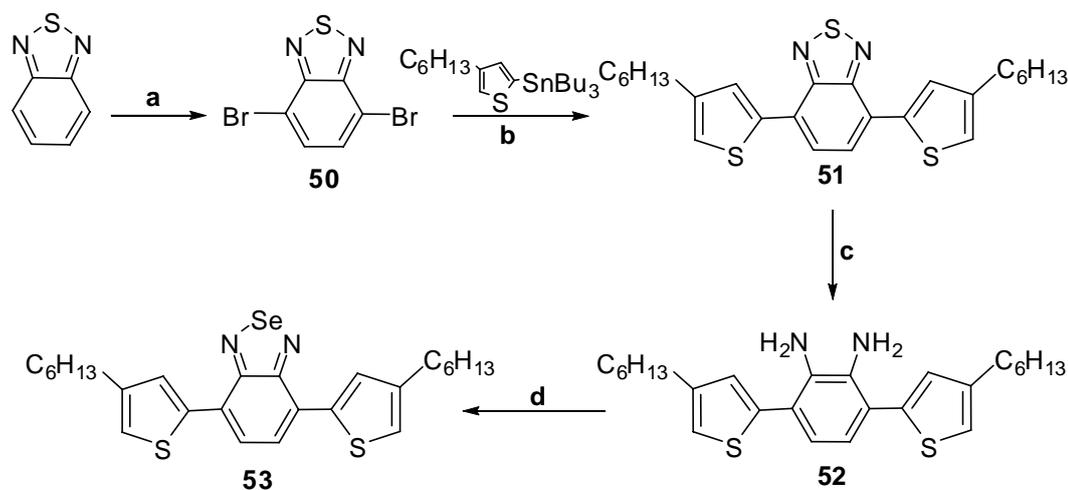
a) HBr, Br$_2$, reflux, 6 h **b)** Pd(PPh$_3$)$_2$Cl$_2$, dry THF, reflux **c)** Zn, acetic acid, 60°C, 1 h
d) SeO$_2$, EtOH, rt, 1h

Scheme 19

The Stille coupling reaction between 4,7-dibromo-5,6-dinitrobenzo[*c*][1,2,5] thiadiazole **50** and tributyl(4-hexylthiophen-2-yl)stannane resulted in 4,7-bis(4-hexylthiophen-2-yl)benzo[*c*][1,2,5]thiadiazole **51**. The obtained product, orange

solid, was reduced with Zn/acetic acid system. It was reacted with SeO_2 without further purification to obtain 4,7-bis(4-hexylthiophen-2-yl)benzo[c][1,2,5] selenadiazole **53**. After purification of the product by column chromatography on silica, the product **53** was isolated as red solid (84 % yield). NMR spectroscopy was used for structure elucidation. In ^{1}H-NMR spectrum, it was observed that benzene ring protons resonate at 7.66 ppm as singlet due to the symmetry and thiophene ring protons resonate as doublet *(J=1.1 Hz)* at 6.96 ppm and at 7.80 ppm, respectively. In ^{13}C-NMR spectrum, hexyl carbons resonate in the range of 13.0 and 30.7 ppm.

2.2. Characterization of Conducting Polymers

2.2.1. Dibenzo[*a,c*]phenazine Derivatives

2.2.1.1 Cyclic Voltammograms

Electroactivities of monomers were investigated using cyclic voltammetry. Analysis of **31** showed poor film-forming ability in dichloromethane (DCM), acetonitrile (ACN), benzonitrile and tetrahydrofurane (THF). Hence, this polymer was not good enough to produce films with a sufficient quality for electrochromic studies. The cyclic voltammograms corresponding to the potentiodynamic polymerization of **29** and **30** by application of potential scans are shown in Figure 21. In each case, the first cycle shows an irreversible anodic wave corresponding to the oxidation of the monomer forming a radical cation. Subsequent cycling leads to a new redox couple associated with the oxidation and reduction of the polymer growth onto the electrode surface.

Table 2 Experimental conditions and results of the electrochemical studies of dibenzophenazine derivatives.

Monomer	Supporting electrolyte	Solvent	Monomer $E_{p,a}$ (V)	Polymer $E_{p,a}$(V)	$E_{p,c}$(V)
29	TBAPF$_6$	DCM	1.27	1.17	0.93
30	TBAPF$_6$	DCM	1.12	1.0	0.77
31	TBAPF$_6$	THF	1.38	1.30	1.23
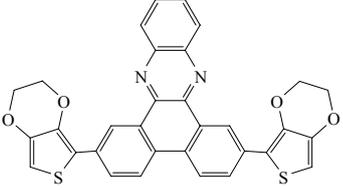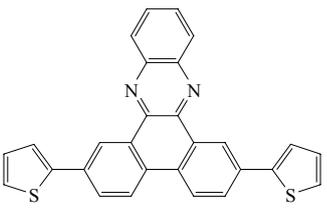
Cyclic voltammograms of **29** and **30** were obtained in dichloromethane (DCM) 0.1M tetrabutylammonium hexafluorophosphate (TBAPF$_6$) at a scan rate of 100 mV/s. Electropolymerization of **30** was performed using multiple scan voltammetry between +0.4 V and +1.3 V on an ITO electrode. The monomer **30** started to get oxidized at +1.1 V vs the Ag wire pseudo-reference electrode during the first anodic sweep. The redox behavior of **29** was studied by scanning potential between +0.3 V and +1.4 V. For monomer **29**, the onset of oxidation started at a slightly higher potential (+1.2 V vs the Ag wire pseudo-reference electrode). As expected, the oxidation of **29** was observed at higher potential than that of **30** due to the difference in electronic nature of the external moities (3-hexyl thiophene and EDOT).
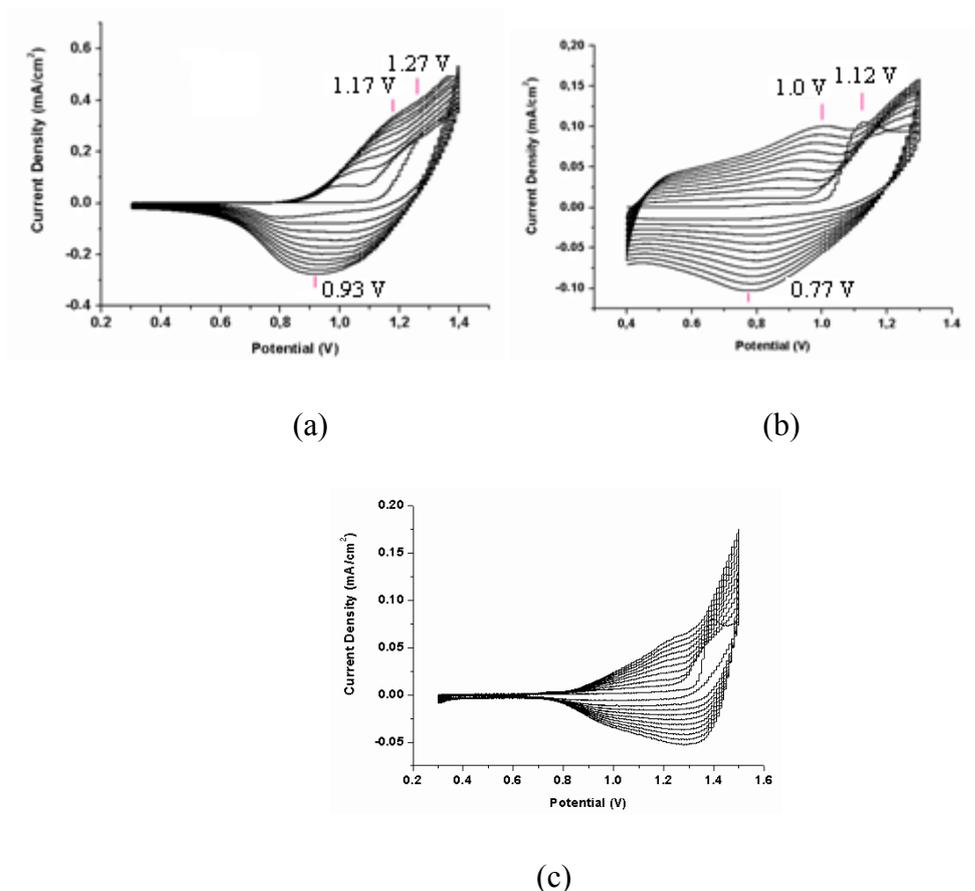
Figure 21 Cyclic voltammograms of a) **29** b) **30** c) **31.**

Upon repeated scanning the increased current response of the polymer redox process illustrates that electrochemical polymerization is proceeding at the electrode surface to form an electroactive polymer film. On the anodic scans, polymer oxidation potentials were evolved at about + 1.0 V for **P30** and + 1.17 V for **P29**. Reduction of the polymers evolved at + 0.77 V for **P30** and + 0.93 V for **P29** vs the same reference electrode.

Cyclic voltammograms were obtained at different scan rates in order to test adherence of the polymers to the electrode surface (Figure 22). Anodic and cathodic peak currents reveal a linear relationship as a function of scan rate for both polymers, which proves that the films were well-adhered and electroactive. The linear increase

of the current upon incrementing the scan also indicates that the electrochemical processes are not diffusion limited and are quasi-reversible even at high scan rates.
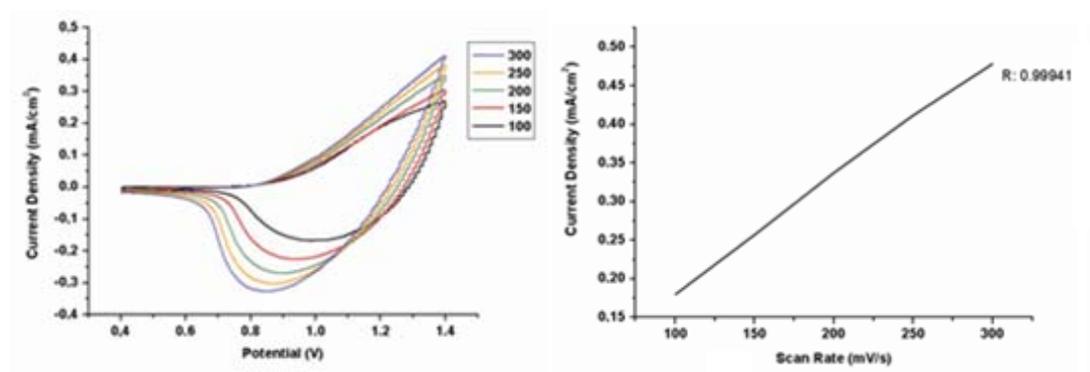
(a)
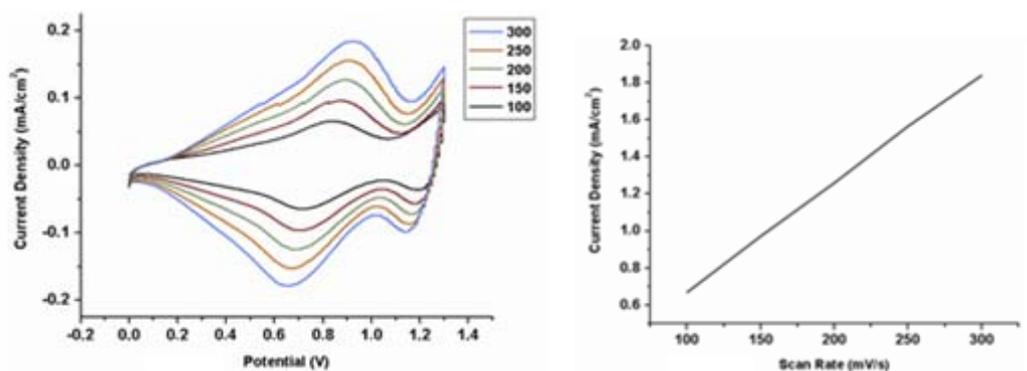
(b)

Figure 22 Scan rate dependence and relation between current density and scan rate of a) **P29** b) **P30.**

2.2.1.2 Spectroelectrochemistry

In order to probe the electronic structure of the polymers and examine the optical changes upon doping, spectroelectrochemical analyses were performed. For these measurements, polymer films were deposited on ITO-coated glass slides from 10^{-2} M monomer solutions in 0.1 M TBAPF$_6$/DCM. The optical changes were investigated

by UV–Vis-NIR spectroscopy in a monomer free TBAPF$_6$/DCM solution by applying different voltages (Figure 23).
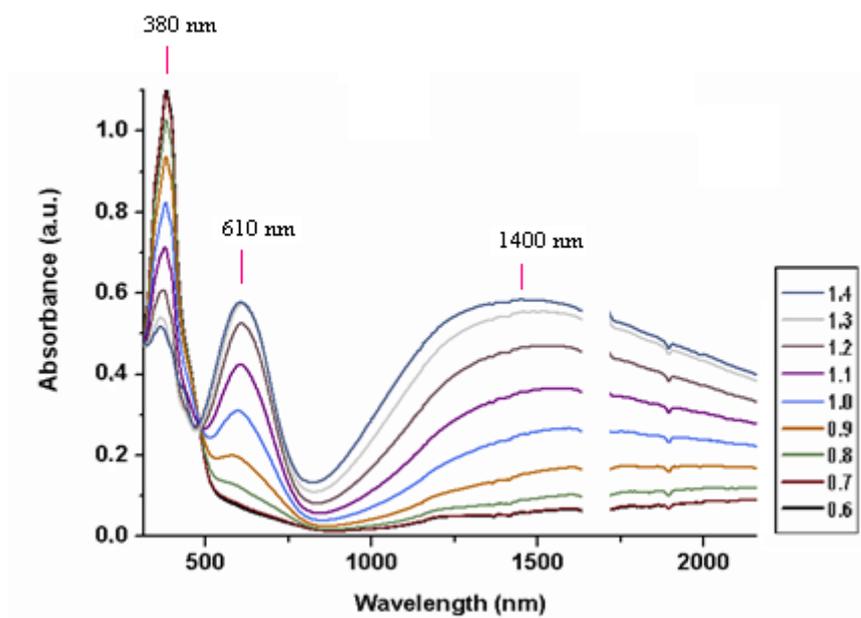
(a)
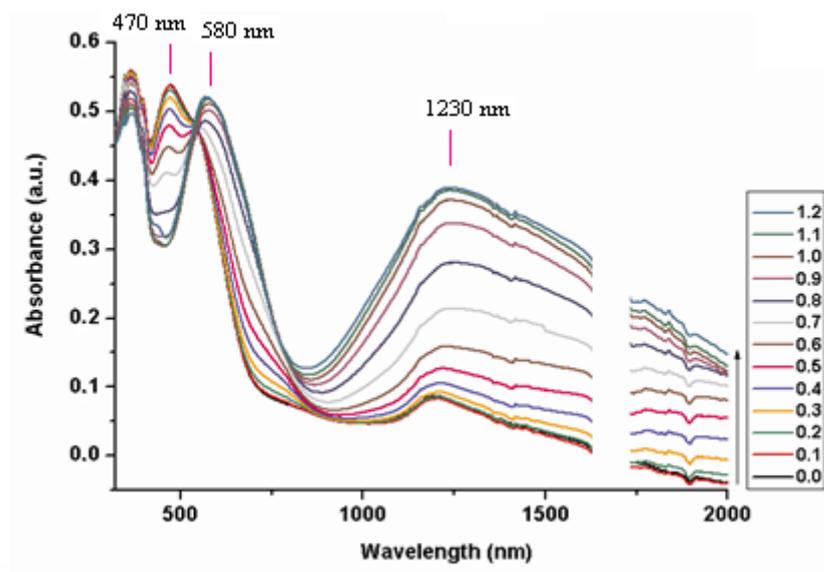
(b)

Figure 23 Spectroelectrochemical spectra of **a) P29** with applied potential between 0.6 V and +1.4 V in DCM/TBAPF$_6$ **b) P30** with applied potential between 0.0 V and +1.2 V in DCM/TBAPF$_6$.

Oxidation of an electrochromic material produces radical cations (polarons) and further oxidation produces dications (bipolarons), allowing new electronic transition thereby changing absorption spectra. As seen from the spectroelectrochemical series, upon stepwise oxidation of all the polymers, the absorbance of π-π* transition decreased while those of the polaron and bipolaron peaks increased. The absorbance assigned to π-π* transition for **P30** is at 470 nm. The band gap of the polymer was calculated as 1.7 eV according to the onset of the π-π* transition. As the potential applied increases, the broad absorption peaks at about 580 and 1230 nm, corresponding to polaron and bipolaron species, respectively, also increase. Presence of alkyl chains at the β-position of thiophene ring has influence on the electronic structure of the π-conjugated system in which the onset of the π-π* transition shifts shorter wavelength. **P29** exhibits larger Eg value; 2.4 eV than **P30** (Table 3).

Table 3 Spectroelectrochemical properties of **P29** and **P30.**

Polymer	E_g	λ_{max}
P29	2.4 eV	380 nm
P30	1.7 eV	470 nm

The different structures of the polymers due to the differences in donor moiety affect not only the monomer oxidation and the polymer redox couple potential but also the maximum absorption wavelengths of the corresponding transition. The introduction of alkyl substituent on polymer causes steric hindrance, resulting in less order and less conjugation by the red shift in absorption spectra and the increase in polymer's band gap.

2.2.1.3 Electrochromic Switching

For the double potential step experiment for **P29**, the potential was set at an initial value (+0.6 V) for a set period of time (5s) and was stepped to a second potential (+1.4 V) for the same period of time, before being switched back to the initial potential again (Figure 24). Electrochromic contrast was reported as a percent transmittance change (T %) at λ_{max}. The optical contrasts for **P29** were calculated as 17 % at 380 nm, 38 % at 610 nm and 54 % at 1400 nm. **P30** achieves 22 % at 470 nm, 8 % at 580 nm and 50 % at 1230 nm of its total optical change.

(a)   (b)
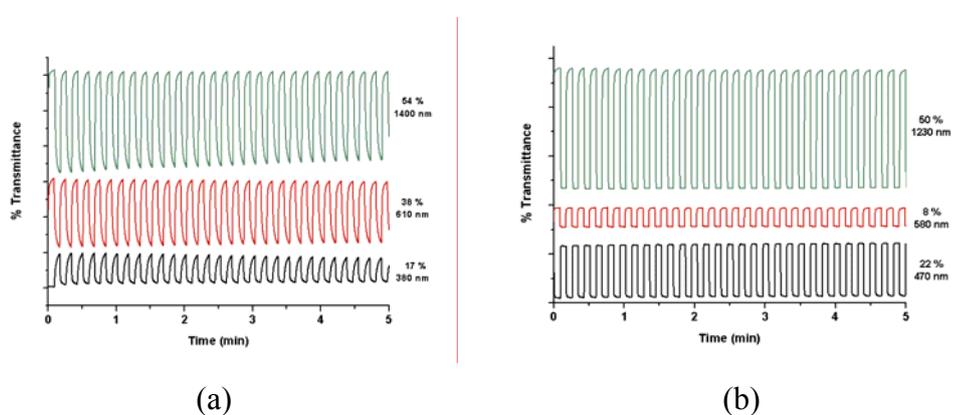
Figure 24 Electrochromic switching, optical absorbance change monitored **a)** at 380 nm, 610 nm and 1400 nm for **P29** between 0.6 V and +1.4 V **b)** at 470 nm, 580 nm and 1230 nm for **P30** between 0.0 V and +1.2 V.

Table 4 shows optical contrast ratio and switching times at all of the λ_{max} for **P29** and P30 where the latter has faster switching times than **P29**.

Table 4 Optical contrast and switching times for **P29** and **P30**

λ_{max} **P29**	380 nm	610 nm	1400 nm
Optical Contrast P29	17 %	38 %	54 %
Switching Time P29	2.8 s	1.8 s	1.2 s

Table 4 continue

λ_{max} **P30**	**470 nm**	**580 nm**	**1230 nm**
Optical Contrast P30	22 %	8 %	50 %
Switching Time P30	0.4 s	0.6 s	1.0 s

2.2.1.4 Colorimetry

Colorimetry was used to make the measurement of the color in an objective and quantitative practice, which determines the colors in electrochromic devices. The Commission Internationale de l'Eclairage (CIE) system was employed as the quantitative scale to define and compare colors. The color coordinates, Y, x, y values, were measured for polymer films and summarized in Table 5.

P30 becomes red (Y: 176; x: 0.395; y: 0.337) in the neutral state, while the oxidized state is blue (Y: 204; x: 0.251; y: 0.273). **P29** film changed from a yellow neutral state (Y: 821; x: 0.352; y: 0.386) to a blue oxidized state (Y: 538; x: 0.263; y: 0.30).

Table 5 Electrochromic properties of (a) **P29** and (b) **P30.**

+ 0.4 V	+ 1.4 V
Y: 821 x: 0.352 y: 0.386	Y: 533 x: 0.263 y: 0.309

(a)

+ 0.0 V	+ 1.4 V
Y: 176 x: 0.395 y: 0.337	Y: 204 x: 0.251 y: 0.273

(b)

2.2.2 Dibenzo[*f,h*]pyrido[3,4-*b*]quinoxaline Derivatives

2.2.2.1 Cyclic Voltammograms

Electrochemical behavior of **32**, **33** and **34** were examined in appropriate solvent/supporting electrolytes system using cyclic voltammetry. Working conditions and data evaluated from CV are given for each monomer in Table 6.

Table 6 Experimental conditions and results of the electrochemical studies of dibenzopyridoquinoxaline derivatives.
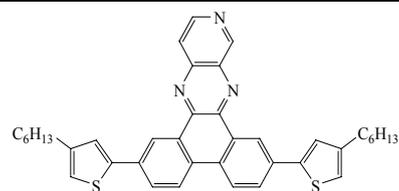
Monomer	Supporting electrolyte	Solvent	Monomer $E_{p,a}$(V)	Polymer	
				$E_{p,a}$(V)	$E_{p,c}$ (V)
32	LiClO$_4$	DCM:ACN 5:95	0.98V	0.85V	0.45V
33	TBAPF$_6$	DCM:ACN 5:95	>1.2V	0.91V	0.71V
34	LiClO$_4$	DCM:ACN 5:95	1.11V	0.87V	0.75V
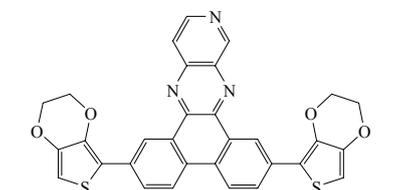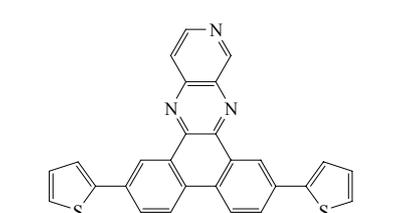
According to these data (Figure 25) the lowest oxidation and reduction potentials were observed for monomer **32** and its polymer, which may be due to better HOMO-LUMO match between donor and acceptor units.

Monomer **34** was slightly soluble in common solvents such as DCM, ACN, benzonitrile. The film formation on ITO was poor so further characterization could not be achieved.

(a)   (b)

(c)
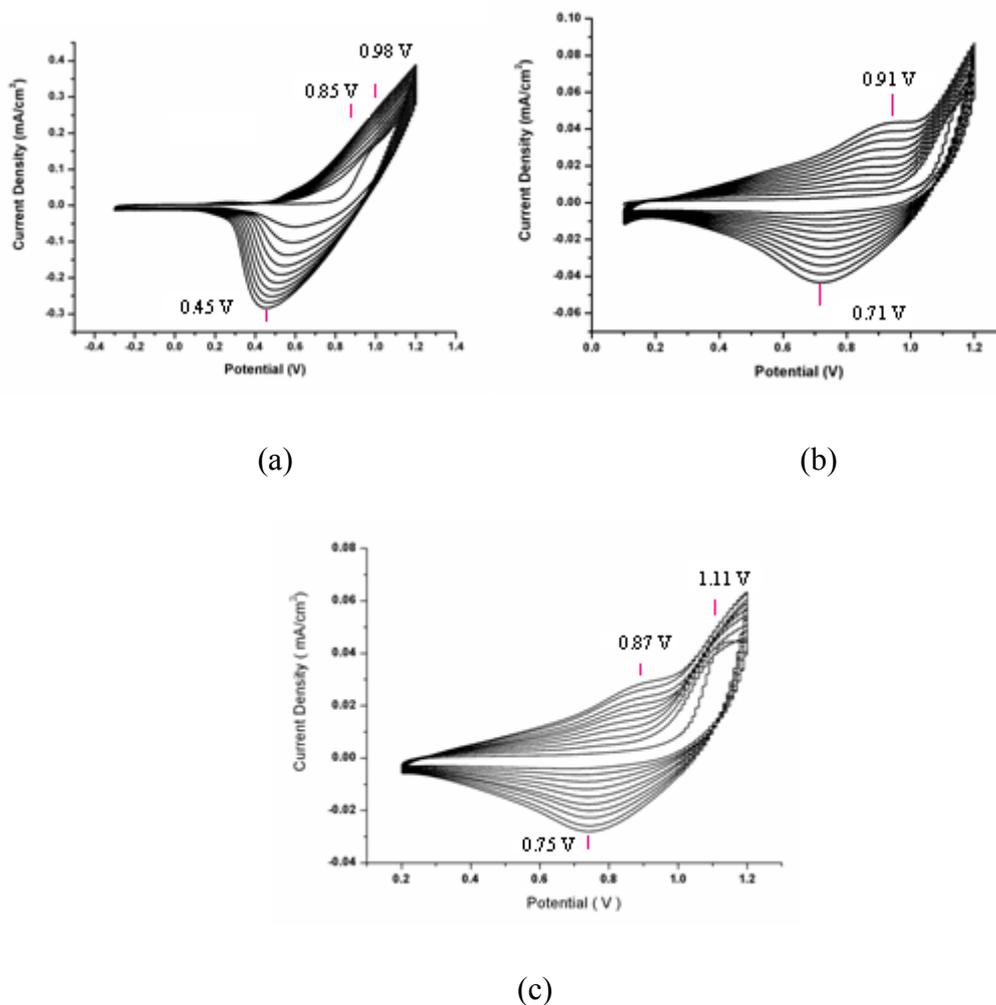
Figure 25 Cyclic voltammograms of a) **32**, b) **33** and c) **34.**

2.2.2.2 Spectroelectrochemistry

Polymer films were potentiodynamically synthesized on an ITO electrode in the presence of 0.01 M monomer, while the potential was swept between the appropriate potential intervals in LiClO$_4$/DCM/ACN for **32** and TBAPF$_6$/DCM/ACN for **33**. The electrochemical and electrochromic properties of the polymer film were studied with a monomer-free medium. A π-π* transition was revealed at 372 nm and the band gap

(Eg) was calculated as 2.43 eV for **P32** (Figure 26 a). The polaron and bipolaron band were observed at 560 nm and 1200 nm, respectively.

Table 7 Spectroelectrochemical properties of **P32** and **P33.**

Polymer	E_g	λ_{max}
P32	2.43 eV	372nm
P33	1.8 eV	474 nm

When EDOT was used as the donor moiety instead of 3-hexylthiophene not only band gap but also the colors of the **P33** film change. The peak at 474 nm corresponds to the π-π* transition of the neutral polymer. Hence, the polymer is pink in the neutral state. The band gap of the polymer is 1.8 eV, which was calculated from the onset of the π-π* transition (Figure 26 b).
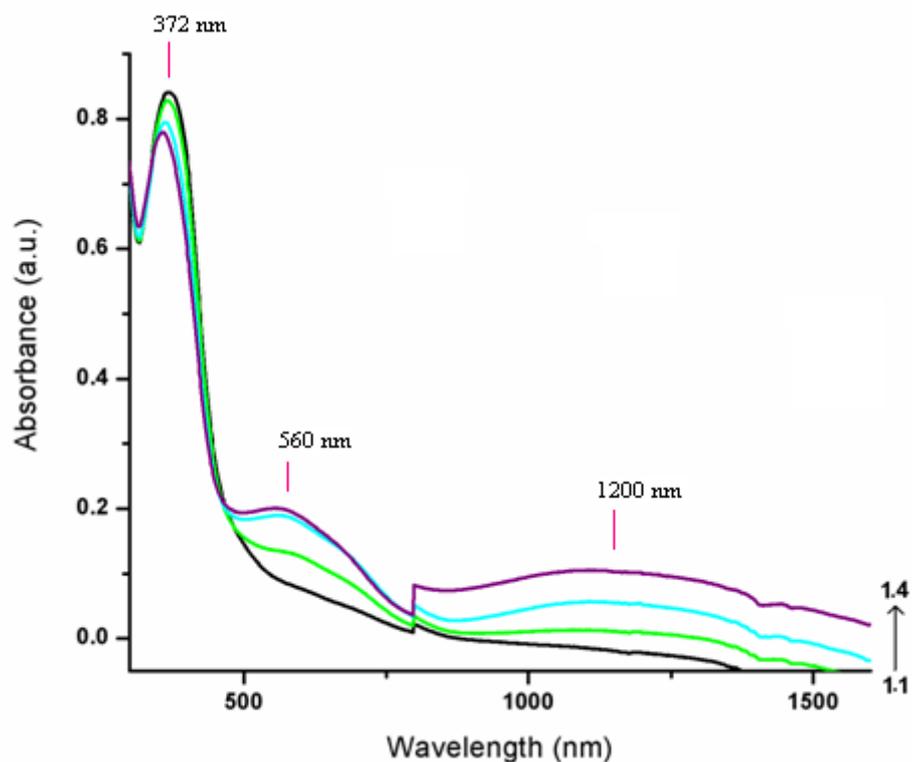
(a)
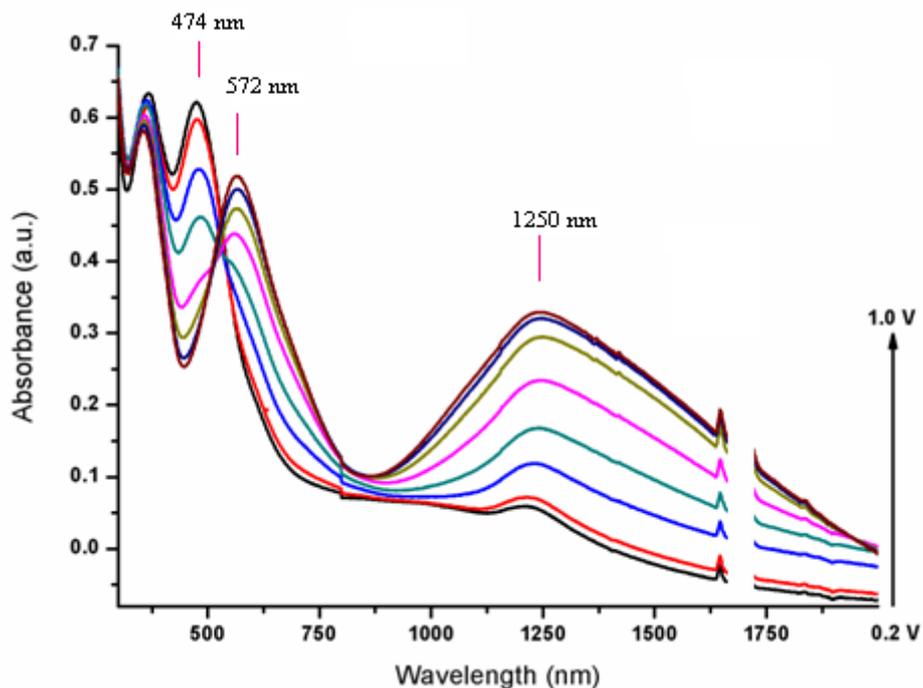
(b)

Figure 26 Spectroelectrochemical spectra of **a) P32** with applied potential between +1.1 V and +1.4 V in ACN/DCM/LiClO$_4$ **b**) **P33** with applied potential between +0.2 V and +1.0 V in ACN/DCM/TBAPF$_6$.

As a result of the charge carrier formation upon oxidation, new absorption bands evolve at 572 nm and 1250 nm representing the formation of polaronic and bipolaronic bands. Since the polaron formation is at visible region, the color of the **P33** film reveals two different colors.

2.2.2.3 Electrochromic Switching

To monitor the percent transmittance as a function of time and to determine the switching time of the polymers at a given λ_{max}, electrochromic switching studies were performed by stepping potential repeatedly between the neutral and oxidized states.

P32 revealed optical contrast of 5 % at 560 nm and 6 % at 1200 nm. **P33** has better optical contrast and switching times than **P32**.

Table 8 Optical contrast and switching times for **P32** and **P33**

λ_{max} P32	560 nm	1200 nm	
Optical Contrast P32	5 %	6 %	
Switching Time P32	2.3 s	1.5 s	

λ_{max} P33	474 nm	572 nm	1250 nm
Optical Contrast P33	17 %	10 %	13 %
Switching Time P33	1.2 s	1.3 s	1 s

2.2.2.4 Colorimetry

P32 displays yellow color (Y: 84.7, x: 0.37, y: 0.24) in the neutral form and blue color (Y: 39.16, x: 0.24, y: 0.21) in the oxidized state. **P32** has pink color in the neutral state (Y: 35.04, x: 0.36, y: 0.32) and violet color (Y: 39.83, x: 0.32, y: 0.27) in the oxidized state.

Table 9 Electrochromic properties of (a) **P32** and (b) **P33.**

- 0.1 V	+ 1.4 V		+ 0.2 V	+ 1.0 V
Y: 84.7 x: 0.37 y: 0.43	Y: 39.16 x: 0.24 y: 0.21		Y: 35.04 x: 0.36 y: 0.32	Y: 39.83 x: 0.32 y: 0.27
(a)			(b)	

2.2.3 Tetrahydrodibenzo[*a,c*]phenazine Derivatives

2.2.3.1 Cyclic Voltammograms

Multiple scan voltammetry on ITO was performed in a solution containing 0.1 M TBAPF$_6$ and 10^{-2} M monomer solutions. Applied potentials were changed between +0.5V and +1.4V for **35**, between +0.1V and +1.1V for **36** and from +0.2V to +1.3V for **37** at a scan rate of 100 mV/s (Figure 27). The solvent was chosen as a mixture ACN and DCM (95:5) for **36** due to the poor solubility of the monomer in ACN. On the other hand, the electrochemical behaviors of **35** and **37** were examined in DCM. While the monomer oxidation potential of **35** was observed at 1.28 V, they were at 0.97 V for **36** and >1.3 V for **37.** After the first cycle, an oxidation peak at 1.16 V and its reverse cathodic peak at 1.00 V appeared in CV of **35**. Upon repeated scanning, a reversible redox couple developed at 0.84 V and 0.77 V for **36** and at 1.11 V and 0.70 V for **37** (Table 10).

Table 10 Experimental conditions and results of the electrochemical studies of tetrahydrodibenzophenazine derivatives.
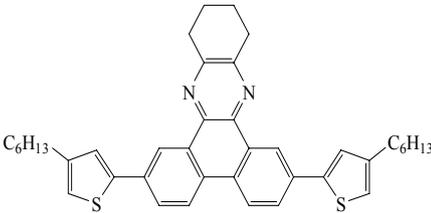
Monomer	Supporting electrolyte	Solvent	Monomer $E_{p,a}$(V)	Polymer	
				$E_{p,a}$(V)	$E_{p,c}$(V)
35	TBAPF$_6$	DCM	1.27	1.16	1.0
36	TBAPF$_6$	DCM:ACN (5:95)	0.97	0.83	0.77
37	TBAPF$_6$	DCM	>1.3	1.11	0.70
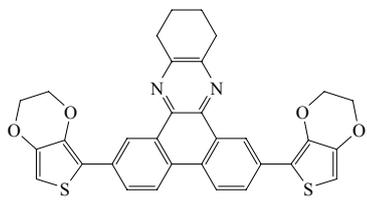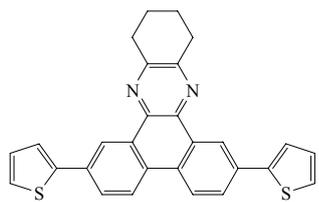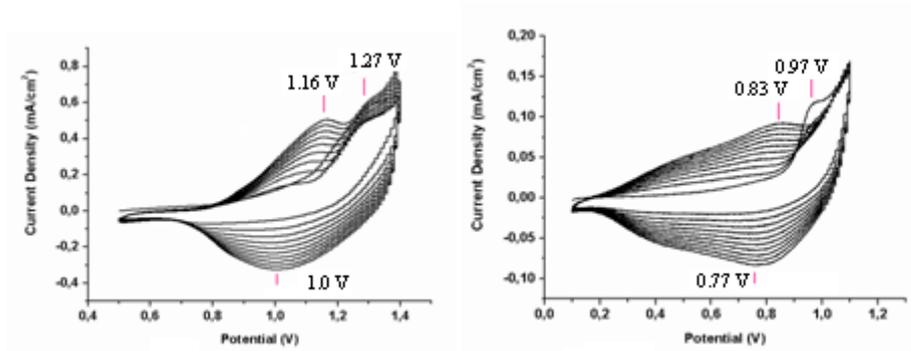
(a)   (b)
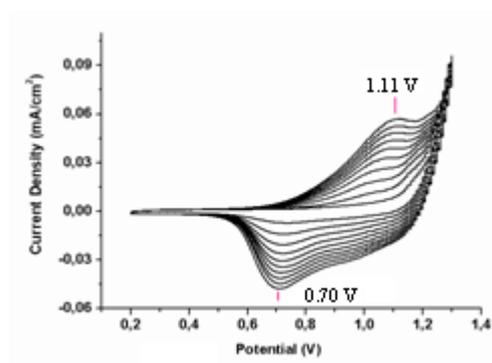
(c)

Figure 27 Cyclic voltammograms of a) **35** b) **36** and c) **37.**

The scan rate dependence of the polymer films were investigated by CV and true linear relations were observed between the peak current and the scan rate, which indicates the presence of a well adhered electroactive film with a non-diffusion limited redox process (Figure 28).
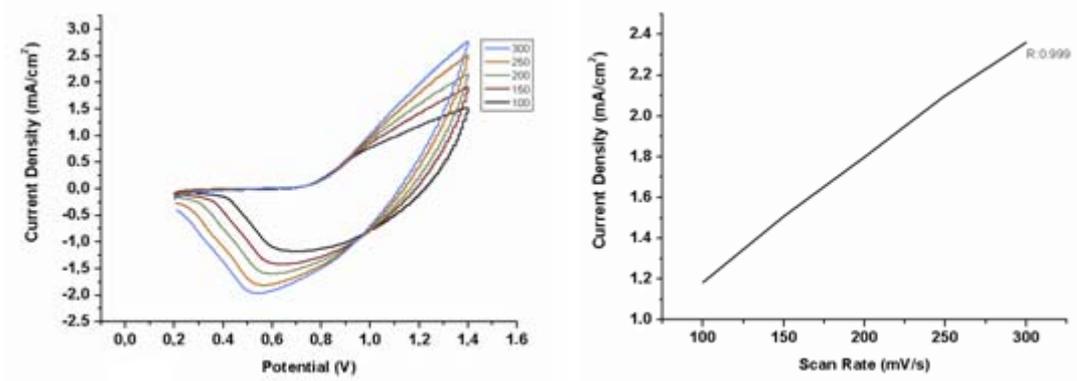
(a)
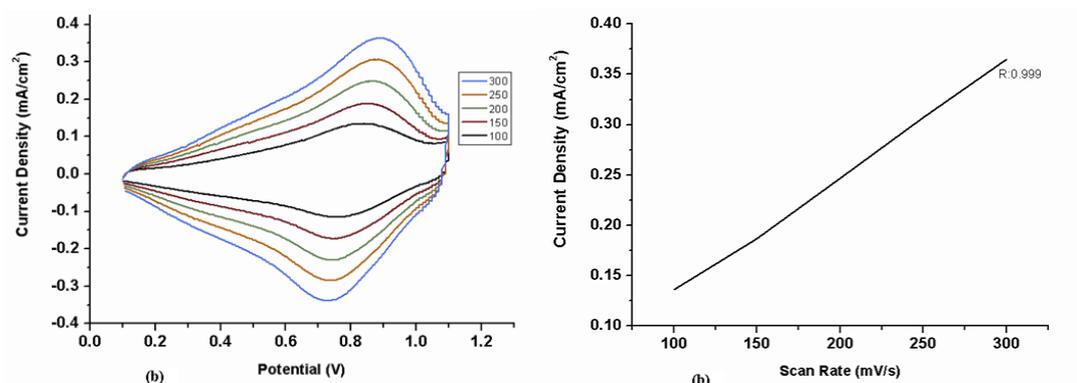
(b)

Figure 28 Scan rate dependence and relation between current density and scan rate of a) **P35** b) **P36.**

2.2.3.2 Spectroelectrochemistry

To investigate optoelectrochemical property, polymer films of **P35** and **P37** were electrochemically deposited on ITO coated glass in DCM with $TBAPF_6$. ACN/DCM (95:5) mixture was used as the solvent for **P36**. UV-Vis spectra were taken in a monomer free solution at various potentials to monitor the changes in absorbance as the polymer film is oxidized (Figure 29).
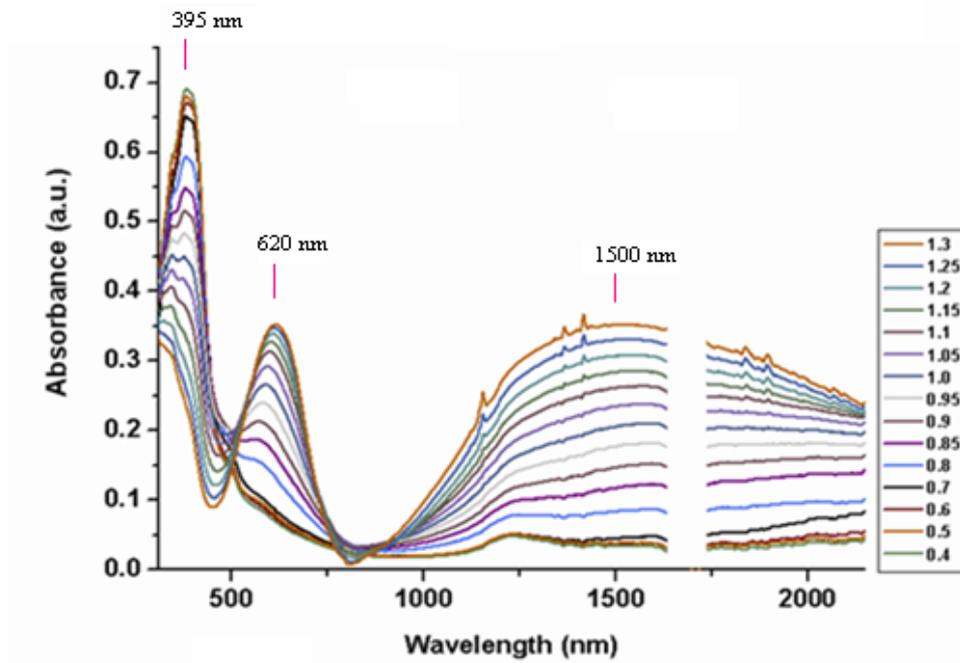
(a)
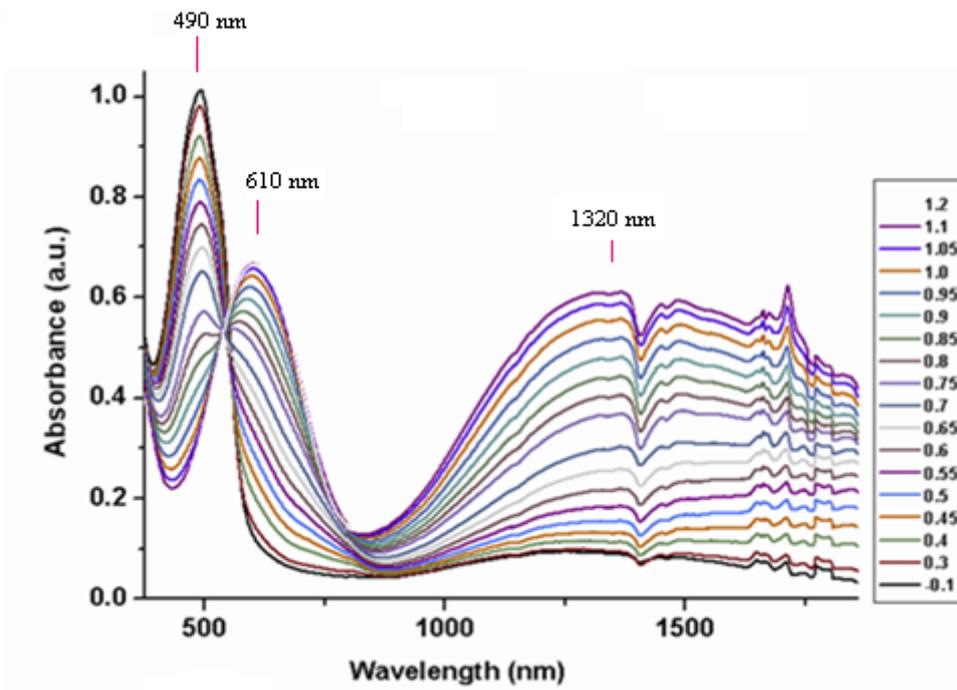
(b)
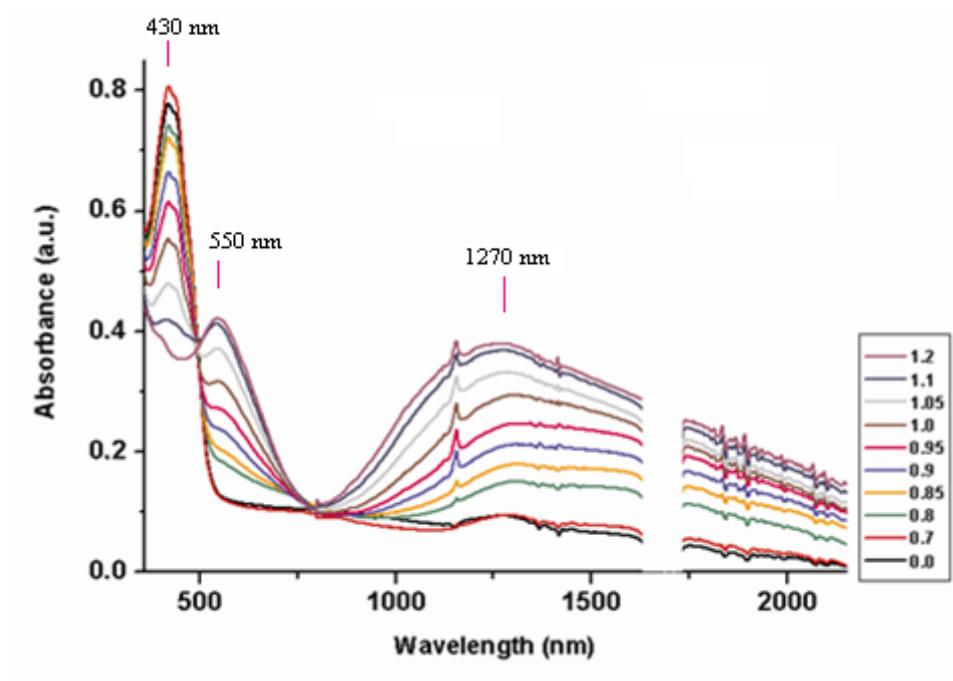
(c)

Figure 29 Spectroelectrochemical spectra of **a) P35** with applied potential between +0.4 V and +1.3 V in DCM/TBAPF$_6$ **b) P36** with applied potential between -0.1 V and +1.2 V in ACN/DCM/TBAPF$_6$ **c) P37** with applied potential between 0.6 V and +1.2 V in DCM/TBAPF$_6$.

Stepwise oxidation of the **P35** shows the fading of absorbance at 395 nm and typical evolution of peaks at 620 nm and 1500 nm corresponding to polaronic and bipolaronic bands, respectively. The band gap of **P35**, onset of the π-π^* transition for the neutral polymer is calculated as 2.5 eV using the absorption band centered at 395 nm. The absorbance assigned to π-π^* transition for **P36** is at 490 nm and this transition is observed at 430 for **P37**. The band gap of **P36** was calculated as 2.0 eV and that of **P37** was calculated as 2.2 eV according to the onset of the π-π^* transition.

Table 11 Spectroelectrochemical properties of **P35**, **P36** and **P37.**

Polymer	E_g	λ_{max}
P35	2.5 eV	395 nm
P36	2.0 eV	490 nm
P37	2.2 eV	430 nm

The polymers of **P36** and **P37** reveal several distinct colors since the polaron bands of the polymers are still in the visible region during the depletion of π-π^* absorption. The polymers of **P36** and **P37** have the ability to achieve multi-colors with small structural modifications. Multicolored electrochromism observed in a polymer is a promising property since these types of materials can be utilized as active layers in many device applications especially in the information technologies. On the other hand, **P35** film changes from a yellow neutral state to a blue oxidized state.

P36 is orange in its neutral state. Upon oxidation, the orange color of the polymer turns into brown. Further oxidation results in purple, A gray color was observed when 0.7 V potential was applied. When the potential is further increased the polymer turns into a blue color**.**

The color of the **P37** film is yellow in its neutral state. Its color switches from yellow to greenish brown due to further oxidation. When 0.9 V potential is applied, the polymer turns into gray. Further oxidation causes blue color.

2.2.3.3 Electrochromic Switching

Switching time is an important parameter for a polymer since it indicates the speed of ions move into the polymer chains during doping process. The switching times of **P35**, **P36** and **P37** were determined by kinetic studies via measuring the transmittance (%T) at a maximum contrast and were presented in Table 12. The

optical contrast was measured as the difference in percent transmittance between neutral and oxidized forms and noted as ΔT% (Figure 30).

(a)

(b)

(c)
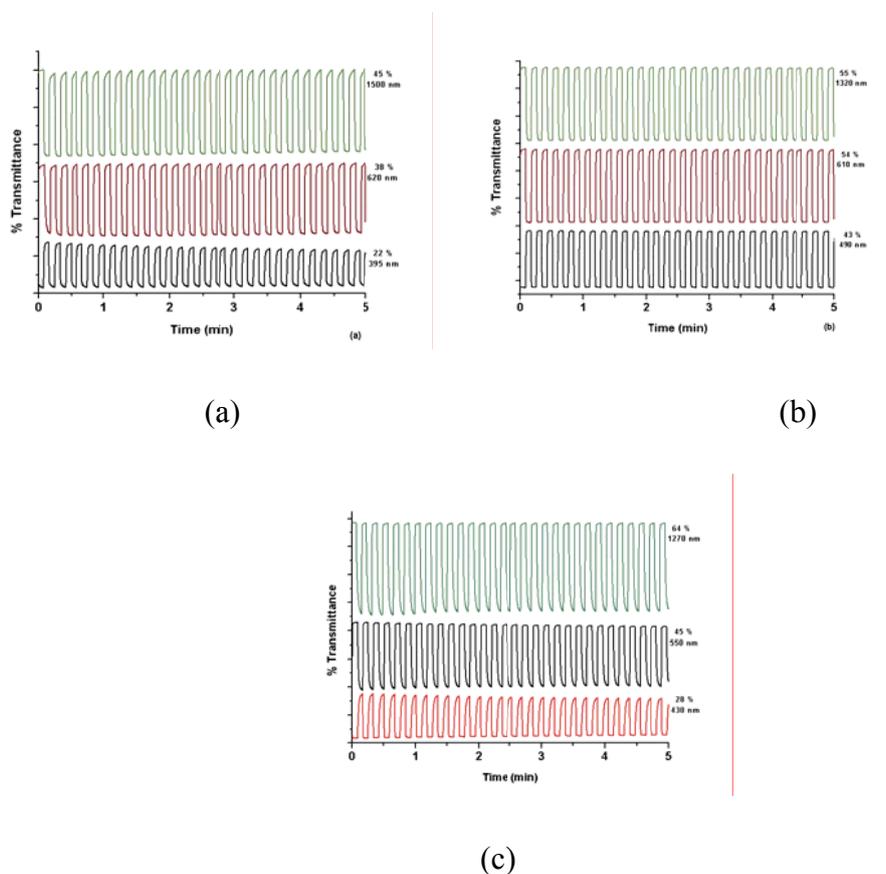
Figure 30 Electrochromic switching, optical absorbance change monitored **a)** at 395 nm, 620 nm and 1500 nm for **P35** between +0.4 V and +1.3 V **b)** at 490 nm, 610 nm and 1320 nm for **P36** between -0.1 V and +1.2 V **c)** at 430 nm, 550 nm and 1270 nm for **P37** between 0.0 V and +1.2 V.

Table 12 Optical contrast and switching times for **P35, P36** and **P37.**

λ_{max} **P35**	**395 nm**	**620 nm**	**1500 nm**
Optical Contrast P35	22 %	38 %	45 %
Switching Time P35	1.7 s	1.5 s	1.8 s

Table 12 continue

λ$_{max}$ P36	490 nm	610 nm	1320 nm
Optical Contrast P36	43 %	54 %	55 %
Switching Time P36	0.8 s	0.7 s	0.6 s

λ$_{max}$ P37	430 nm	550 nm	1270 nm
Optical Contrast P37	28 %	45 %	64 %
Switching Time P37	2.3 s	0.5 s	0.5 s

2.2.3.4 Colorimetry

The color changes were further investigated by colorimetry using the CIE 1931 Yxy color space to define color precisely. Polymer films show different colors in the neutral and fully oxidized states. The color of the polymer film **P35** switches between yellow reduced state and blue oxidized state. On the other hand, **P36** and **P37** show multichromic properties.

Table 13 Electrochromic properties of (a) **P35**, (b) **P36** and **(c) P37.**

+0.4 V	+1.3 V
Y: 99.9 x: 0.320 y: 0.366	Y: 48.7 x: 0.258 y: 0.297

(a)

0.0 V	+0.7 V	+0.9 V	+1.2 V
Y: 798 x: 0.348 y: 0.397	Y: 625 x: 0.353 y: 0.399	Y: 499 x: 0.321 y: 0.363	Y: 446 x: 0.280 y: 0.312

(c)

-0.1 V	+0.3 V	+0.4 V	+0.7 V	+1.0 V
Y: 389 x: 0.489 y: 0.398	Y: 329 x: 0.437 y: 0.398	Y: 327 x: 0.376 y: 0.385	Y: 348 x: 0.316 y: 0.329	Y: 348 x: 0.209 y: 0.219

(b)

2.2.4. Selenadiazole Derivatives

2.2.4.1 Cyclic Voltammograms

The polymer of **53** was synthesized on ITO coated glass slides by oxidative electropolymerization in DCM/ACN (5:95) mixture containing 10^{-2} M NaClO$_4$. However polymerization of **49** was performed in the presence of NaClO$_4$/LiClO$_4$

81

mixture as the supporting electrolyte and DCM/ACN (1:1) as the solvent. The monomer oxidation of **53** occurs at 0.94 V vs, Ag wire pseudo reference electrode. The monomer **49** revealed an irreversible oxidation peak at + 0.71 V whose intensity decreases upon consecutive cycles along with the leakage of the oligomers (Figure 31).

Table 14 Experimental conditions and results of the electrochemical studies of selenadiazole derivatives.
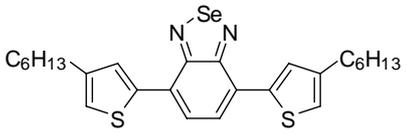
Monomer	Supporting electrolyte	Solvent	Monomer $E_{p,a}$ (V)	Polymer $E_{p,a}$(V)	$E_{p,c}$(V)
53	NaClO$_4$	DCM:ACN (5:95)	+0.94	+0.80	+0.73
49	NaClO$_4$/ LiClO$_4$	DCM:ACN (1:1)	+0.71	+0.53	+0.35
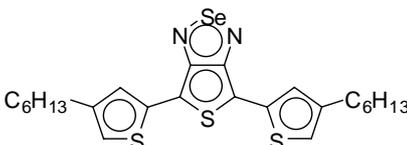
The resultant polymers **53** and **49** revealed p doping properties. The p-doping, for conjugated polymer **53**, was clearly observed by CV studies for **P53** with a definite reversible redox couple with an $E_{p,a}$ of +0.80 V and $E_{p,c}$ of +0.73 V vs. the same reference electrode.
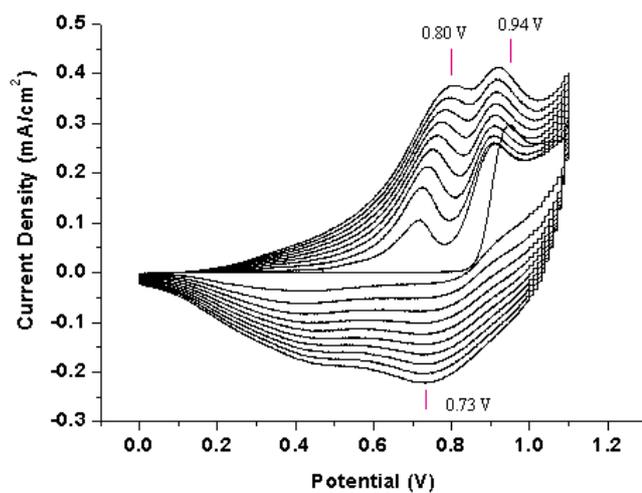
(a)
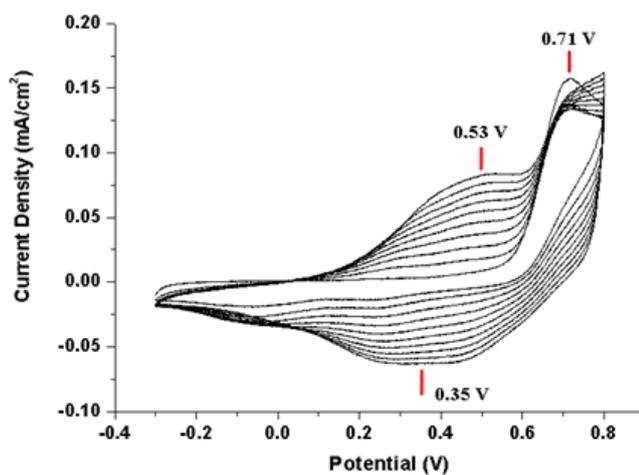
(b)

Figure 31 Cyclic voltammograms of a) **53** b) **49.**

A true linear relation was observed between the peak current and the scan rate during the scan rate studies of **53**, which indicates the presence of a well adhered electroactive film with a non-diffusion limited redox process (Figure 32).
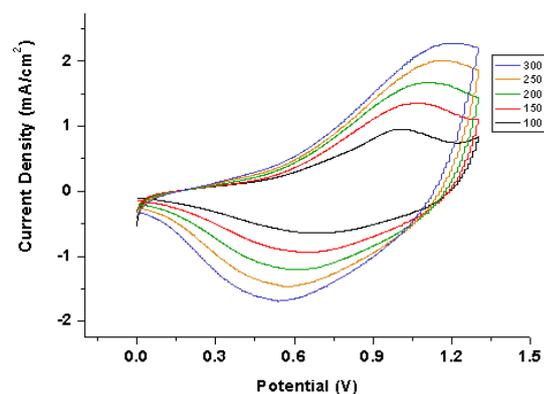
Figure 32 Scan rate dependence of **P53.**

2.2.4.2 Spectroelectrochemistry

Spectroelectrochemical analysis of **53** and **49** were studied to clarify electronic transitions upon doping the polymer. The film was deposited on ITO via potentiodynamic electrochemical polymerization of **53** in the presence of $NaClO_4$ / DCM / ACN at 0.0 V and +1.1 V. **P53** coated ITO was investigated by UV-Vis spectroscopy in the same but monomer free electrolyte system by switching between -0.0 V and +1.3 V with an incremental increase in applied potential (Figure 33).

(a)
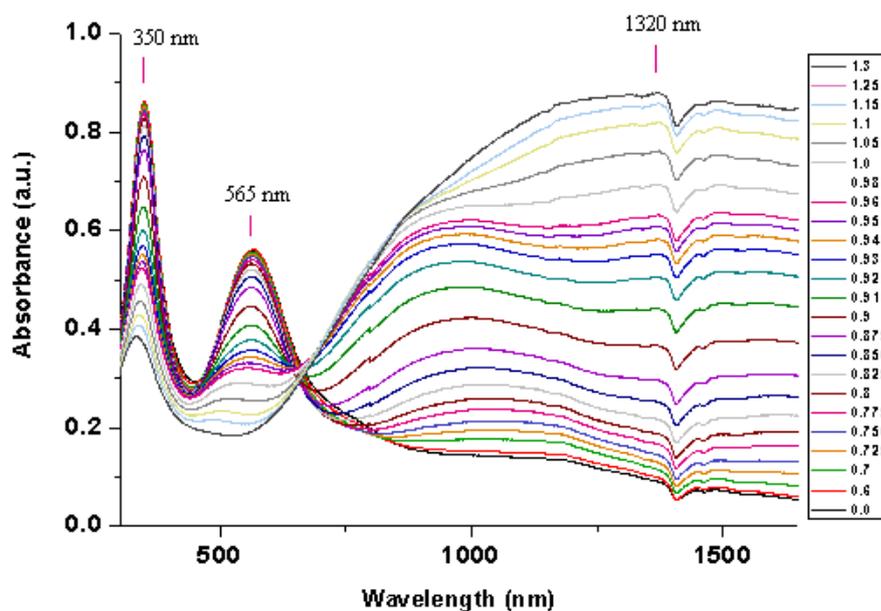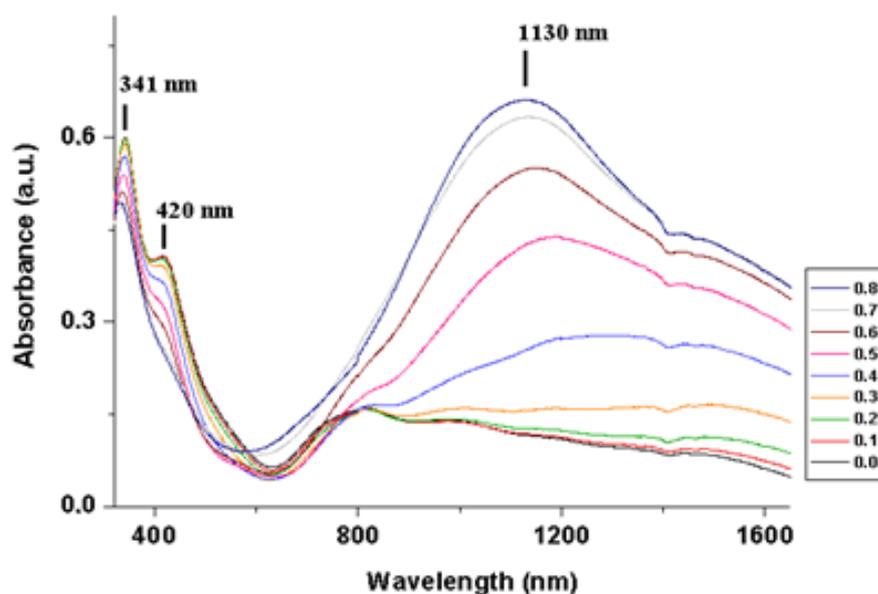
(b)

Figure 33 Spectroelectrochemical spectra of **a) P53** with applied potential between 0.0 V and +1.3 V in ACN/DCM/NaClO$_4$ **b) P49** with applied potential between 0.0 V and 0.8 V in ACN/DCM/NaClO$_4$/LiClO$_4$.

There was a gradual decrease in the peak intensity of the π-π* transition upon increasing the applied voltage. The electronic band gap of **53** was found to be 1.5 eV and λ$_{max}$ was 565 nm. Upon applying voltage, formation of charge carrier bands was observed. Thus, appearance of peak at around 1349 nm could be attributed to the evolution of charge carriers. This resulting UV-Vis spectrum confirmed the typical bipolaronic nature of charge carriers.

Table 15 Eg and λ$_{max}$ of **P53** and **P49.**

Polymer	E$_g$	λ$_{max}$
P53	1.5 eV	565 nm
P49	2.2 eV	420 nm

To probe the optical changes of **49** upon doping, spectral changes were investigated in a monomer free, supporting electrolyte/solvent couple, the same with the electropolymerization process, while increasing the applied potential from 0.0 V to 0.8 V. Although **49** showed electroactivity, its polymer did not show electrochromic properties, which can be deduced from UV-vis-NIR spectrum of **P49**.

2.2.4.3 Electrochromic Switching

Electrochromic contrast was calculated as the percent transmittance change (T %) at 1320 nm where the electrochromic material has the highest optical contrast, 61 % (Figure 34). Switching speed reported as the time required for the coloring/bleaching process was 0.7 s at 1320 nm.

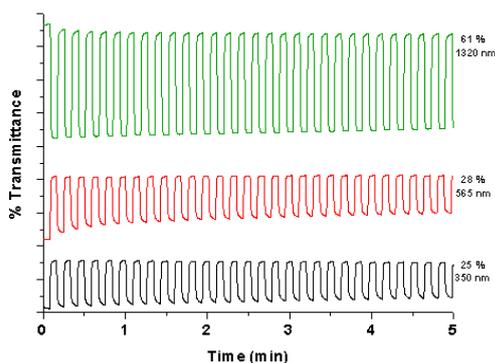**Figure 34** Electrochromic switching, optical absorbance change monitored of **P53** at 350 nm, 565 nm and 1320 nm for P53 between 0.0 V and +1.3 V.

Table 16 Optical contrast and switching times for **P53.**

λ_{max} **P53**	**350 nm**	**565 nm**	**1320 nm**
Optical Contrast	25 %	28 %	61 %
Switching Time	0.8 s	0.9 s	0.7 s

2.2.4.4 Colorimetry

The color coordinates of the **P53** were also determined by colorimetry in order to have an accurate objective measurement. When the polymer was completely reduced, it had violet color. With the application of +1.3 V, the **P53** was oxidized and at this voltage its color was pale blue. Table shows Y, x, y values of the film of **P53** in neutral and oxidized states.

Table 17 Electrochromic properties of **P53.**

+ 0.2 V	+1.3 V
Y: 30.1 x : 0.289 y : 0.273	Y: 58.7 x : 0.286 y : 0.340

2.2.5 5,7-Bis(4-hexylthiophen-2-yl)-2,3-di(thiophen-2-yl)thieno[3,4-*b*]pyrazine 48

2.2.5.1 Cyclic Voltammogram

Multiple scan voltammetry on ITO was performed in a 0.1 M TBAPF$_6$/LiClO$_4$ and 10^{-2} M monomer solution applying potentials between -0.1 V and +0.8 V at a scan rate of 100 mV/s (Figure 35). The solvent was chosen as a mixture of acetonitrile and dichloromethane (95/5) due to the poor solubility of the monomer in ACN. On the other hand, since the monomer bears an alkyl chain in the structure, the oligomers are soluble in pure DCM. Hence a mixture of these two solvents was used as the solvent system. The monomer oxidation potential was observed at 0.62 V. After the

first cycle, an oxidation peak at 0.46 V and its reverse cathodic peak at 0.41 V appeared.

Table 18 Experimental conditions and results of the electrochemical studies of thienopyrazine derivative.
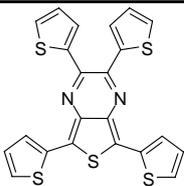
Monomer	Supporting electrolyte	Solvent	Monomer $E_{p,a}$(V)	Polymer $E_{p,a}$(V)	$E_{p,c}$(V)
48	$NaClO_4$/ $LiClO_4$	DCM:ACN (5:95)	0.62	0.46	0.41
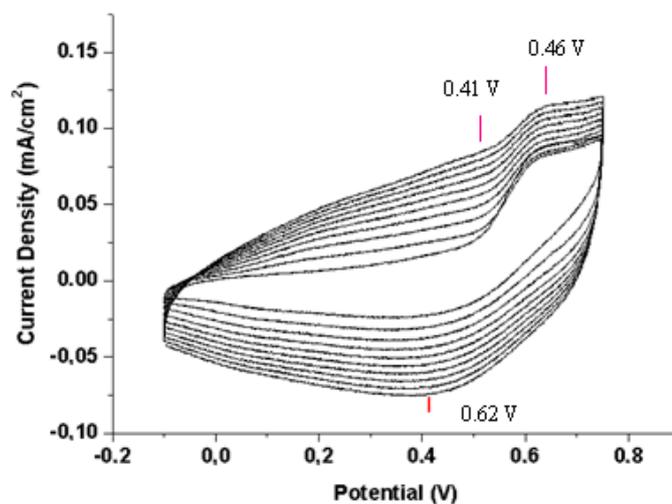
Figure 35 Cyclic voltammogram of **48.**

2.2.5.2 Spectroelectrochemistry

To probe the optical changes upon doping, spectral changes were investigated by UV-vis-NIR spectrophotometer in a monomer free, 0.1 M $TBAPF_6$/$LiClO_4$, ACN/DCM (95:5) solution while increasing the applied potential from -0.4 to 0.9 V (Figure 36).
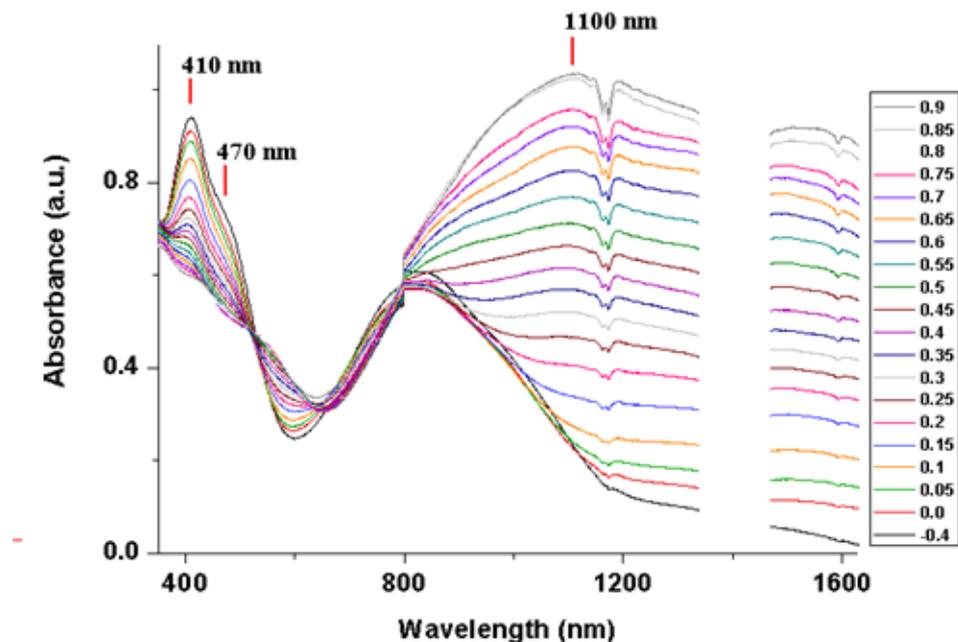
Figure 36 Spectroelectrochemical spectrum of **P48** with applied potential between -0.4 V and 0.9 V in ACN/DCM/NaClO$_4$/LiClO$_4$.

There was a gradual decrease in the peak intensity of the π-π* transition upon increasing the applied voltage. The onset energy for the π-π* transition which is called the electronic band gap (Eg), was found to be 0.95 eV and λ$_{max}$ was 830 nm. Upon applying voltage, formation of charge carrier band was observed at 1100 nm (Table 19).

Table 19 Spectroelectrochemical properties of **P48.**

Polymer	E_g	λ_{max}
P48	0.95 eV	830 nm

2.2.5.3 Electrochromic Switching

The optical switching studies were investigated using a square wave potential step method coupled with optical spectroscopy known as chronoabsorptometry in a monomer free solution. Figure 37 reveals the electrochromic switching properties of **P48**. The optical contrast for **P48** is 16 % at 410 nm, 18 % at 470 nm and 60 % at 1100 nm.
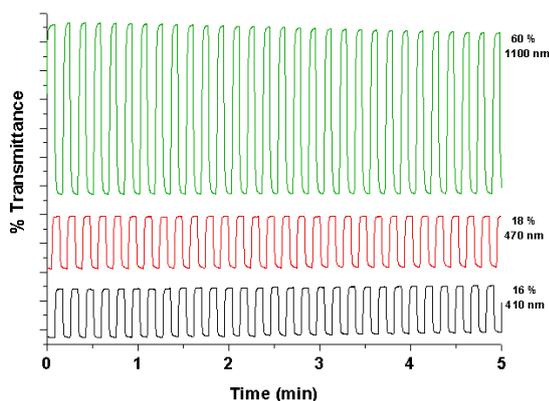
Figure 37 Electrochromic switching, optical absorbance change monitored of **P48** at 410 nm, 470 nm and 1100 nm for P53 between -0.4 V and +0.9 V.

The switching time was determined by monitoring the absorption intensity at 511 nm and 1200 nm while switching the applied voltage between -0.4 V and + 0.9 V. The polymer revealed a switching time of 1.2 s, 1.5 s and 2.0 s at 410 nm, 470 nm and 1200 nm, respectively.

Table 20 Optical contrast and switching times for **P48.**

λ_{max} P48	410 nm	470 nm	1100 nm
Optical Contrast	16 %	18 %	60 %
Switching Time	1.2 s	1.5 s	2.0 s

2.2.5.4 Colorimetry

The color coordinates of the polymer were also determined by colorimetry in order to have an accurate objective measurement.

The polymer has a dark yellow in the neutral state (Y: 36.4, x: 0.402, y: 0.429). Upon further oxidation the yellow color of the polymer turns into green (Y: 40.4, x: 0.369, y: 0.409). Further oxidation gives brown color (Y: 31.7, x: 0.383, y: 0.373).

Tablo 21 Electrochromic properties of **P48.**

-0.3 V	+0.5 V	+0.9V
Y: 36.4 x : 0.402 y : 0.429	Y: 40.4 x : 0.369 y : 0.409	Y: 31.7 x : 0.383 y : 0.373

2.2.6 Quinoxaline Derivatives

2.2.6.1 Cyclic Voltammograms

In order to investigate the electrochemical behaviors of **43** and **44**, CV experiments were performed in (5:95) DCM/ACN/TBAPF$_6$ solvent-electrolyte couple for **44**. As reflected in Figure 38 a, voltammogram of the monomer **44** exhibited an irreversible electroactivity at 0.97 V. At first glance, monomer peak intensity seems to increase with increasing number of scans. However; polymer oxidation peak revealed in the second run and the monomer peak lay under the polymer oxidation peak. This was confirmed with single scan polymer cyclic voltammogram in a monomer free

solution. When there was no monomer in the solution the polymer characteristic peaks were still observable (Figure 39).

Table 22 Experimental conditions and results of the electrochemical studies of quinoxaline derivatives.
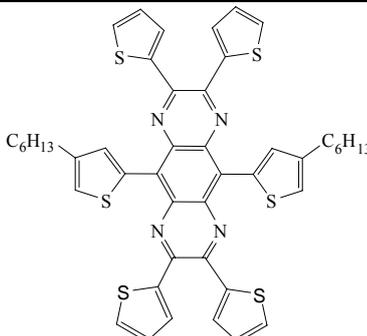
Monomer	Supporting electrolyte	Solvent	Monomer $E_{p,a}$ (V)	Polymer $E_{p,a}$ (V)	$E_{p,c}$(V)
44	TBAPF$_6$	DCM/ACN 5:95	0.97	0.95	0.80
43	LiClO$_4$	DCM/ACN 1:1	1.16	0.83	0.62
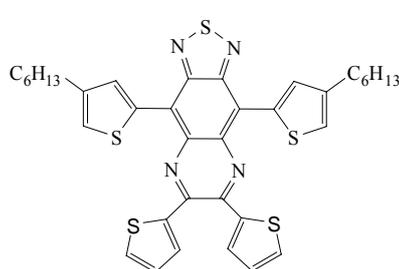
On the other hand, the monomer oxidation peak of **43** was observed at 1.16 V. However, current decreased upon repetitive cycles. Continuous deposition of the polymer onto the ITO was monitored by the increase in the polymer's anodic and cathodic peak currents. As seen in Figure 41b, the **P43** revealed an oxidation peak at 0.83 V and a reduction peak at 0.62 V, lower than that of **P44**.
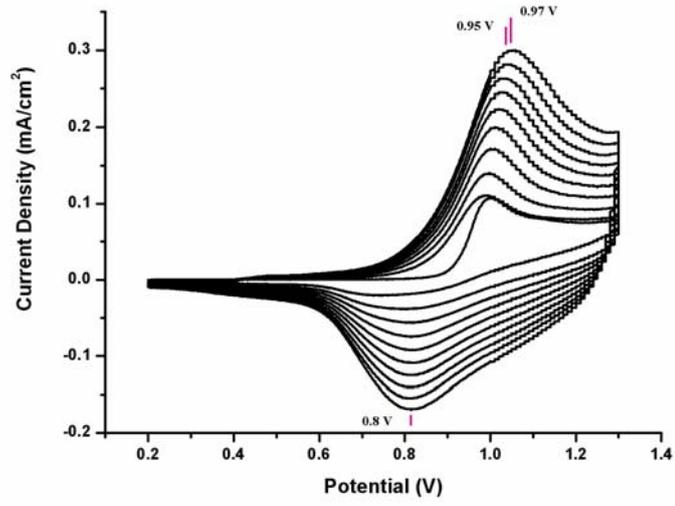
(a)
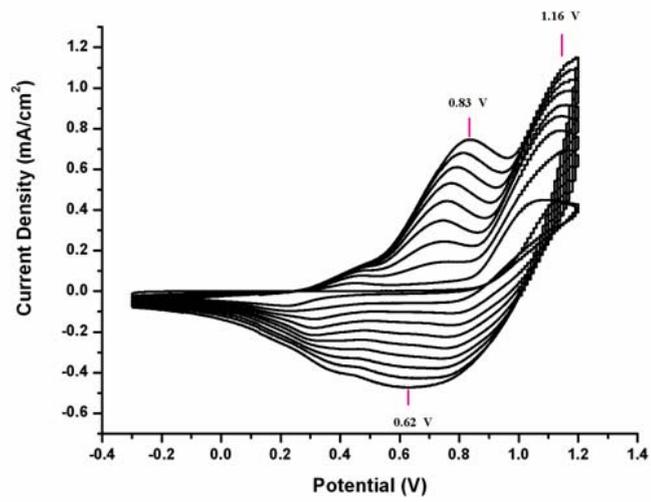
(b)

Figure 38 Cyclic voltammograms of a) **44** b) **43.**
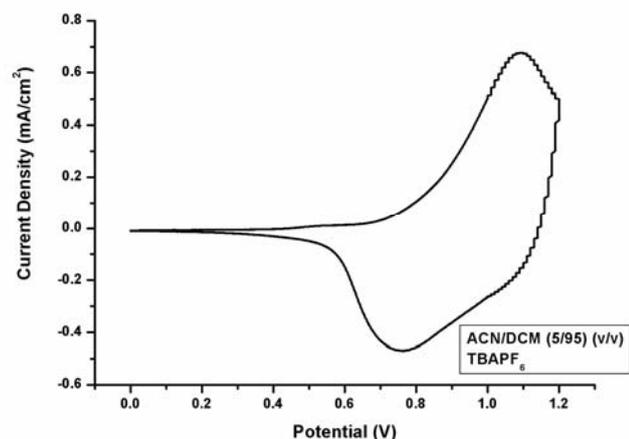
Figure 39 Cyclic voltammograms of **P44** .

The scan rate dependence of the polymer films of **P43 and P44** were investigated by CV. There is a linear relationship between scan rate and current density of the anodically electropolymerized **P44 and P43**, which indicates the presence of a well adhered electroactive film with a non-diffusion limited redox process (Figure 40,41).

Figure 40 Scan rate dependence and relation between current density and scan rate of **P44.**

Figure 41 Scan rate dependence and relation between current density and scan rate of **P43.**

2.2.6.2 Spectroelectrochemistry

In order to investigate the spectroelectrochemistry of the **P43** and **P44**, the polymer films were deposited on ITO via potentiostatic electrochemical polymerization of **44** and **43** (0.01 M) in the presence of suitable solvent/electrolyte system. **P44** coated ITO was investigated by UV-Vis spectroscopy in the same but monomer free electrolytic systems by switching between 0.0 V and +1.3 V with gradual increase in applied potential.

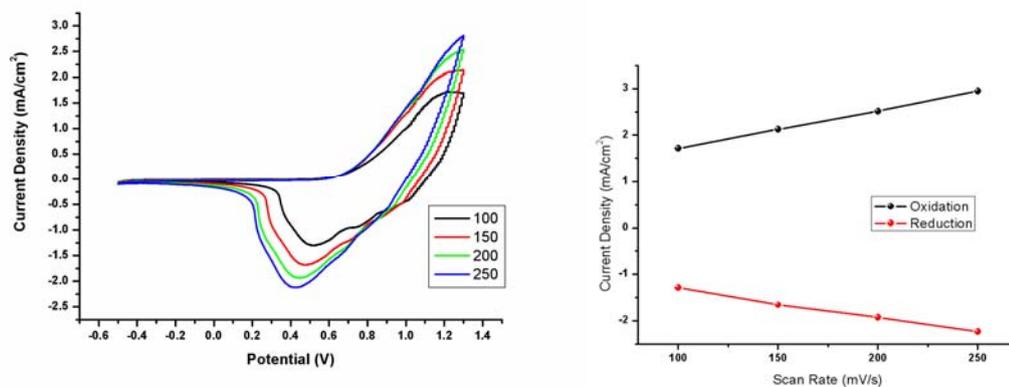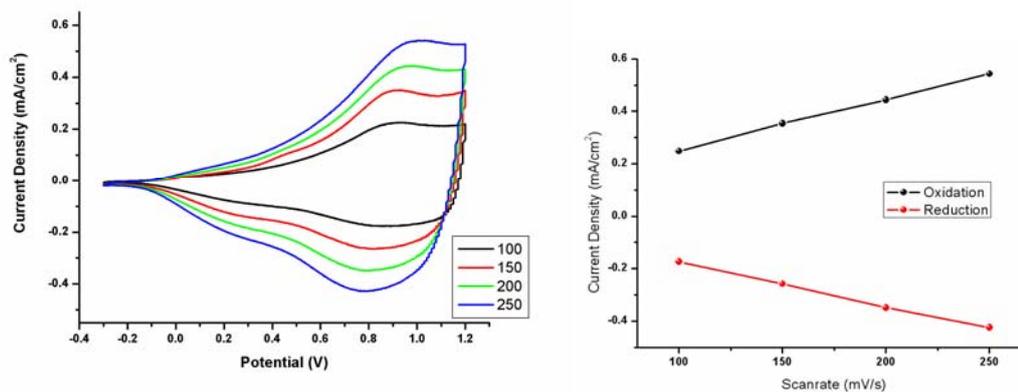Figure 42 a shows the spectroelectrochemistry of **P44**, monitored while the polymer was sequentially stepped between its fully oxidized and reduced forms. This polymer has three absorbance maxima of 352 nm, 535 nm and 750 nm. The electronic band gap, defined as the onset energy for the π- π * transition, was found to be 1.0 eV and λ_{max} was 750 nm.

P44 is brown in its neutral state. When the polymer is oxidized, it turns into deep purple, almost black as it can be easily figured out from UV-Vis spectrum of **P44.** Having black color in any state makes the polymer a significant candidate for smart window applications [127]. Upon oxidation the peak at 750 nm reaches a minimum value and then it starts to increase to absorb almost the complete visible region, which is a clear proof of black color.
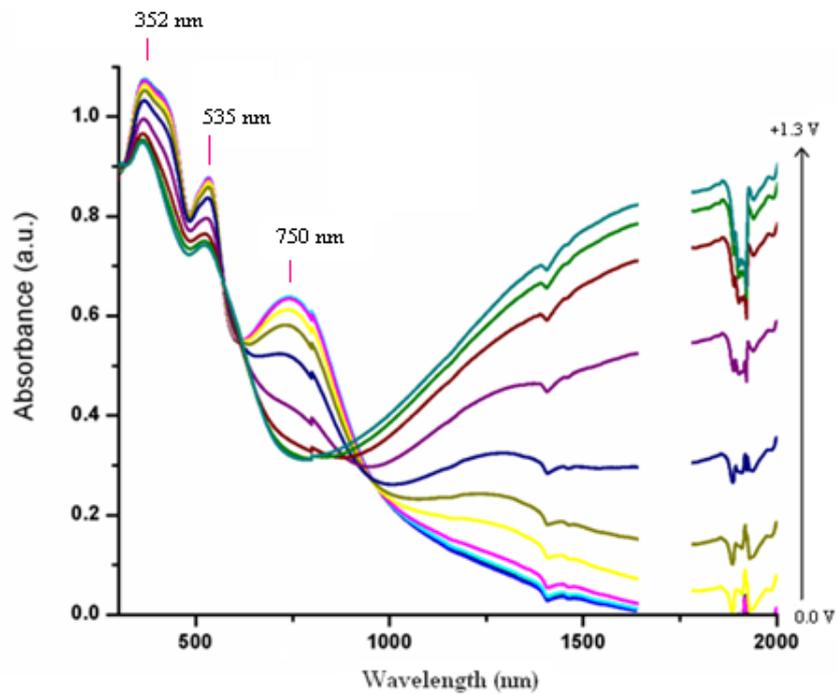
(a)
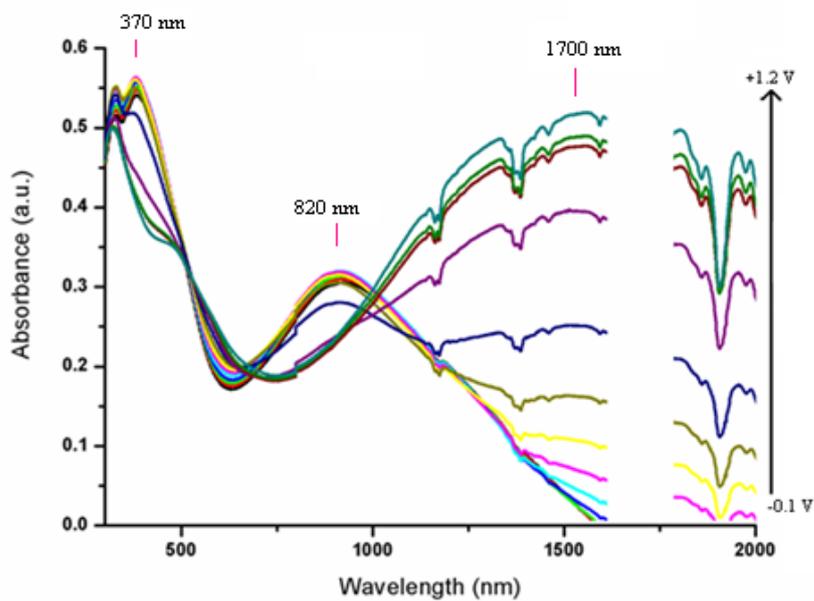
(b)

Figure 42 Spectroelectrochemical spectra of **a) P44** with applied potential between 0.0 V and +1.3 V in ACN/DCM/TBAPF$_6$ **b) P43** with applied potential between -0.1 V and 1.2 V in ACN/DCM/LiClO$_4$.

Optoelectrochemical spectra of **P43** as a function of applied voltage are given in Figure 42 b revealing λmax as 820 nm with a band gap of 0.8 eV. The absorption observed at around 1700 nm were attributed to the evolution of charge carriers.

Table 23 Spectroelectrochemical properties of **P44** and **P43.**

Polymer	E_g	λ_{max}
P44	1.0 eV	750 nm
P43	0.8 eV	820 nm

2.2.6.3 Electrochromic Switching

Electrochromic switching studies were performed to monitor the percent transmittance changes as a function of time and to determine the switching time of the polymer at its max by stepping potential repeatedly between the neutral and oxidized states.

The optical contrast of the **P44** in the NIR region (at 1800 nm) was found to be 84 % with a switching time of 2.0 s (Figure 43 a). This high optical contrast makes this polymer also a powerful candidate for NIR electrochromic applications. NIR applicable materials are of particular interest since they are used for optical data transmission and as NIR dyes [128,129].

(a)

(b)
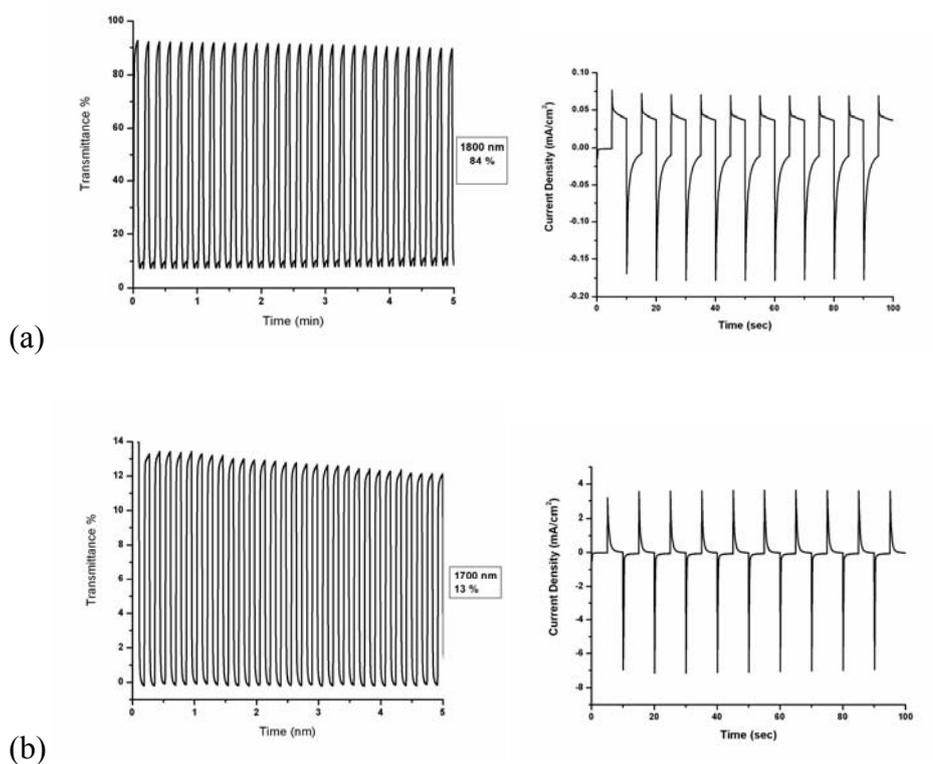
Figure 43 Electrochromic switching, optical absorbance change monitored **a)** at 1800 nm for **P44** between 0.0 V and +1.3 V **b)** at 1700 nm for **P43** between -0.1 V and +1.2 V.

The optical contrasts for **P43** were measured at 370 nm and at 1700 nm as 6 % and 13 % with switching times of 1.6 s and 2.0 s, respectively (Figure 43 b).

Table 24 Optical contrast and switching times for **P43** and **P44.**

λ_{max} **P44**	**1800 nm**
Optical Contrast P44	84 %
Switching Time P44	2.0 s

Table 24 continue

λ_{max} P43	370 nm	1700 nm
Optical Contrast P43	6 %	13 %
Switching Time P43	1.6 s	2.0 s

2.2.6.4 Colorimetry

The color of the film of **P44** switches from deep purple in the reduced state (-0.0 V) to orange in the oxidized state (+1.3 V). The colorimetry studies were carried out at the fully oxidized and reduced states of **P44**, at which Y, x, y values were measured as 25.1, 0.376 and 0.363, in the order given. Y, x, y values of **P44** at neutral state are 14.9, 0.310 and 0.346, respectively. These values show that the color of **P44** at neutral state is orange.

The colorimetry measurements of **P43** were performed at its neutral state (-0.1V) and oxidized state (1.2V). **P43** had a pale yellow in the neutral state and a pale brown in the oxidized state.

Table 25 Electrochromic properties of (a) **P43** and (b) **P44.**

(a)   (b)

CHAPTER 3

EXPERIMENTAL

3.1 Materials and Methods

In this study all compounds were identified using Nuclear Magnetic Resonance Spectrometer (NMR) (Bruker Spectrospin Avance DPX-400 Spectrometer at 400MHz) and chemical shifts (δ) were determined relative to tetramethylsilane as the internal standard. Deutereo chloroform and dimethyl formamide were used as solvent. Chemical shifts were reported in ppm and coupling constants were given as Hz.

Column chromatography was done for purification the products by using Merck Silica Gel (70 -230 mesh). TLC was carried out on aliminium sheets precoated with silica gel 60 F 254 (Merck), and the spots were visualized with UV light (l = 254 and 366 nm). Melting points were determined by help of capillary tube apparatus. For the samples, which are degraded in capillary tube apparatus, DSC method was performed.

The cyclic voltammograms were recorded using VoltaLab PST050 and Solartron 1285 Potentiostats. A Varian Cary 5000 UV-Vis spectrophotometer was used to perform the spectroelectrochemical studies. Colorimetry measurements were done via a Conica Minolta CS-100 spectrophotometer.

3.2 Synthetic Procedures of Monomers

3.2.1 Synthesis of Dibenzo[*a,c*]phenazine Derivatives

3.2.1.1 2,7-Dibromophenantherene-9,10-dione 25
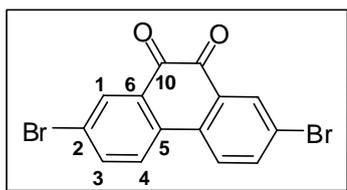
NBS (1.795g, 10.09 mmol) was added to a well stirred solution of phenanthrene-9,10-dione (1g, 4.80 mmol) in 98 % H_2SO_4 and stirred at room temperature for 3 h. After that the mixture poured on crushed ice. The orange product was filtered off, washed with cold water. To purify **25**, recrystallization was done in DMSO. (1.31 g, 75%) M.p.:326.8°C by DSC (Lit.[115] m.p.=337 °C). ^{1}H-NMR (400MHz d_6-DMSO): δ (ppm) 8.25 (d, 2H, J= 8.4 Hz, H-4), 8.09 (d, 2H, J= 1.9 Hz, H-1), 7.96 (dd, 2H, J=8.4, 1.9 Hz, H-3) ^{13}C-NMR (100 MHz, d_6-DMSO): δ (ppm) 177.1, 137.8, 134.0, 133.5, 131.4, 127.3, 123.2.

3.2.1.2. General Procedure for The Synthesis of Dibenzo[*a,c*]phenazine Derivatives

9,10-Phenanthraquinone (300 mg, 0.82 mmol), ethanol (50 mL), catalytic amount PTSA and diamino compounds (0.82 mmol) were placed in a round-bottomed flask fitted with a condenser. The mixture was heated under reflux. At the end of the reaction, cloudy mixture was observed. Upon cooling, filtration of the reaction mixture followed by washing with ethanol afforded the desired products, 2,7-dibromodibenzo[*a,c*]phenazine and 2,7-dibromodibenzo[*f,h*]pyrido[3,4-*b*]quinoxaline. To purify 2,7-dibromo-10,11,12,13-tetrahydrodibenzo[*a,c*]phenazine, column chromatography was performed over silica gel, eluting with 1:5 (chloroform: hexane).

3.2.1.2.1. 2,7-Dibromodibenzo[*a,c*]phenazine 26
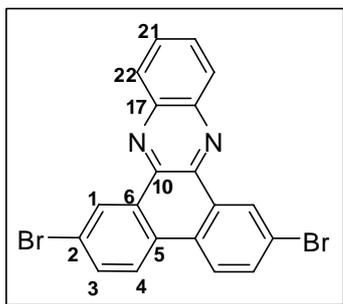
Pale yellow solid (310 mg, 86 %) ^{1}H-NMR (400 MHz, CDCl$_3$): δ (ppm) 9.46 (d, 2H, J= 2.2 Hz, H-1), 8.29 (m, 4 H), 7.83(m, 4H) ^{13}C-NMR (100 MHz, CDCl$_3$): δ (ppm) 142.7, 133.7, 132.2, 130.8, 130.4, 129.8, 129.4, 124.9, 123.2, 100.3.

3.2.1.2.2. 2,7-Dibromodibenzo[*f,h*]pyrido[3,4-*b*]quinoxaline 27
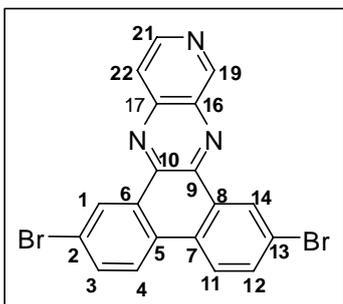
Yellowish orange solid (240 mg, 67% yield) ^{1}H-NMR (400MHz *d$_6$*-DMSO): δ (ppm) 9.80 (s, 1H, H-19), 9.28 (d, 2H, J=1.7 Hz, H-1, H-14), 8.95 (d, 1H, J=5.9 Hz, H-21), 8.72 (d, 1H, J=8.7 Hz), 8.71 (d, 1H, J=8.4 Hz), 8.26 (d, 1H, J=5.9 Hz, H-22), 8.075 (2H, td, H-3, H-12).

3.2.1.2.3. 2,7-Dibromo-10,11,12,13-tetrahydrodibenzo[*a,c*]phenazine 28
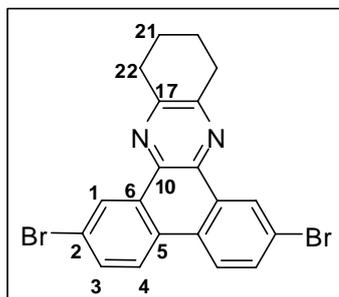
White solid (180 mg, 49%) IR υ = 3074, 2931, 1878, 1598, 1479, 1427, 1371, 1323, 1263, 1197, 1074, 955, 898, 797, 733, 655, 526 cm^{-1}. ^{1}H-NMR (400MHz CDCl$_3$): δ (ppm) 9.04 (d, 2H, *J*=2.2 Hz, H-1), 8.12 (d, 2H, *J*=8.7 Hz, H-4), 7.64 (dd, 2H, *J*=8.7, 2.2 Hz, H-3), 3.10 (m, 4H, H-22), 2.00 (m, 4H, H-21) ^{13}C-NMR (100 MHz, CDCl$_3$): δ (ppm) 153.3, 137.4, 131.7, 131.4, 128.7, 127.6, 124.1, 122.1, 32.7, 22.8.

3.2.1.3. General Procedure for The Synthesis of 29, 30, 31 via Stille coupling

2,7-Dibromodibenzo[*a,c*]phenazine (100 mg, 0.23 mmol), and tributylstannane (0.92 mmol) were dissolved in anhydrous THF (150 ml), the solution was purged with argon for 30 min and dichlorobis(triphenyl phosphine)palladium(II) 40 mg, 0.057 mmol) was added at room temperature. The mixture was refluxed over night under argon atmosphere. If necessary, the crude products were purified by column chromatography using CHCl$_3$ – hexane as eluent.

3.2.1.3.1 2,7-Bis(4-hexylthiophen-2-yl)dibenzo[*a,c*]phenazine 29
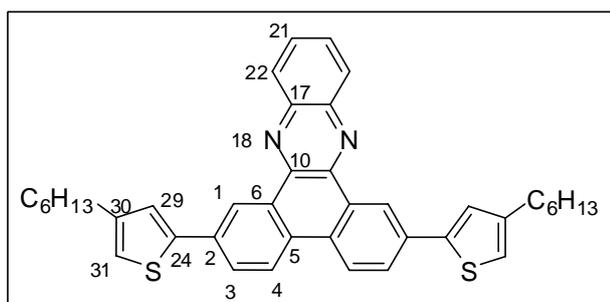
The crude product was purified by column chromatography (chloroform/hexane 1:2) to give **29** (96 mg, 64 %) as a lemon yellow solid. IR υ = 3061, 2921, 2852, 1731, 1608, 1509, 1464, 1340, 1061, 905, 819, 766, 722, 578 cm^{-1}. ^{1}H-NMR (400 MHz, CDCl$_3$) : δ (ppm) 9.48 (s, 2H, H-1), 8.39 (d, 2H, J = 8.4 Hz, H-4), 8.31 (dd, 2H, J = 6.4, 3.3 Hz, H-22), 7.89 (d, 2H, J = 8.4, H-3), 7.80 (dd, 2H, J = 6.4, 3.3 Hz, H-21), 7.40 (s, 2H, H-31), 6.92 (s, 2H, H-29), 2.63 (t, 4H, J = 7.6 Hz, thiophene-CH$_2$-), 1.65 (m, 4H), 1.33 (m, 12 H), 0.87 (t, 6H, J= 6.8 Hz, -CH$_3$). ^{13}C-NMR (100 MHz, CDCl$_3$) : δ (ppm) 144.9, 143.8, 142.6, 142.5, 134.4, 130.9, 130.8, 130.1, 129.8, 127.9, 125.6, 123.7, 122.9, 120.5, 32.0, 31.0, 30.8, 29.4, 22.9, 14.4.

3.2.1.3.2 2,7-Bis(2,3-dihydrothieno[3,4-*b*][1,4]dioxin-5-yl)dibenzo[*a,c*]phenazine 30
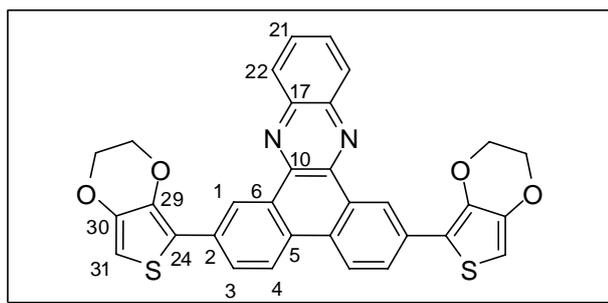
The crude product was purified by column chromatography (chloroform/hexane 2:1) to give **30** (85 mg, 66 %) as a brownish orange solid. IR υ = 3105, 2922, 1611, 1496, 1433, 1362, 1254, 1175, 1126, 1072, 909, 821, 761, 720, 578 cm^{-1}. ^{1}H-NMR (400 MHz, CDCl$_3$) : δ (ppm) 9.59 (d, 2H, J = 2.0 Hz, H-1), 8.43 (d, 2H, J = 8.5 Hz, H-4), 8.31 (dd, 2H, J = 6.5, 3.3 Hz, H-22), 8.11 (dd, 2H, J = 8.5, 2.0 Hz, H-3), 7.79 (dd, 2H, J= 6.5, 3.3 Hz, H-21), 6.36 (s, 2H, H-31), 4.39 (m, 4H), 4.27 (m, 4H) ^{13}C-NMR (100 MHz, CDCl$_3$): δ (ppm) 141.4, 141.2, 141.0, 137.8, 131.6, 129.3, 129.0, 128.5, 128.4, 126.9, 122.1, 121.8, 116.1, 97.3, 63.8, 63.4. HRMS *m/z* calcd for (C$_{32}$H$_{20}$N$_2$O$_4$S$_2$) 561.0943; found 561.0961.[M+H]+.

### 3.2.1.3.3　2,7-Di(thiophen-2-yl)dibenzo[*a,c*]phenazine 31
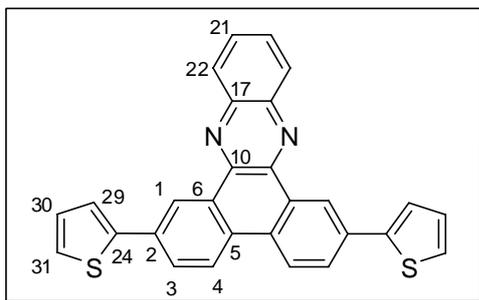
Solvent was filtered and the solid washed with dichloromethane to give a goldish yellow solid (73 mg, 71 %). IR υ = 3067, 1649, 1610, 1523, 1484, 1346, 1062, 907, 815, 759, 722, 578 cm^{-1}. ^{1}H-NMR (400MHz, d_6-DMF) : δ (ppm) 9.83 (d, 2H, J = 1.6 Hz, H-1), 9.10 (d, 2H, J = 8.3 Hz, H4), 8.64 (dd, 2H, J = 6.4, 3.2 Hz, H-22), 8.47 (d, 2H, J = 8.3 Hz, H-3), 8.26 (dd, 2 H, J = 6.4, 3.2 Hz, H-21), 8.06 (d, 2H, J = 3.3 Hz), 7.93 (d, 2H, J = 5.0 Hz), 7.50 (t, 2H, J = 5.0, 3.3 Hz, H-30) HRMS m/z calcd for (C$_{28}$H$_{16}$N$_2$S$_2$) 445.0833; found 445.0814.[M+H]+.

3.2.1.4. General Procedure for The Synthesis of 32, 33, 34 via Stille coupling

2,7-Dibromodibenzo[*f,h*]pyrido[3,4-*b*]quinoxaline (100 mg, 0.23 mmol), and tributylstannane (0.92 mmol) were dissolved in anhydrous THF (170 ml), the solution was purged with argon for 30 min and dichlorobis(triphenyl phosphine)palladium(II) 40 mg, 0.057 mmol) was added at room temperature. The mixture was refluxed over night under argon atmosphere. The crude products were purified by column chromatography using CHCl$_3$ – hexane as eluent.

3.2.1.4.1 2,7-Bis(4-hexylthiophen-2-yl)dibenzo[*f,h*]pyrido[3,4-*b*]quinoxaline 32
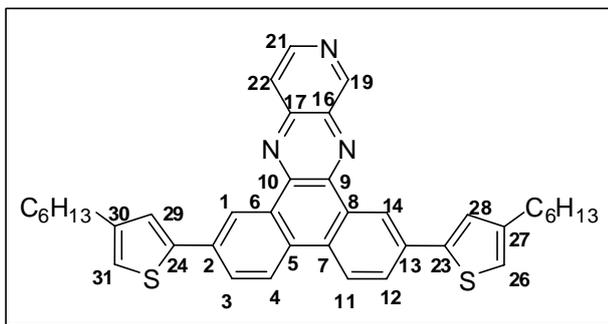

The crude product was purified by column chromatography (chloroform/hexane 2:1) to give **32** (63 %) as a yellow solid. ^{1}H-NMR (400 MHz, CDCl$_3$): δ (ppm) 9,57 (s, 1H, H-19), 9.11 (t, 2H, J=1.9 Hz, H-1, H-14), 8.73 (d, 1H, J=5.7 Hz, H-21), 8.01 (d, 2H, J=8.3 Hz, H-4), 7.91 (d, 1H, J=5.7 Hz, H-22), 7.68 (dd, 1H, J=8.3, 1.9 Hz, H-3), 7.67 (dd, 1H, J=8.3, 1.9 Hz), 7.29 (d, 1H, J=1.6 Hz), 7.27 (d, 1H, J=1.6 Hz), 6.91 (d, 2H, J=1.6 Hz, H-28, H-29), 2.63 (td, 4H, thiophene-CH$_2$-), 1.67 (p, 4H), 1.34 (m, 12 H), 0.87 (t, 6H, J=7.0 Hz, -CH$_3$). ^{13}C-NMR (100 MHz, CDCl$_3$): δ (ppm) 153.9, 144.8, 144.3, 143.5, 143.5, 142.4, 142.2, 141.9, 141.8, 135.5, 132.8, 132.7, 129.6, 128.9, 128.2, 128.0, 126.9, 126.5, 124.2, 124.1, 121.9, 121.9, 121.4, 121.0, 120.1, 119.2, 30.7, 29.7, 29.4, 28.1, 21.6, 13.1. HRMS *m/z* calcd for (C$_{39}$H$_{39}$N$_3$S$_2$) 614.2642; found 614.2444M+H]+.

3.2.1.4.2 2,7-Bis(2,3-dihydrothieno[3,4-*b*][1,4]dioxin-5-yl)dibenzo[*f,h*]pyrido[3,4-*b*] quinoxaline 33
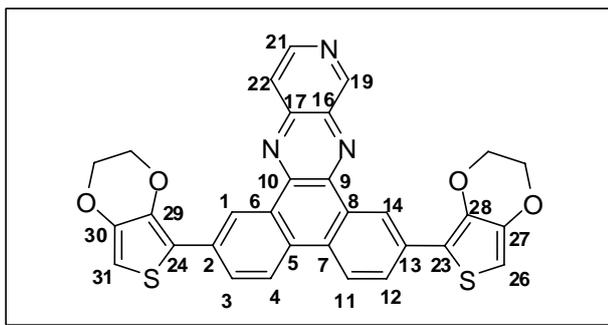
The crude product was purified by column chromatography (chloroform/hexane 7:1) to give **33** (58 %) as a red solid. IR υ = 3115, 2929, 1610, 1501, 1439, 1368, 1258, 1171, 1073, 892, 809, 722, 674, 564 cm^{-1}. ^{1}H-NMR (400 MHz, CDCl$_3$) : δ (ppm) 9.77 (s, 1H, H-19), 9.59 (d, 1H, J=1.8 Hz), 9.57 (d, 1H, J=1.9 Hz), 8.82 (d, 1H, J=5.7 Hz, H-21), 8.43 (d, 1H, J=8.7 Hz), 8.42 (d, 1H, J=9.1 Hz), 8.15 (m, 3H), 6.38 (s, 1H), 6.39 (s, 1H), 4.40 (m, 4H), 4,28 (m,4H). HRMS m/z calcd for (C$_{31}$H$_{19}$N$_3$O$_4$S$_2$) 572.0872; measured 572.0749[M+H]+.

### 3.2.1.4.3 2,7-Di(thiophen-2-yl)dibenzo[*f,h*]pyrido[3,4-*b*]quinoxaline 34
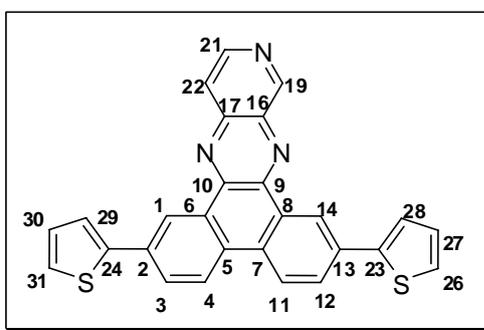
The crude product was filtered over silica gel (chloroform as eluent) to give **34** (65 %) as a yellowish orange solid. IR υ = 3068, 1650, 1602, 1539, 1478, 1420, 1342, 1257, 1062, 903, 815, 697, 559 cm^{-1}. ^{1}H-NMR (400 MHz, CDCl$_3$) : δ (ppm) 9.77 (s, 1H, H-19), 9.53 (d, 2H, J=1.9Hz, H-1, H-14), 8.84 (d, 1H, J=5.9 Hz, H-21), 8.45 (d, 1H, J=8.7 Hz), 8.44 (d, 1H, J=8.5 Hz), 8.12 (d, 1H, J=5.9 Hz, H-22), 8,00 (m,2H, H-3, H-12), 7.59 (m, 2H), 7.37 (t, 1H, J=1.3 Hz), 7.36 (t, 1H, J=1.3 Hz), 7.15 (m, 2H). HRMS m/z calcd for (C$_{27}$H$_{15}$N$_3$S$_2$) 446.0764; measured 446.0627[M+H]+.

3.2.1.5. General Procedure for the Synthesis of 35, 36, 37 via Stille coupling

2,7-dibromo-10,11,12,13-tetrahydrodibenzo[*a,c*]phenazine (100 mg, 0.23 mmol), and tributylstannane (0.92 mmol) were dissolved in anhydrous THF (80 ml), the solution was purged with argon for 30 min and dichlorobis(triphenyl phosphine)palladium(II) 40 mg, 0.057 mmol) was added at room temperature. The

mixture was refluxed over night under argon atmosphere. The crude products were purified by column chromatography using CH$_2$Cl$_2$ – hexane as eluent.

3.2.1.5.1 2,7-Bis(4-hexylthiophen-2-yl)-10,11,12,13-tetrahydrodibenzo[a,c] phenazine 35
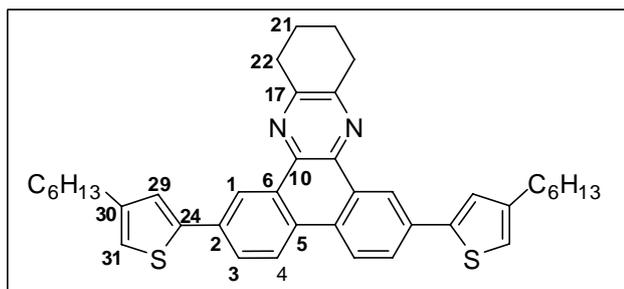
The crude product was purified by column chromatography (dichloromethane/hexane 1:3) to give **35** (82 mg, 58 %) as pale yellow solid. IR υ = 3055, 2925, 2852, 1611, 1460, 1371, 1323, 903, 810, 724, 580 cm^{-1}. ^{1}H-NMR (400MHz CDCl$_3$): δ (ppm) 9.21 (s, 2H, H-1), 8.33 (d, 2H, J=8.5 Hz, H-4), 7.79 (d, 2H, J=8.5 Hz, H-3), 7.34 (s, 2H, H-31), 6.88 (s, 2H, H-29), 3.15 (m, 4H, H-22), 2.60 (t, 4H, J=7.6 Hz, thiophene-CH$_2$-), 1.99 (m, 4H, H-21), 1.63 (p, 4H), 1.30 (m, 12H), 0.84 (t, 6H, J=7.0 Hz, -CH$_3$) ^{13}C-NMR (100 MHz, CDCl$_3$): δ (ppm) 152.8, 144.8, 144.1, 138.9, 133.8, 130.4, 129.9, 126.6, 125.5, 123.4, 121.6, 120.2, 33.0, 32.0, 31.0, 30.8, 29.3, 23.2, 22.9, 14.4.

### 3.2.1.5.2 2,7-Bis(2,3-dihydrothieno[3,4-b][1,4]dioxin-5-yl)-10,11,12,13-tetrahydrodibenzo [a,c]phenazine 36
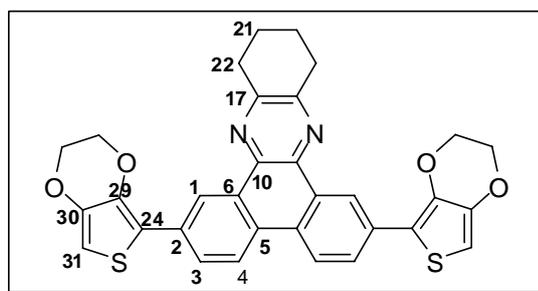
The crude product was purified by column chromatography (dichloromethane:hexane 3:1) to give **36** (86 mg, 66 %) as a yellow solid. IR υ = 3112, 2932, 1610, 1503, 1437, 1365, 1168, 1071, 897, 810, 755, 605 cm^{-1}. ^{1}H-NMR (400MHz CDCl$_3$): δ (ppm) 9.31 (d, 2H, J=1.8 Hz, H-1), 8.37 (d, 2H, J=8.7 Hz, H-4), 7.99 (dd, 2H, J=8.7, 1.8 Hz, H-3), 6.30 (s, 2H, H-31), 4.32 (m, 4H, H-22), 4.22 (m, 4H, H-21), 3.15 (m, 4H), 1.98 (m, 4H). ^{13}C-NMR (100 MHz, CDCl$_3$): δ (ppm) 151.3, 141.3, 137.7, 137.6, 131.1, 129.1, 128.1, 125.5, 121.8, 120.5, 116.6, 97.0, 63.8, 63.4, 31.8, 21.9.

3.2.1.5.3 2,7-Di(thiophen-2-yl)-10,11,12,13-tetrahydrodibenzo[*a,c*]phenazine 37
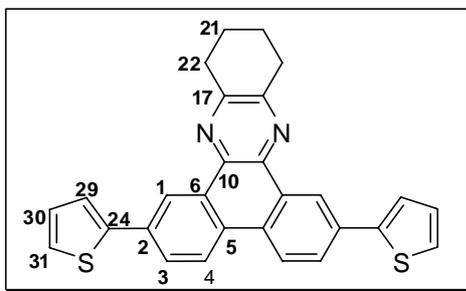
The crude product was purified by column chromatography (dichloromethane:hexane 5:1) to give **37** (68 mg, 66%) as yellow solid. IR υ = 3067, 2934, 1898, 1610, 1446, 1371, 1193, 1075, 903, 811, 696, 592 cm^{-1}. ^{1}H-NMR (400MHz CDCl$_3$): δ (ppm) 9.35 (d, 2H, J=1.9 Hz, H-1), 8.49 (d, 2H, J=8.5 Hz, H-4), 7.91 (dd, 2H, J=8.5, 1.9 Hz, H-3), 7.53 (dd, 2H, J=3.5, 1.0 Hz), 7.30 (dd, 2H, J=5.1, 1.0 Hz), 7.10 (dd, 2H, J=5.1, 3.5 Hz, H-30), 3.19 (m,4H), 2.03 (m, 4H).

3.2.2 Synthesis of Quinoxaline Derivatives

3.2.2.1 4,7-Dibromobenzo[c][1,2,5]thiadiazole 38
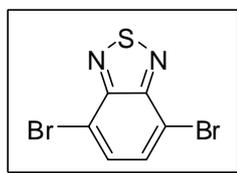
To a 250 ml two-necked round bottom flask were added benzothiadiazole (5 g, 36.7 mmol) and 75 ml of HBr (47%). A solution containing Br_2 (17.6 g, 110.16 mmol) in 50 ml of HBr was added dropwise very slowly (slow addition is essential!). After total addition of the Br_2, the solution was refluxed for 6 h. Precipitation of an orange solid was noted. The mixture was allowed to cool to room temperature and sufficient saturated solution of $NaHSO_3$ added to consume completely any excess Br_2. The mixture was filtered under vacuum and washed exhaustively with water. The solid was then washed once with cold Et_2O and dried under vacuum, affording the desired dibrominated product 4,7-dibromobenzo[c][1,2,5]thiadiazole **38** in 88% yield (9.53 g).^{1}H-NMR (400MHz $CDCl_3$): δ (ppm) 7.73 (s, 2H). ^{13}C-NMR (400MHz $CDCl_3$): δ (ppm) 152.6; 132.1; 113.6. Mp 187–188 ºC.

3.2.2.2 4,7-Dibromo-5,6-dinitrobenzo[c][1,2,5]thiadiazole 39
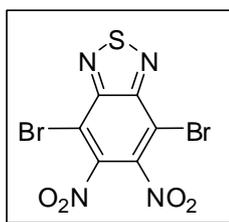
4,7-dibromobenzo[c][1,2,5]thiadiazole **39** (5 g, 17 mmol) was added in small portion to a mixture of conc. sulfuric acid and fuming nitric acid (1:1, 50 ml) with stirring at 0-5 ºC over 30 min. After stirring for 3 h at room temperature, the mixture was poured into the ice-water, and the yellow precipitate was collected by filtration, washed with water. Purification by chromatography on silica gel (EtOAc:hexane,

1:4) gave 1.78 g of the product **39** as a beige solid (27% yield). ^{13}C-NMR (400 MHz, CDCl3): δ (ppm) 151.4, 144.9, 110.3.

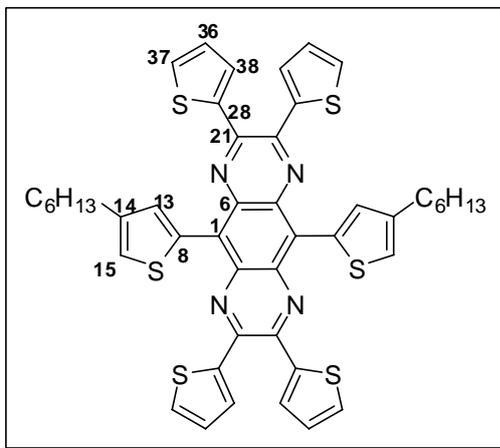### 3.2.2.3 4,7-Bis(4-hexylthiophen-2-yl)-5,6-dinitrobenzo[*c*][1,2,5]thiadiazole 40
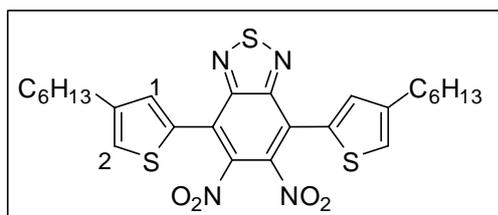
4,7-Dibromo-5,6-dinitrobenzo[*c*][1,2,5]thiadiazole (400 mg, 1.04 mmol) and tributyl(4-hexylthiophen-2-yl)stannane (1.85 g, 4.16 mmol) were dissolved in anhydrous THF (100 ml). The solution was purged with argon for 30 min and dichlorobis(triphenyl phosphine)palladium(II) (70.2 mg, 0.10 mmol) was added at room temperature. The mixture was refluxed for 16 h under argon atmosphere. Solvent was evaporated under vacuum and the crude product was purified by column chromatography over silica gel, eluting with 1:2 (dichloromethane:hexane) and give orange-brown oil **40** (380 mg, 68 %).^{1}H-NMR (400MHz CDCl3): δ (ppm) 7.23 (s, 4H, H-1, H-2), 2.57 (t, 4H, *J*=7.6 Hz, thiophene-CH2-), 1.56 (p, 4H), 1.26 (m, 12H), 0.81 (t, 6H, *J*=6.7 Hz, -CH3) ^{13}C-NMR (100 MHz, CDCl3) : δ (ppm) 149.8, 142.0, 139.2, 129.8, 126.8, 124.0, 118.9, 29.2, 27.9, 27.8, 26.5, 20.2, 11.7.

3.2.2.4 4,9-Bis(4-hexylthiophen-2-yl)-6,7-di(thiophen-2-yl)-[1,2,5]thiadiazolo[3,4-*g*] quinoxaline 43
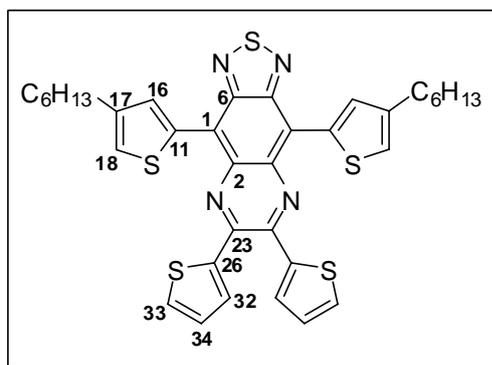
A mixture of dinitro compound **43** (200 mg, 0.36 mmol) and iron dust (0.24 g, 4.29 mmol) in acetic acid (4 mL) was stirred at 30 °C for 4 h. The reaction mixture was poured into cold 5% NaOH (5 mL), and then a yellow solid appeared. The solution was extracted with Et_2O. The organic layer was washed with brine and dried over Na_2SO_4. After removal of the solvent under reduced pressure, the residue was used without purification for the synthesis of 4,9-bis(4-hexylthiophen-2-yl)-6,7-di(thiophen-2-yl)-[1,2,5]thiadiazolo[3,4-g]quinoxaline **43**. The product, 4,7-bis(4-hexylthiophen-2-yl)benzo[c][1,2,5]thiadiazole-5,6-diamine **41**, was dissolved in 5 ml EtOH. 2,2'-Thenil (79 mg, 0.36 mmol) and catalytic amount PTSA were added to the reaction medium. The reaction mixture was stirred at room temperature for 6 hours. The solvent was evaporated and the product was purified by column chromatography (1:1 CH_2Cl_2:Hexane). Green solid, 132.3 mg (54%) IR υ = 3099, 2919, 1650, 1520, 1453, 1373, 1243, 1189, 1060, 901, 845, 706, 579 cm^{-1}. ^{1}H-NMR (400MHz $CDCl_3$): δ (ppm) 8.62 (d, 2H, J=1.1 Hz, H-18), 7.51 (dd, 2H, J=5.0, 0.9 Hz), 7,44 (dd, 2H, J=3.7, 0.9 Hz), 7.19 (brs, 2H, H-16), 6.97 (dd, 2H, J=5.0, 3.7 Hz, H-34), 2.68 (t, 4H, J=7.7 Hz, thiophene-CH_2-), 1.68 (p, 4H), 1.32 (m, 12H), 0.84 (t, 6H, J=6.8 Hz, -CH_3) ^{13}C-NMR (100 MHz, $CDCl_3$): δ (ppm) 150.4, 144.3, 141.5, 140.2, 133.9, 133.3, 132.7, 129.9, 129.2, 126.0, 125.0, 119.1, 30.3, 29.2, 29.2, 27.7, 21.2, 12.7.

### 3.2.2.5 5,10-Bis(4-hexylthiophen-2-yl)-2,3,7,8-tetra(thiophen-2-yl)pyrazino[2,3-g] quinoxaline 44

A mixture of 4,7-bis(4-hexylthiophen-2-yl)-5,6-dinitrobenzo[c][1,2,5]thiadiazole **40** (200 mg, 0.36 mmol) and zinc dust (489 mg, 7.48 mmol) in acetic acid (3 mL) was stirred at 60 °C for 1 h until the reaction mixture turned white. After this was cooled to room temperature, 2-2'-thenil (0.159 g, 0.72 mmol) was added to the solution and the mixture was stirred for 1 h. After removal of the solvent under reduced pressure, the residue was purified by column chromatography on silica gel (eluent 1:1 CH_2Cl_2: Hexane) to obtain the title compound **44** (145 mg, 48%) as a shiny-black solid. IR υ = 3088, 2925, 1520, 1426, 1310, 1233, 1173, 1060, 853, 701, 598 cm^{-1}. ^{1}H-NMR (400MHz CDCl$_3$): δ (ppm) 8.16 (s, 2H, H-15), 7.48 (d, 4H, J=3.7 Hz), 7,46 (d, 4H, J=5.0 Hz), 7.27 (s, 2H, H-13), 6.94 (dd, 4H, J=5.0, 3.7 Hz, H-36), 2.75 (t, 4H, J=7.7 Hz, thiophene-CH$_2$-), 1.77 (p, 4H), 1.35 (m, 12H), 0.84 (t, 6H, J=7.0 Hz, -CH$_3$) ^{13}C-NMR (100 MHz, CDCl$_3$): δ (ppm) 144.0, 141.3, 141.1, 135.2, 134.8, 132.7, 129.5, 129.2, 126.5, 125.9, 124.7, 30.8, 29.8, 28.2, 21.6, 13.1.

3.2.3 Synthesis of 5,7-bis(4-hexylthiophen-2-yl)-2,3-di(thiophen-2-yl)thieno[3,4-b] pyrazine
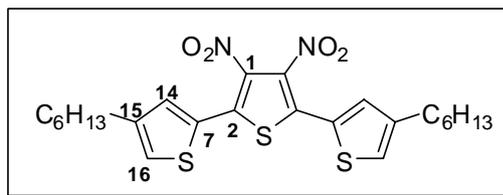
3.2.3.1. 2,5-Dibromo-3,4-dinitrothiophene 45
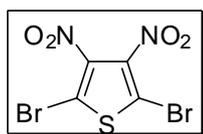
Concentrated sulfuric acid (18.58 mL) and fuming sulfuric acid (30% SO$_3$, 18.58 mL) were combined in a flask equipped with a mechanical stirrer and cooled with an ice bath. 2,5- dibromothiophene (10 g, 41 mmol) was then added maintaining a temperature below 20°C. Nitric acid (6.5 mL) was then added dropwise, being careful to keep the temperature under 30°C. Once the addition was complete, the mixture was allowed to react for an additional three hours and then poured over 150 g of ice. Upon the melting of the ice, the solid residue was recovered by vacuum filtration and washed well with water to produce a light yellow powder.

Recrystallization with methanol gave 11.2 g (82%) of analytically pure material; mp 136.2°C. ^{13}C-NMR (100 MHz, CDCl$_3$): δ (ppm) 139.6, 112.4.

3.2.2.2. 5-5'-Bis(4-hexylthiophen-2-yl)-3,4-dinitrothiophene 46

2,5-Dibromo-3,4-dinitrothiophene (400 mg, 1.20 mmol) and tributyl(4-hexylthiophen-2-yl)stannane (2.20 g, 4.82 mmol) were dissolved in anhydrous THF (100 ml). The solution was purged with argon for 30 min and dichlorobis(triphenyl phosphine)palladium(II) (84 mg, 0.12 mmol) was added at room temperature. The mixture was refluxed for 16 h under argon atmosphere. Solvent was evaporated under vacuum and the crude product was purified by column chromatography over silica gel, eluting with 1:2 (dichloromethane:hexane) and give yellow needle (422 mg, 69 %). ^{1}H-NMR (400MHz CDCl$_3$): δ (ppm) 7.26 (d, 2H, J=1.3 Hz, H-16), 7.07 (brs, 2H, H-14), 2.51 (t, 4H, J=7.7 Hz, thiophene-CH$_2$-), 1.53 (p, 4H), 1.25 (m, 12H), 0.79 (t, 6H, J=6.6 Hz, -CH$_3$) ^{13}C-NMR (100 MHz, CDCl$_3$) : δ (ppm) 143.9, 134.4, 132.9, 131.2, 136.7, 125.0, 30.5, 29.3, 29.2, 27.8, 21.5, 13.0.

### 3.2.2.3. 5-5'-Bis(4-hexylthiophen-2-yl)-3,4-diaminothiophene 47
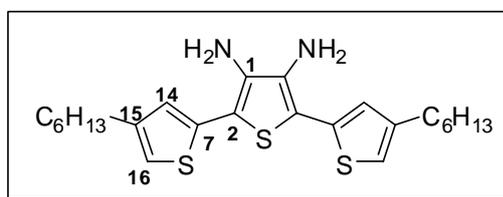
46 (200 mg, 0.39 mmol) and tin(II) chloride dihydrate (1.87 g, 9.87 mmol) were dissolved in ethyl acetate (50ml) and stirred at reflux for 2 h. The mixture was added to a solution of Na2CO3 (50 ml, 0.25 M), stirred vigorously with dichloromethane

(50 ml) and the mixture was filtered over celite. The phases were separated and the organic phase was washed with water (3 × 25 mL), dried with MgSO$_4$ and the solvent was evaporated. Yield: 156 mg (89%) ^{1}H-NMR (400MHz CDCl$_3$): δ (ppm) 6.85 (s, 2H, H-16), 6.77 (s, 2H, H-14), 3.25 (brs, 4H, -NH$_2$), 2.52 (t, 4H, J=7.7 Hz, thiophene-CH$_2$-), 1.56 (p, 4H), 1.25 (m, 12H), 0.82 (t, 6H, J=6.8 Hz, -CH$_3$) ^{13}C-NMR (100 MHz, CDCl$_3$): δ (ppm) 143.0, 134.4, 132.0, 124.2, 117.5, 109.8, 30.6, 29.5, 29.3, 28.0, 21.5, 13.0.

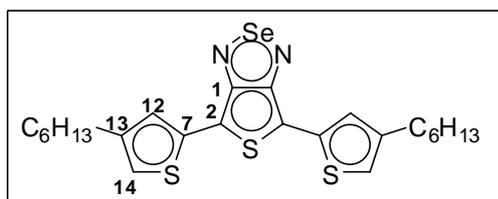### 3.2.2.4. 5,7-Bis(4-hexylthiophen-2-yl)-2,3-di(thiophen-2-yl)thieno[3,4-*b*]pyrazine 48
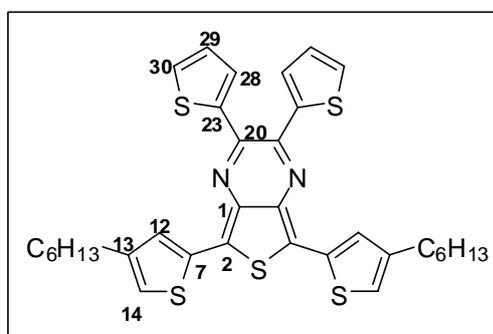
Diamino compound **47** (100 mg, 0.22 mmol) and 2,2'-thenil (50 mg, 0.22 mmol) were dissolved in 4 ml ethanol and stirred at room temperature for 10 minute. Then, catalytic amount PTSA was added in the mixture. After the reaction was completed, the solvent was removed under vacuum. The residue was purified by coloumn chromatography over silica gel, eluting with 1:2 (chloroform:hexane) and give greenish blue solid (105 mg, 74 %). IR υ = 2950, 1426, 1362, 1268, 1060, 851, 700, 641cm^{-1}. ^{1}H-NMR (400MHz CDCl$_3$): δ (ppm) 7.39 (dd, 2H, J=4.9, 0.7 Hz), 7.36 (d, 2H, J=1.0 Hz, H-14), 7.22 (dd, 2H, J=3.8, 0.7 Hz), 6.90 (dd, 2H, J=4.9, 3.8 Hz, H-29), 6.85 (brs, 2H, H-12), 2.53 (t, 4H, J=7.6 Hz, thiophene-CH$_2$-), 1.57 (p, 4H), 1.26 (m, 12H), 0.81 (t, 6H, J=6.8 Hz, -CH$_3$) ^{13}C-NMR (100 MHz, CDCl$_3$): δ (ppm) 144.0, 141.9, 141.0, 134.8, 132.6, 128.3, 127.7, 125.7, 124.4, 123.0, 120.0, 30.1, 28.9, 28.8, 27.4, 21.0, 12.5.

3.2.4. Synthesis of Selenadiazole Derivatives

3.2.4.1 4,6-Bis(4-hexylthiophen-2-yl)-4,6-dihydrothieno[3,4-*c*][1,2,5] selenadiazole 49

To a solution of **47** (100 mg, 0.22 mmol) in ethanol (2 ml) was added a solution of selenium dioxide (27.74 mg, 0.25 mmol) in hot water (1 ml). The mixture was stirred at room temperature for 1 h. Filtration of the product over AlO_2 gave 4,6-bis(4-hexylthiophen-2-yl)-4,6-dihydrothieno[3,4-*c*][1,2,5]selenadiazole **49** green solid, in70 % (82 mg) yield. ^{1}H-NMR (400MHz CDCl$_3$): δ (ppm) 7.34 (d, 2H, *J*=0.8 Hz, H-14), 6.82 (d, 2H, *J*=0.8 Hz, H-12), 2.55 (t, 4H, *J*=7.6 Hz, thiophene-CH$_2$-), 1.58 (p, 4H), 1.24 (m, 12H), 0.82 (t, 6H, J=6.9 Hz, -CH$_3$) ^{13}C-NMR (100 MHz, CDCl$_3$): δ (ppm) 161.9, 143.5, 134.3, 124.2, 119.2, 109.1, 30.6, 29.4, 29.3, 28.0, 21.6, 13.0.

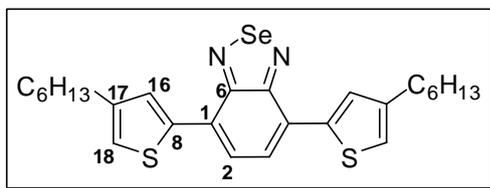### 3.2.4.2 Synthesis of 4,7-Bis(4-hexylthiophen-2-yl)benzo[*c*][1,2,5]selenadiazole

3.2.4.2.1 4,7-Bis(4-hexylthiophen-2-yl)benzo[*c*][1,2,5]thiadiazole 51
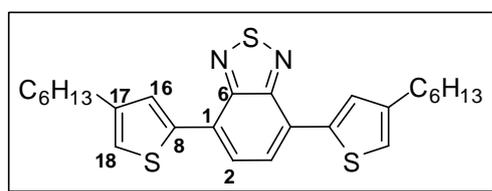
4,7-dibromobenzo[*c*][1,2,5]thiadiazole **50** (300 mg, 1.02 mmol) and tributyl(4-hexylthiophen-2-yl)stannane (1.87 g, 4.08 mmol) were dissolved in anhydrous THF (100 ml). The solution was purged with argon for 30 min and dichlorobis(triphenyl phosphine)palladium(II) (71.6 mg, 0.10 mmol) was added at room temperature. The

116

mixture was refluxed for 14 h under argon atmosphere. Solvent was evaporated under vacuum and the crude product was purified by column chromatography over silica gel, eluting with 1:2 (dichloromethane/hexane) and give orange solid (313mg, 64 %). ^{1}H-NMR (400MHz CDCl$_3$): δ (ppm) 7.90 (d, 2H, J=1.0 Hz, H-18), 7.75 (s, 2H, H-2), 6.97 (d, 2H, J=1.0 Hz, H-16), 2.62 (t, 4H, J=7.6 Hz, thiophene-CH$_2$-), 1.63 (p, 4H), 1.63 (m, 12H), 0.83 (t, 6H, J=7.0 Hz, -CH$_3$) ^{13}C-NMR (100 MHz, CDCl$_3$): δ (ppm) 151.6, 143.3, 138.0, 127.9, 125.0, 124.5, 120.5, 30.6, 29.6, 29.4, 28.0, 21.6, 13.0.

3.2.4.2.2 4,7-Bis(4-hexylthiophen-2-yl)benzo[*c*][1,2,5]selenadiazole 53

To a solution of 3,6-bis(4-hexylthiophen-2-yl)benzene-1,2-diamine **52** (100 mg, 0.23 mmol) in ethanol (2 ml) was added a solution of selenium dioxide (27.74 mg, 0.25 mmol) in hot water (1 ml). The mixture was stirred at room temperature for 1 h. Filtration of the green precipitate gave 4,7-bis(4-hexylthiophen-2-yl)benzo[*c*][1,2,5]selenadiazole **53** in 84% (98 mg) yield. IR υ = 3094, 2922, 1650, 1541, 1473, 1315, 1261, 1087, 820, 581 cm^{-1}. ^{1}H-NMR (400MHz CDCl$_3$): δ (ppm) 7.80 (d, 2H, J=1.1 Hz, H-18), 7.66 (s, 2H, H-2), 6.96 (d, 2H, J=1.1 Hz, H-16), 2.61 (t, 4H, J=7.7 Hz, thiophene-CH$_2$-), 1.62 (p, 4H), 1.28 (m, 12H), 0.82 (t, 6H, J=7.0 Hz, -CH$_3$) ^{13}C-NMR (100 MHz, CDCl$_3$): δ (ppm) 157.2, 143.0, 138.3, 127.9, 126.5, 124.8, 120.8, 30.7, 29.6, 29.4, 28.0, 21.6, 13.0.

3.3 Synthesis of Conducting Polymers

3.3.1. Electrochemical Polymerization

Electrochemical polymerization of monomers were accomplished via potentiodynamic method in single-compartment cell furnished with indium tin oxide (ITO) working, Pt counter, Ag wire reference electrodes in the presence of suitable supporting electrolytes and solvent systems.

3.3.1.1. Polymerization of Dibenzo[*a,c*]phenazine Derivatives

P29 and **P30** were obtained in dichloromethane (DCM) solution containing 0.1 M tetrabutylammonium hexafluorophosphate (TBAPF$_6$). The redox behaviors of **P29** and **P30** were studied via scanning the potential between +0.4 and +1.3 V and between +0.3 V and +1.4 V with 100 mV/s scan rate, respectively. The free standing the polymers were washed with DCM in order to remove the excess TBAPF$_6$ and unreacted monomer after the electrolysis.

3.3.1.2 Polymerization of Dibenzo[*f,h*]pyrido[3,4-*b*]quinoxaline Derivatives

Polymerization of **32** and **34** were performed in the presence of 0.1 M lithium perchlorate (LiClO$_4$) in ACN/DCM (95:5) via potentiodynamic electrolysis by the stepping the potential between 0.3 V and 1.2 V and between 0.2 V and 1.2 V, respectively. TBAPF$_6$ /ACN/DCM (95:5) system was used for the polymerization of **33**. After electrolysis, all polymer films were washed with ACN/DCM mixture.

3.3.1.3. Polymerization of Tetrahydrodibenzo[*a,c*]phenazine Derivatives

While polymerization of **36** was carried out in the presence of 0.1 M TBAPF$_6$ in ACN/DCM(95:5), polymerization of **35** and **37** were performed in the presence of 0.1 M TBAPF$_6$ in DCM. Potentiodynamic electrolysis of **36** was run by sweeping the potential between +0.1V and +1.1 V with 100 mV.s-1 scan rate. Electropolymerization of **35** and **37** was performed using multiple scan voltammetry

from +0.5 V to +1.4 V and from +0.2 V to +1.3 V in the order given. As the free standing films of **P35** and **P37** were washed with DCM, the film of **P36** was washed with ACN/DCM (95:5), to remove unreacted monomer and excess TBAPF$_6$ after electrolysis.

3.3.1.4. Polymerization of Selenadiazole Derivatives

Preparative electrochemical polymerization of **53** was performed by sweeping the potential between 0.0 V and +1.1 V with a scan rate 100 mV/s. NaClO$_4$ (0.1 M) and ACN/DCM (95:5) were used as the supporting electrolyte and solvent. Compound **49** was polymerized in the presence of NaClO$_4$/LiClO$_4$ as the supporting electrolyte in DCM/ACN (1:1) mixture. The free standing films were washed with DCM several times to remove unreacted monomer and the electrolyte.

3.3.1.5. Polymerization of Thienopyrizine Derivative

Electrochemical polymerization of **48** was performed using NaClO$_4$ (0.1 M) and LiClO$_4$ (0.1 M) as the supporting electrolyte in ACN/DCM (95:5) system. Experiments were carried out sweeping the potential between -0.1 V and +0.8 V with 100 mV/s scan rate and the free standing film that formed was washed with DCM to remove unreacted monomer and excess electrolyte after electrolysis.

3.3.1.6. Polymerization of Quinoxaline Derivatives

Electrochemical polymerization of **44** was performed using TBAPF$_6$ as the supporting electrolyte (0.1M) in DCM/ACN (5:95). The electrolysis solution contained 0.01 M **44**. Experiments were carried out sweeping the potential between 0.2 V and +1.3 V with 100 mV/s scan rate. On the other hand, polymerization of **43** was carried out in the presence of LiClO$_4$ in DCM/ACN (1:1) and the potential swept between 0.3 V and 1.3 V. The free standing films that formed were washed with DCM to remove unreacted monomer and excess electrolyte after electrolysis.

3.4 Characterization of Conducting Polymers

3.4.1. Cyclic Voltammetry (CV)

Cyclic voltammetry is a useful tool for understanding a wide range of oxidation and reduction processes, particularly those occurring during the synthesis and redox reactions of conducting polymers. Furthermore, CV reveals information regarding the stability of the product during multiple redox cycles. Since the rate of potential scan is variable, both fast and slow reactions can be followed. A very important aspect of this method is its ability to generate new redox species during the first potential scan and then probe the fate of species on the second and subsequent scans. Therefore, CV allows the growth of a polymer film along with its further characterization during a single experiment.

The experimental setup of cyclic voltammetry consists of a working electrode, a counter electrode and a reference electrode. Indium tin oxide (ITO) as the working electrode, Pt as the counter electrode and a Ag wire as the pseudo reference electrode were used during the CV studies.

3.4.2 Electrochromic Properties of Conducting Polymers

3.4.2.1. Spectroelectrochemical Studies

Spectroelectrochemistry is a combination of electrochemical and spectroscopic techniques operated at the same time. In order to probe the electronic structure of the polymers and to examine the optical changes that occur during redox switching, optoelectrochemical analysis were carried out.

Polymer films were synthesized on a glass slide coated with indium tin oxide (ITO) from a 0.01M monomer solutions in different solvent-electrolyte couples. The

polymers were synthesized by potentiodynamic electrolysis. Then the polymer was reduced, washed with electrolyte solution to remove unreacted monomer.
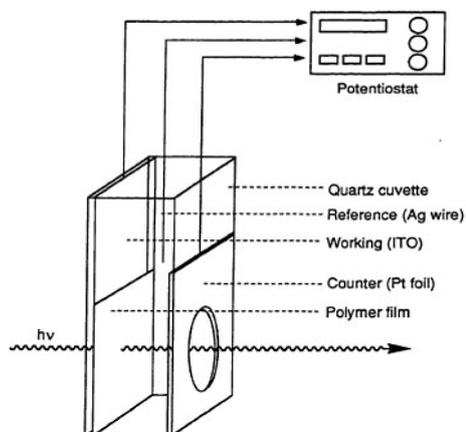

Figure 44 In-situ optoelectrochemical analysis.

For the spectroelectrochemical studies, the polymer film coated ITO was placed in a cuvette that is equipped with a reference electrode (Ag wire) and a Pt wire counter electrode (Figure 44). This cell was then connected to a potentiostat, and the polymer was oxidized stepwise while obtaining a spectrum at each potential. The results were then recorded as a graph of the extent of absorption as a function of wavelength.

3.4.2.2. Switching Studies

To monitor absorbance changes with time during repeated potential stepping between bleached and colored states (to obtain an insight into changes in the optical contrast), long term switching studies were carried out (Figure 45). A square wave potential step method coupled with optical spectroscopy known as chronoabsorptometry was used to probe switching times and contrast in these polymers. Electrochromic contrast is often described as percent transmittance change (T %) at a specified wavelength where the material has the highest optical contrast.
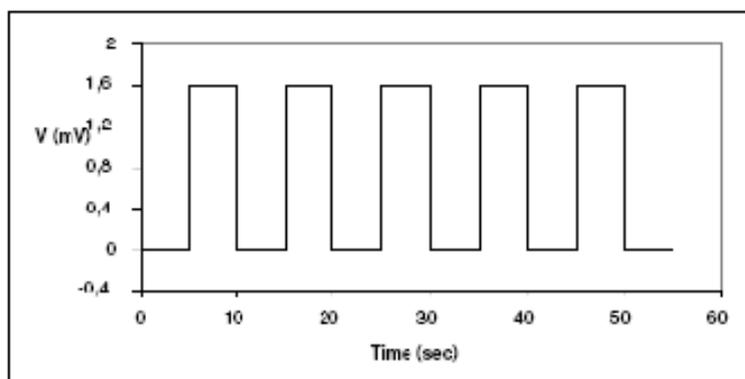
Figure 45 Square wave voltammetry.

In order to examine switching properties, polymers were deposited on ITO-coated glass slides in the form of thin films. After coating the polymers on ITO electrode, a potential square wave was applied in the monomer free solution while recording the percent transmittance between its neutral and doped states at a fixed maximum absorption wavelength. Switching properties of polymer films were investigated using potential square wave technique with a residence time of 5 seconds between oxidation and reduction potentials.

3.4.2.3 Colorimetry

Colorimetry was used to define the color of the polymers. The results were expressed in the CIE 1931 Lab color space.

The experimental setup for Colorimetry analysis is similar to the one used for spectroelectrochemistry. The applied potential is controlled by a Voltalab PST50 potentiostat. The polymer coated ITO/cuvette assembly is placed in a grey painted light booth (chromaticity box) that has a light source D50 (5000K) located in the back. The relative luminance *(L)* and the a and b values were measured at the fully oxidized and reduced states of the polymers with a Minolta CS-100 Chroma Meter colorimeter. In order to obtain accurate values, a background measurement on a bare ITO/cuvette assembly was taken either at the beginning or at the end of the polymer colorimetric analysis.

122

CHAPTER 4

CONCLUSION

In the first part of the thesis, new donor-acceptor type monomers, bearing benzothiadiazole, dibenzophenazine, dibenzoyridoquinoxaline, tetrahydrodibenzophenazine, thienopyrizine, theinoselenadiazlole, benzoselenadiazole, pyrazinoquinoxaline, thiadizoloquinoxaline as the acceptor units and 3-hexylthiophene, thiophene and edot as the donor units were synthesized via well-known synthetic methods such as bromination, nitration , reduction, condensation and Stille coupling reactions. Monomers with 3-hexylthiophene unit in their structure were found to be soluble, hence may as well be considered as potential candidates to be used in devices.

Second part of the study was devoted to investigate one of the most interesting properties of conducting polymers, electrochromism. In recent years there has been a growing interest in the application of conducting polymers in electrochromic devices. Thus, electrochromic properties of the synthesized conducting polymers were investigated by several techniques such as spectroelectrochemistry, kinetic and colorimetry studies.

Spectroelectrochemistry experiments were performed in order to investigate key properties of conjugated polymers such as band gap, maximum absorption wavelength, the intergap states that appear upon doping and evolution of polaron and bipolaron bands.

The polymers with thiadizoloquinoxaline (**P43**), pyridoquinoxaline (**P44**) and thienopyrizine (**P48**), acceptor units, bearing 3-hexylthiophene as the donor unit, revealed low band gaps; 0.8 eV, 1.0 eV and 0.95 eV, respectively.

Switching time and optical contrast of the polymers were evaluated via kinetic studies. Among the synthesized polymers, polypyrazinoquinoxaline (**P44**) exhibited 84% optical contrast, the highest value in these polymers, in near IR region, which makes the polymer a powerful candidate for NIR applications.

Polymers with dibenzohenazine and tetrahydro-dibenzophenazine units exhibited reasonable optical contrasts ranging between 45 % and 64 %. Switching times of the polymers with EDOT units (**P30** and **P36**) were found to be less than 1 s. Benzoselenadiazole (**P53**) and thienopyrazine (**P48**) derivatives showed optical contrasts of about 60 % and the switching time of **P53** was also below 1 s.

Colorimetry measurements revealed that three of the synthesized polymers are multichromic. Two of them are tetrahydrodibenzophenazine derivatives, **P36** and **P37**, and the oher one is thienopyrizine derivative (**P48**). Also, pyrazinoquinoxaline derivative (**P44**) has almost black color in its oxidized state which is very rare and significant property for electrochromic polymers. Due to this nature it may also be used in solar cell applications.

Monomers bearing dibenzophenazine, dibenzopyridoquinoxaline and tetrahydrobenzophenazine as the acceptor units coupled with 3-hexylthiophene had better solubility properties than the others with EDOT and thiophene as the donor units. In the case of EDOT, polymers had lower band gaps and faster switching times. In contrast with dibenzophenazine and dipenzopyridoquinoxaline, the use of tetrahydrodibenzophenazine as the acceptor unit enhanced the solubility of the resulting monomers, significantly. Also in this case polymers bearing thiophene and EDOT showed multichromic properties.

In this study, eight different acceptor units which are coupled with 3-hexylthiophene were synthesized and the polymers obtained from these revealed different characteristics. After the investigation of the optical and electronic properties of these polymers, one can say that the polymers with thienopyrazine unit has multichromic properties, the polymer with pyrazinoquinoxaline unit has almost black

color in its oxidized state, the polymer with thiadiazoloquinoxaline unit has the lowest bad gap and the polymer with benzoselenadiazole unit is highly soluble.

In conclusion, by wise selection of donor-acceptor couples one can optimize solubility properties, low band gap phenomena and electrochromic properties of the resulting polymers.
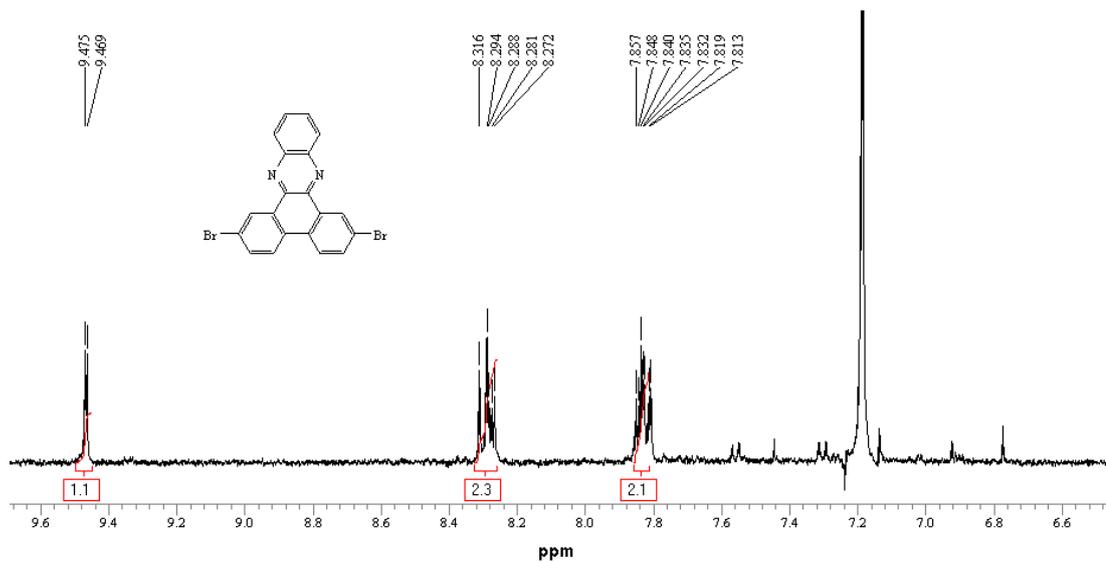
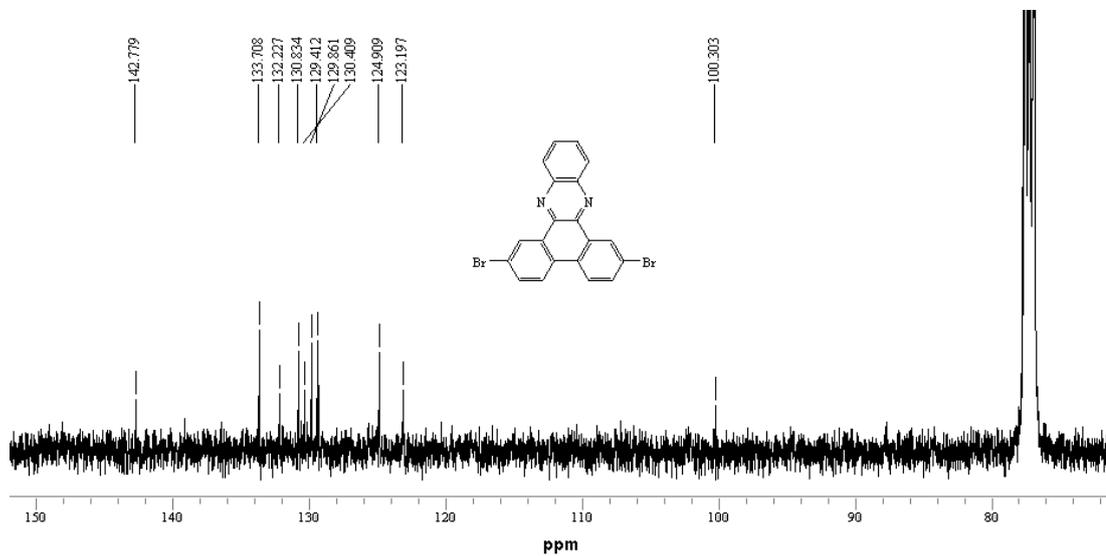**Figure 46** ^{1}H-NMR spectrum of 2,7-dibromodibenzo[*a,c*]phenazine **26.**

Figure 47 ^{13}C-NMR spectrum of 2,7-dibromodibenzo[*a,c*]phenazine**26.**
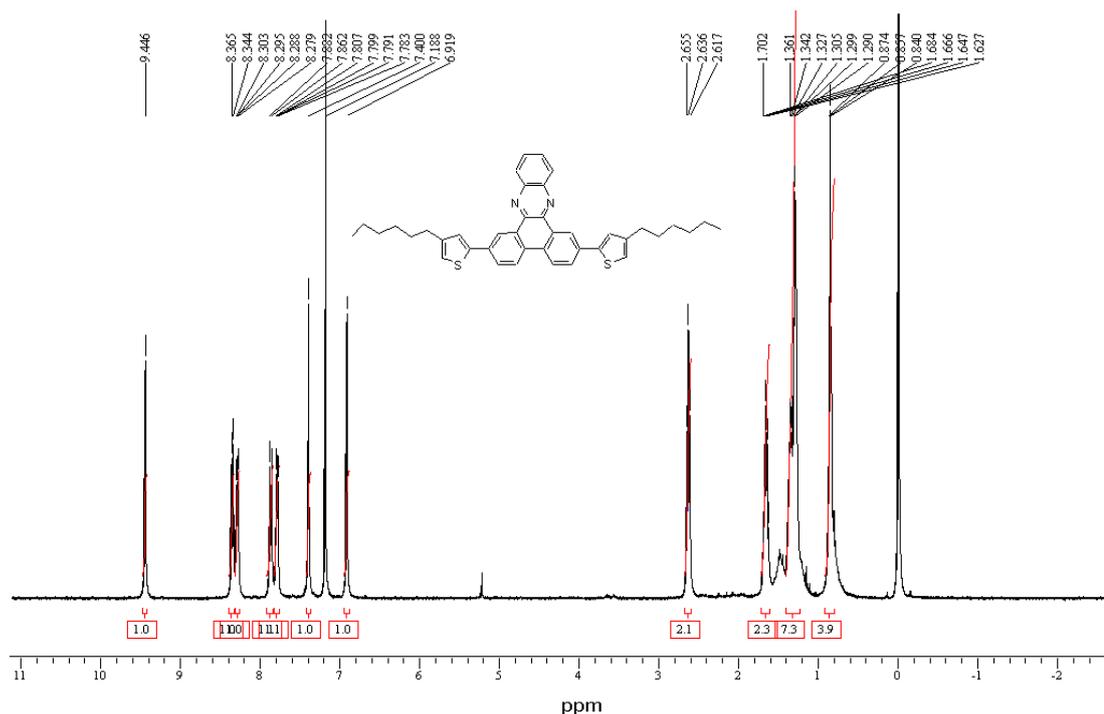
Figure 48 ^{1}H-NMR spectrum of 2,7-bis(4-hexylthiophen-2-yl)dibenzo[*a,c*] phenazine **29.**
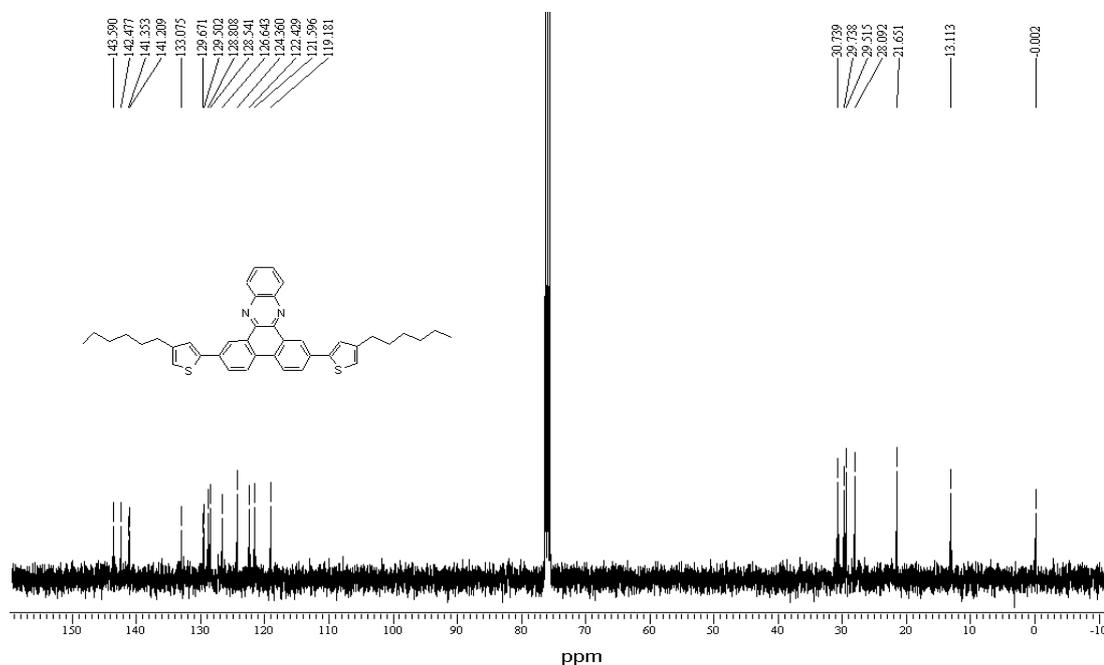
Figure 49 ^{13}C-NMR spectrum of 2,7-bis(4-hexylthiophen-2-yl)dibenzo[*a,c*] phenazine **29.**
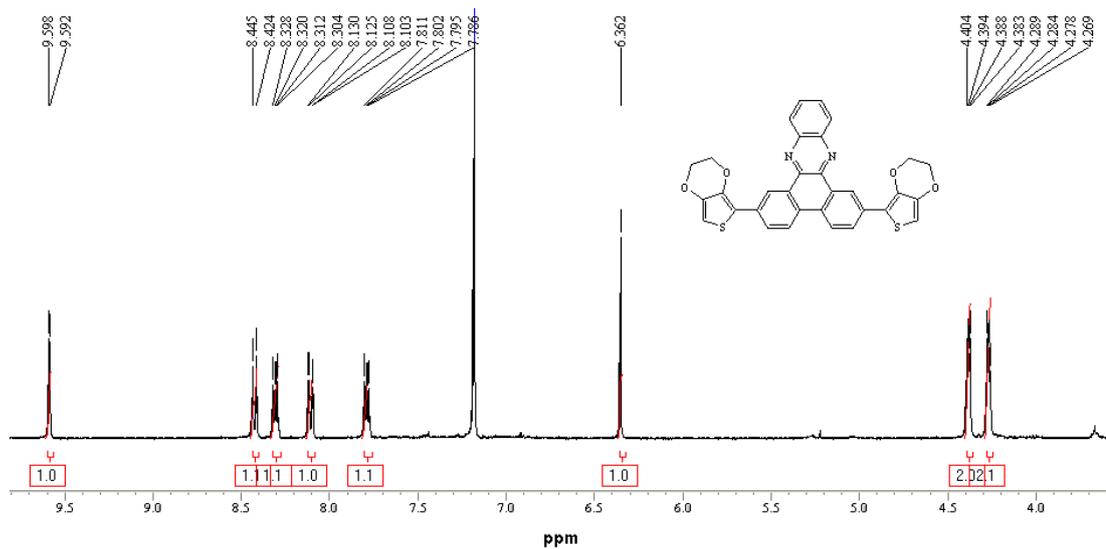
Figure 50 [superscript 1]H-NMR spectrum of 2,7-bis(2,3-dihydrothieno[3,4-*b*][1,4]dioxin-5-yl)dibenzo[*a,c*]phenazine **30.**
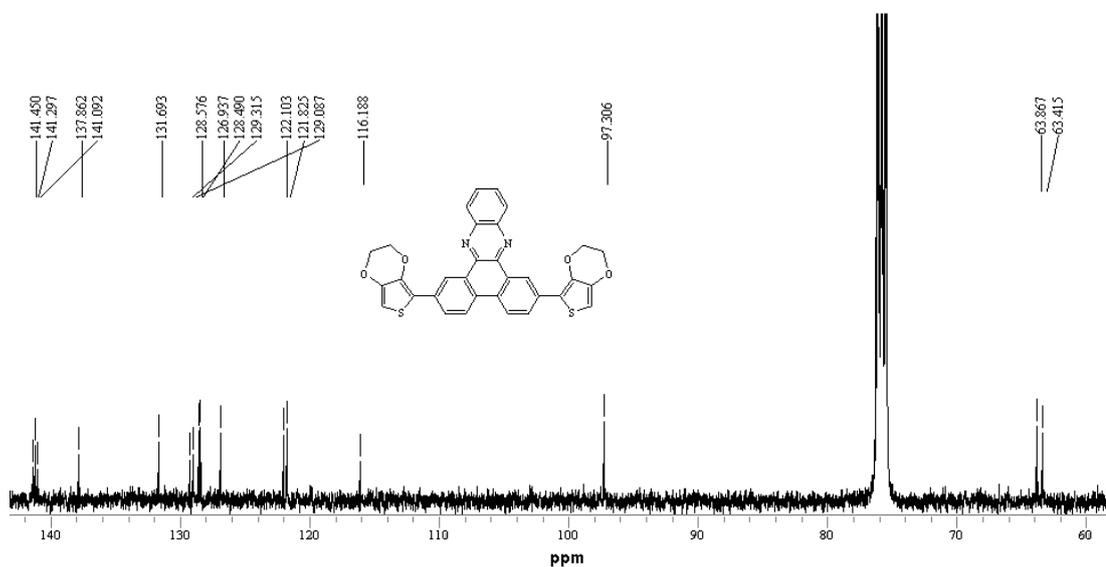
Figure 51 [superscript 13]C-NMR spectrum of 2,7-bis(2,3-dihydrothieno[3,4-*b*][1,4]dioxin-5-yl) dibenzo[*a,c*]phenazine **30.**
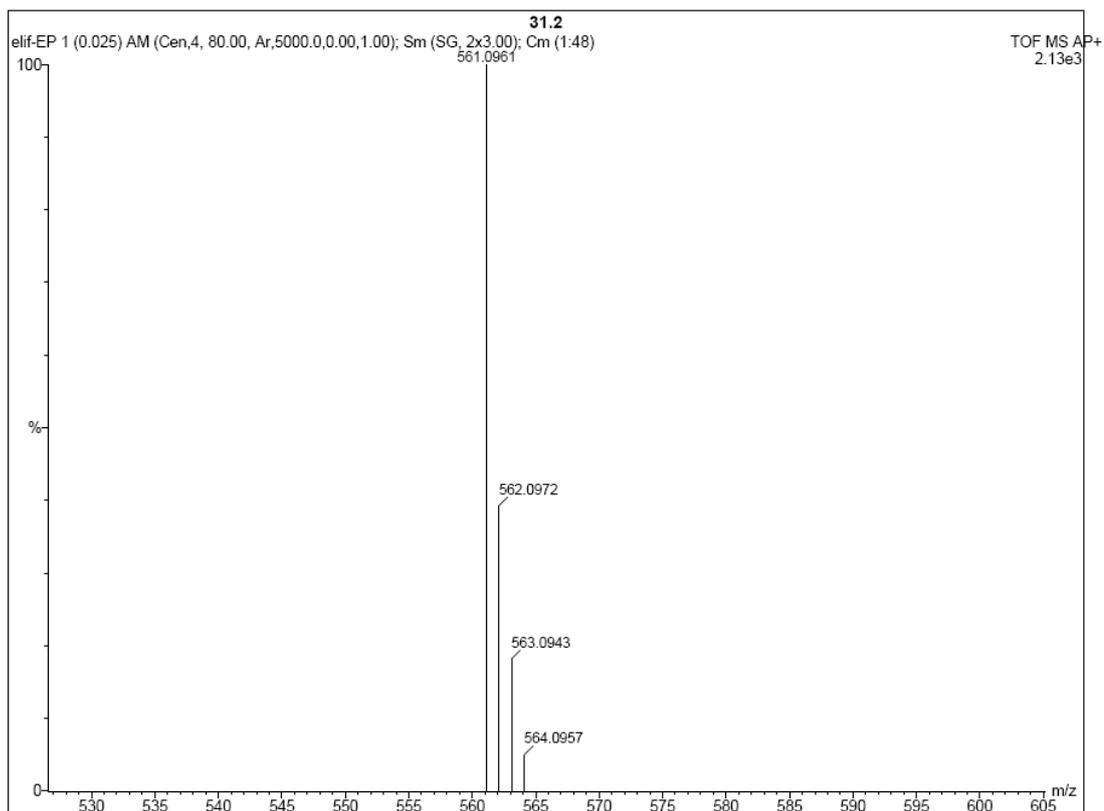
Figure 52 HRMS spectrum of 2,7-bis(2,3-dihydrothieno[3,4-*b*][1,4]dioxin-5-yl) dibenzo[*a,c*]phenazine **30.**
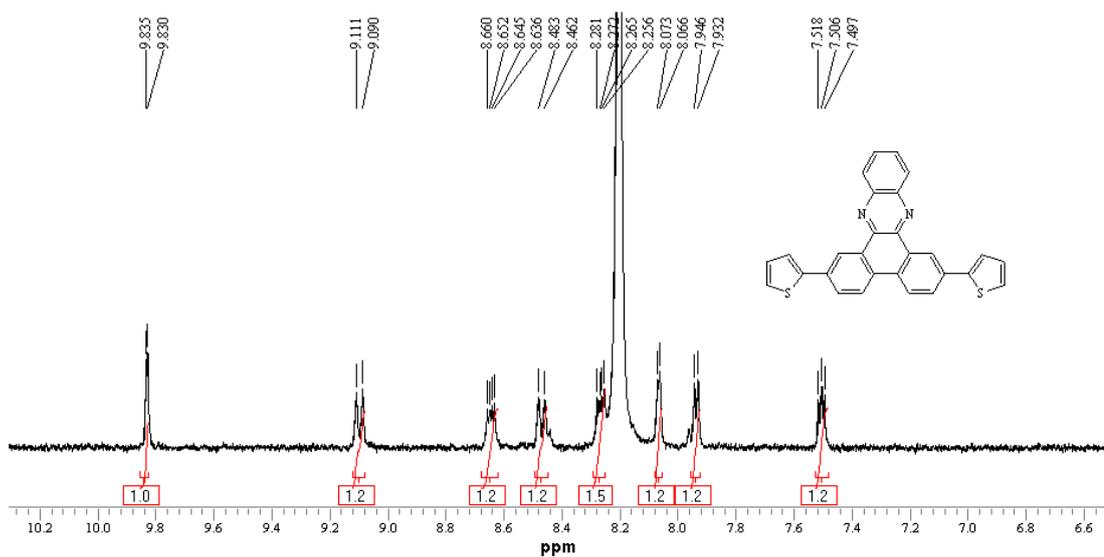
Figure 53 ^{1}H-NMR spectrum of 2,7-di(thiophen-2-yl)dibenzo[*a,c*]phenazine **31.**
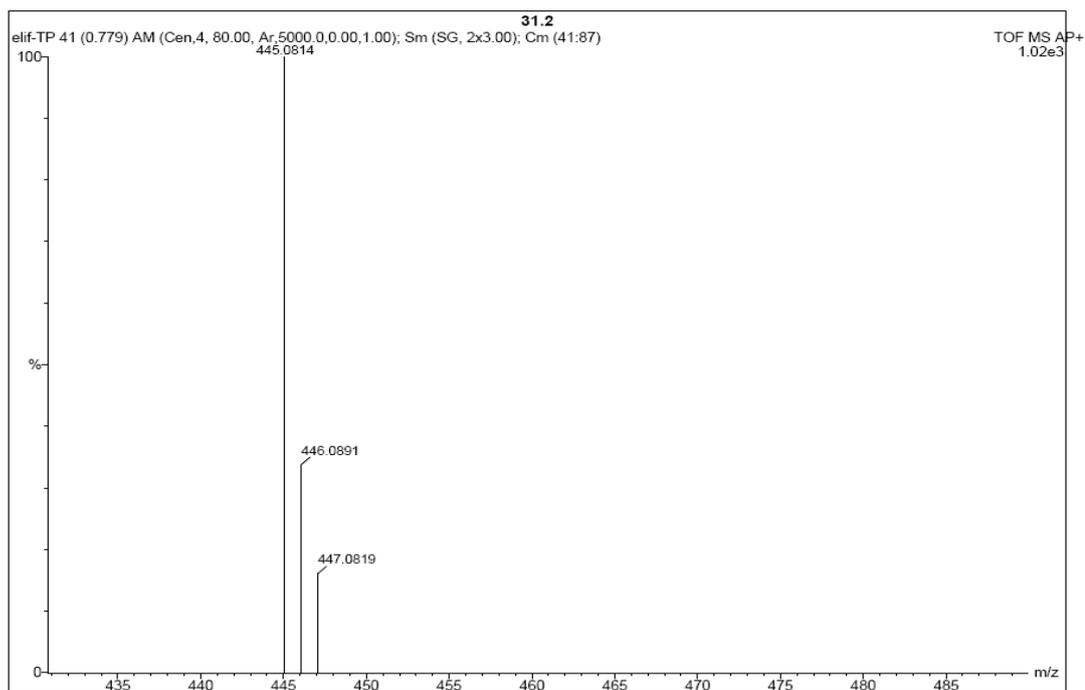
Figure 54 HRMS spectrum of 2,7-di(thiophen-2-yl)dibenzo[*a,c*]phenazine **31.**
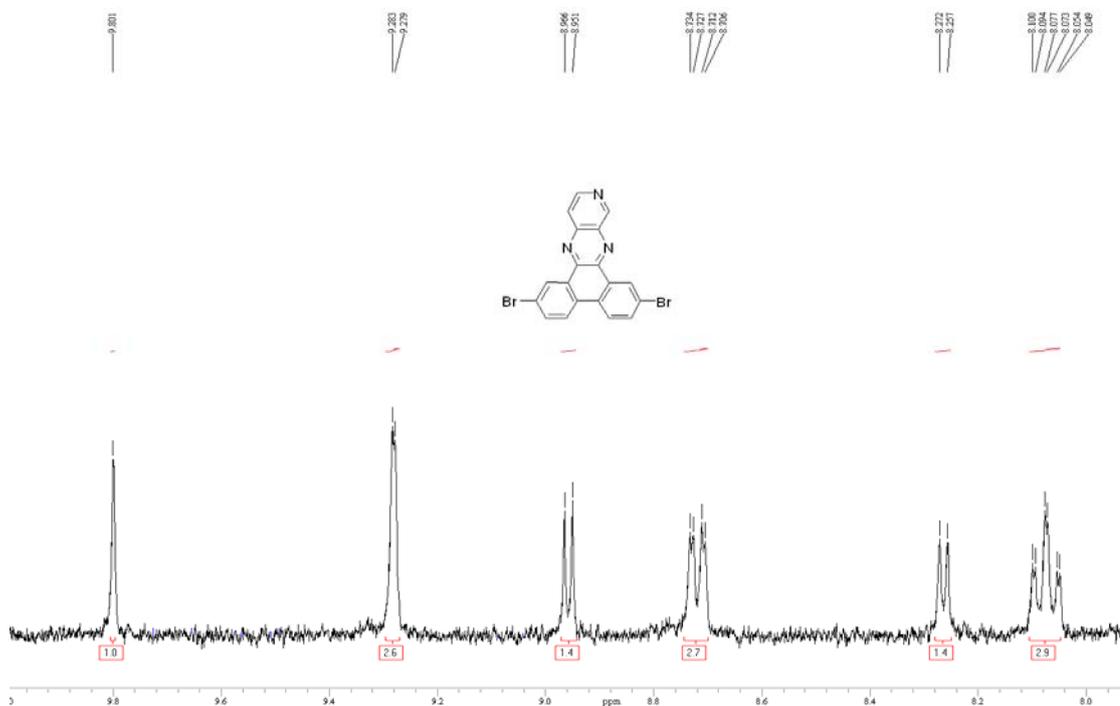
Figure 55 ^{1}H-NMR spectrum of 2,7-dibromodibenzo[*f,h*]pyrido[3,4-*b*]quinoxaline **27.**
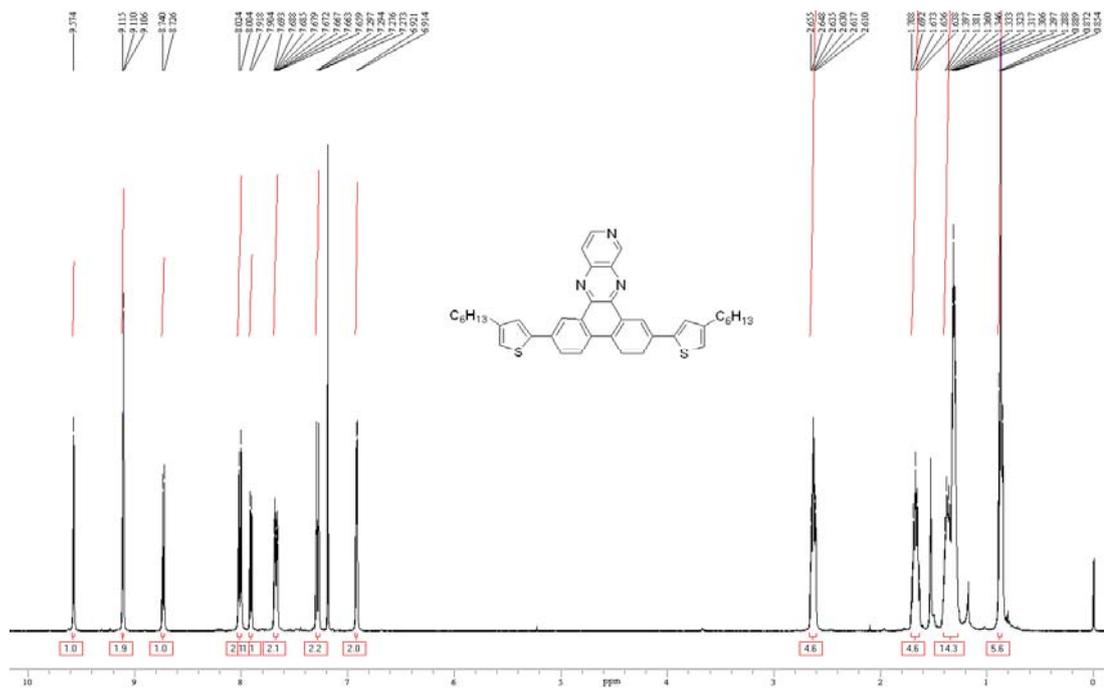
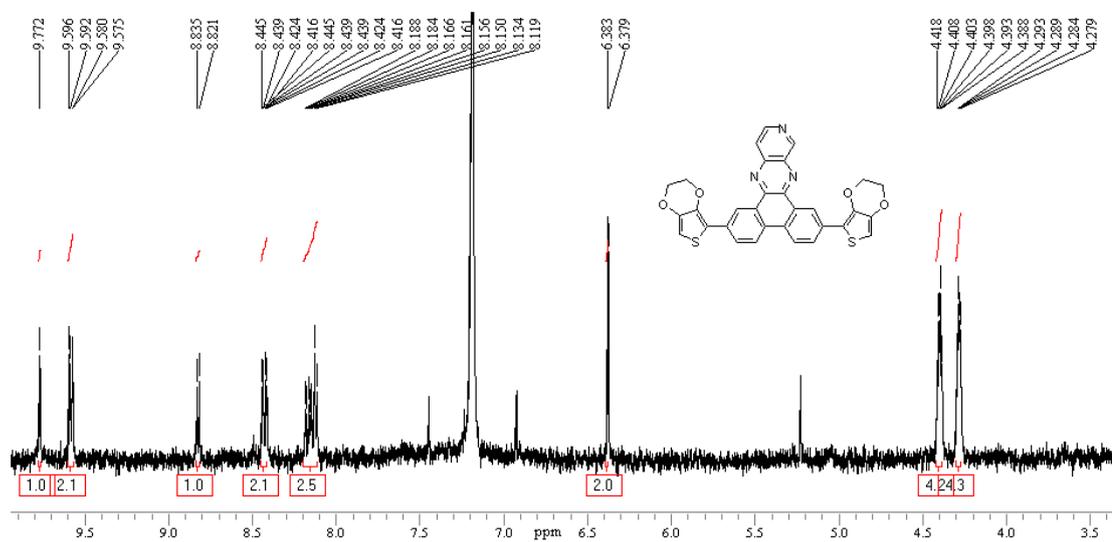**Figure 56** ¹H-NMR spectrum of 2,7-bis(4-hexylthiophen-2-yl)dibenzo[*f,h*]pyrido [3,4-*b*]quinoxaline **32.**
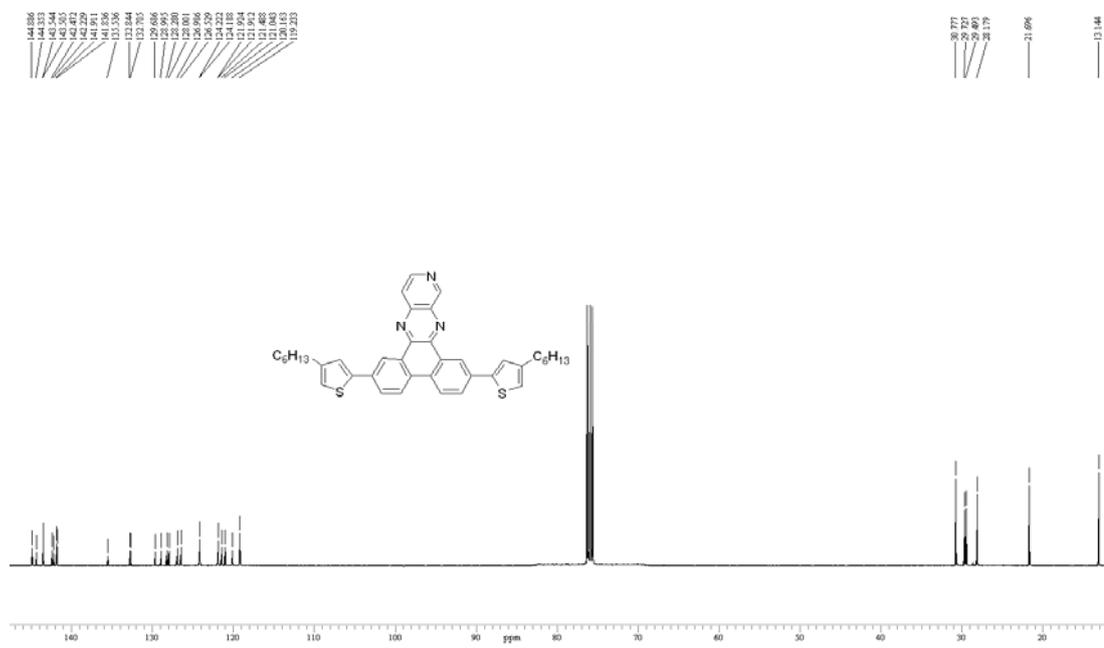
Figure 57 ¹³C-NMR spectrum of 2,7-bis(4-hexylthiophen-2-yl)dibenzo[*f,h*]pyrido [3,4-*b*]quinoxaline **32.**
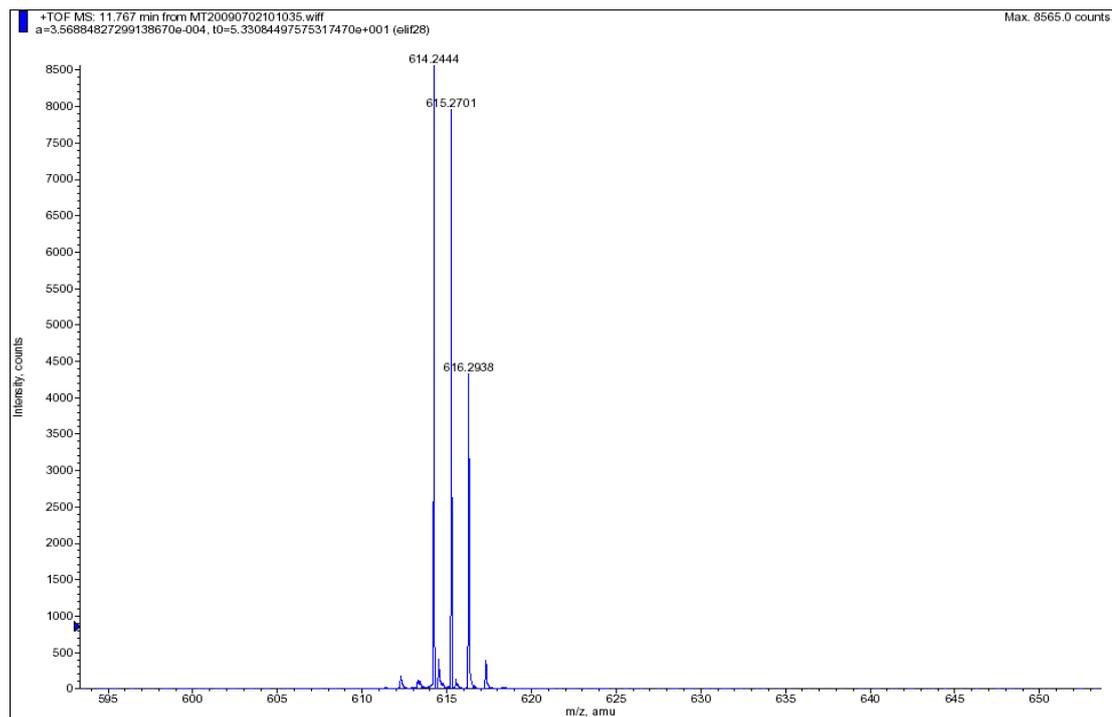
Figure 58 HRMS spectrum of 2,7-bis(4-hexylthiophen-2-yl)dibenzo[*f,h*]pyrido [3,4-*b*]quinoxaline **32.**

Figure 59 ¹H-NMR spectrum of 2,7-bis(2,3-dihydrothieno[3,4-*b*][1,4]dioxin-5-yl)dibenzo[*f,h*]pyrido[3,4-*b*] quinoxaline **33.**
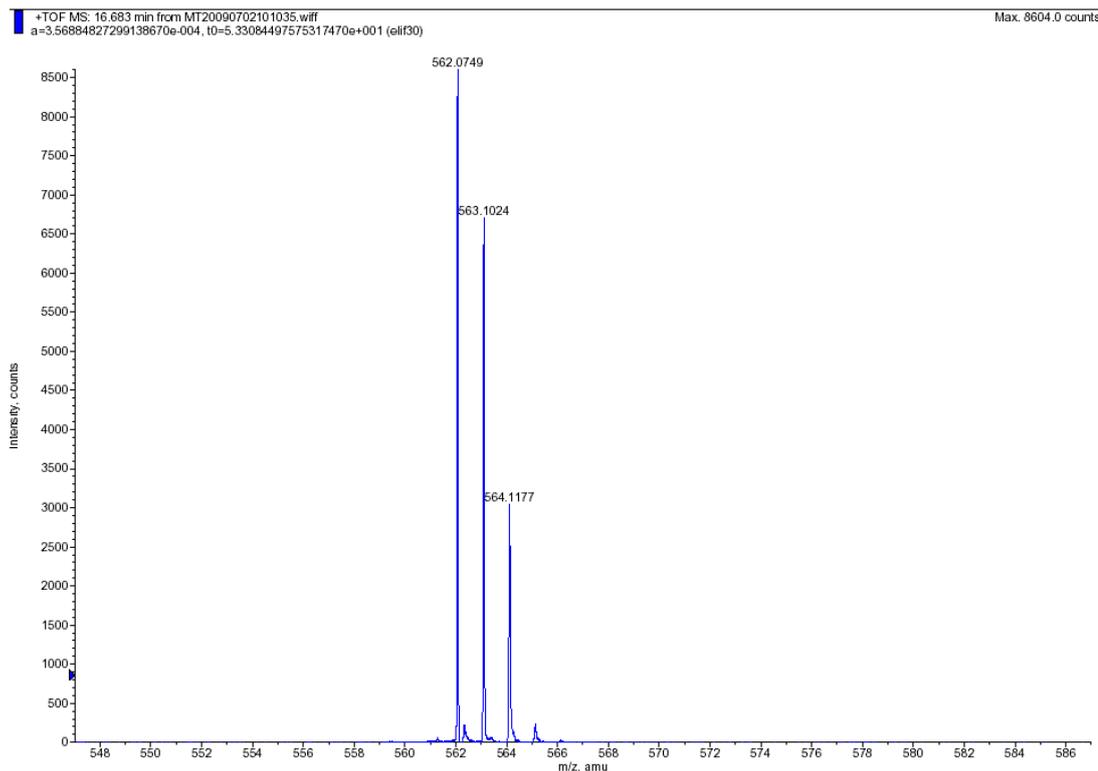
Figure 60 HRMS spectrum of 2,7-bis(2,3-dihydrothieno[3,4-*b*][1,4]dioxin-5-yl)dibenzo[*f,h*]pyrido[3,4-*b*] quinoxaline **33.**
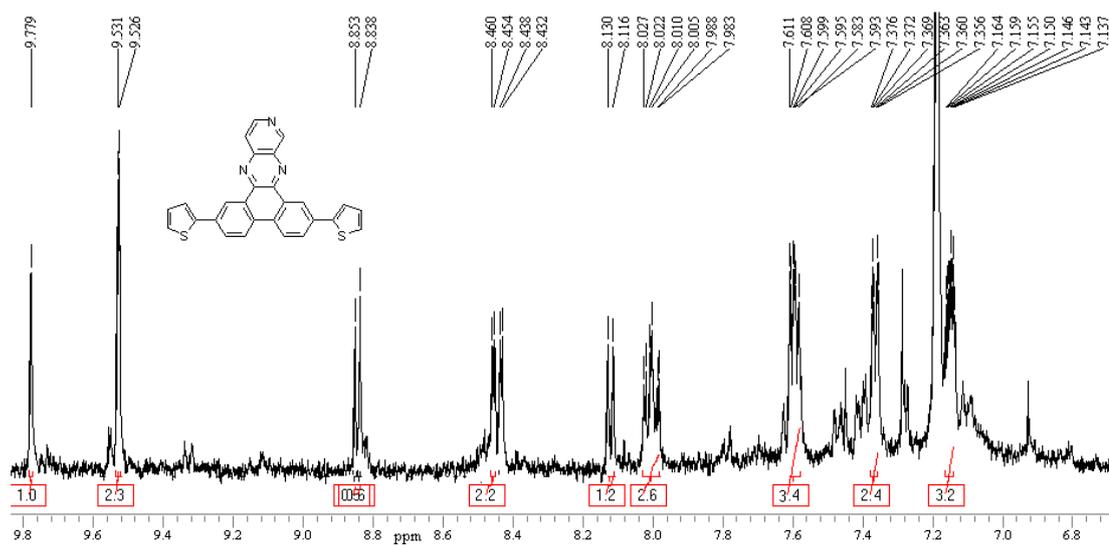

Figure 61 [^1]H-NMR spectrum of 2,7-di(thiophen-2-yl)dibenzo[*f,h*]pyrido[3,4-*b*]quinoxaline **34.**
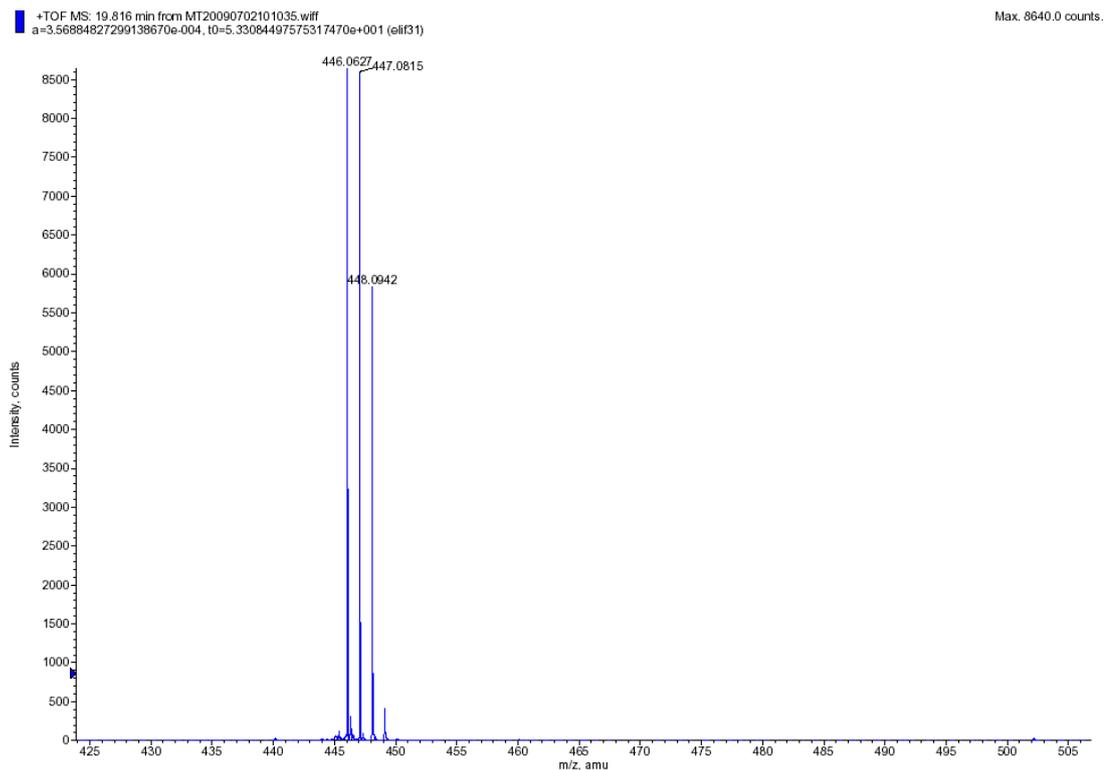
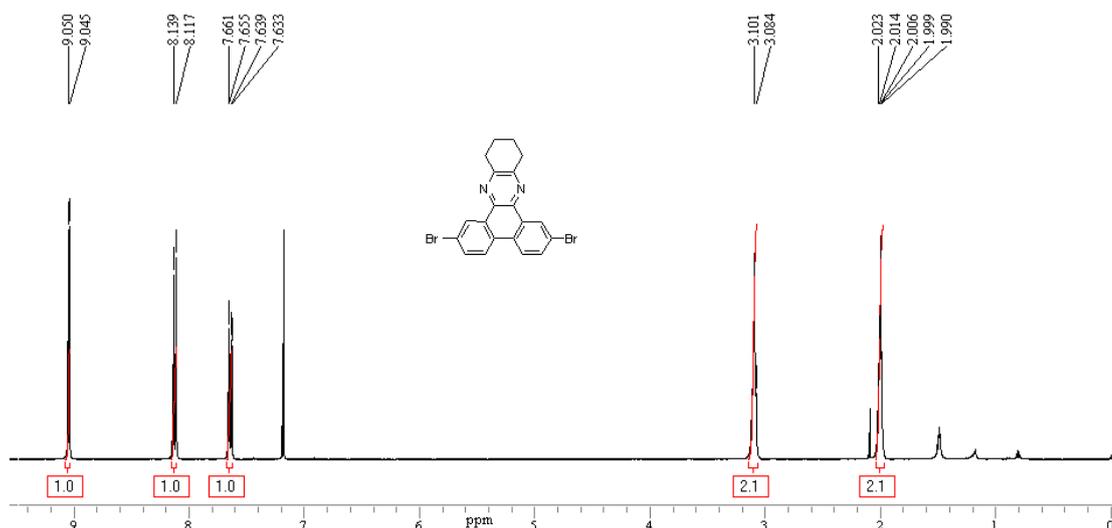**Figure 62** HRMS spectrum of 2,7-di(thiophen-2-yl)dibenzo[*f,h*]pyrido[3,4-*b*]quinoxaline **34.**

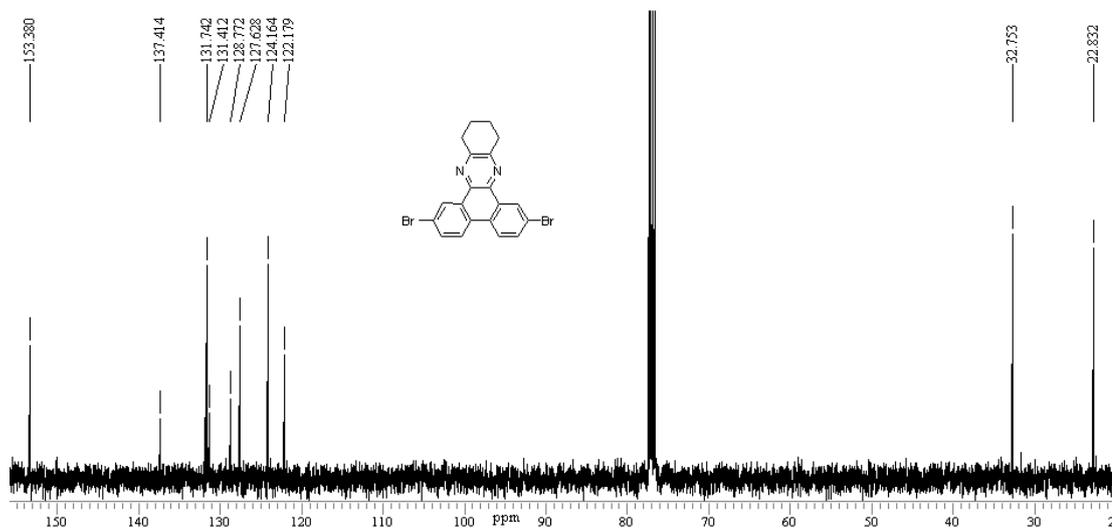**Figure 63** ^{1}H-NMR spectrum of 2,7-dibromo-10,11,12,13-tetrahydrodibenzo[*a,c*]phenazine **28.**

Figure 64 ^{13}C-NMR spectrum of 2,7-dibromo-10,11,12,13-tetrahydrodibenzo[*a,c*]phenazine **28.**
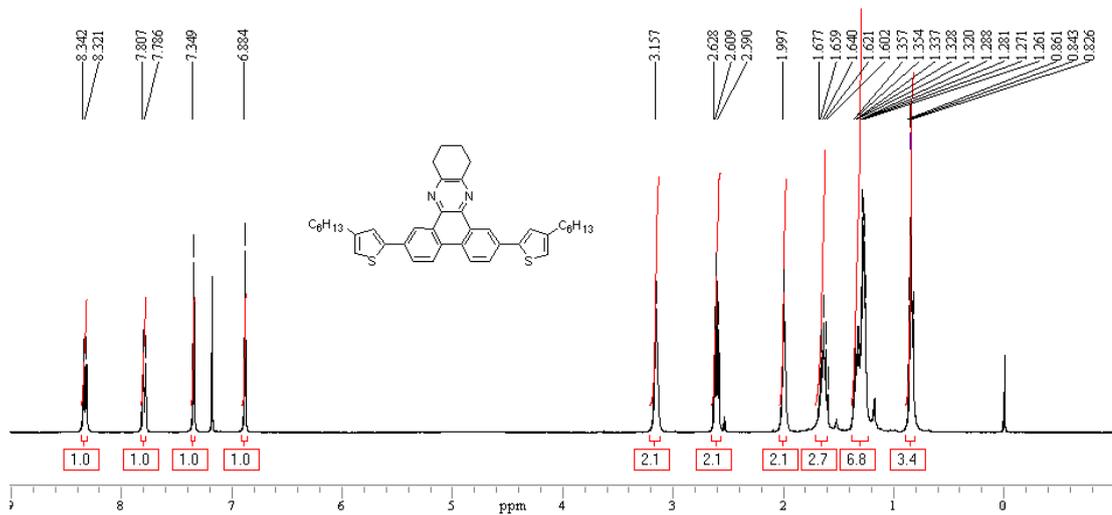

Figure 65 ^{1}H-NMR spectrum of 2,7-bis(4-hexylthiophen-2-yl)-10,11,12,13-tetrahydrodibenzo[*a,c*] phenazine **35.**
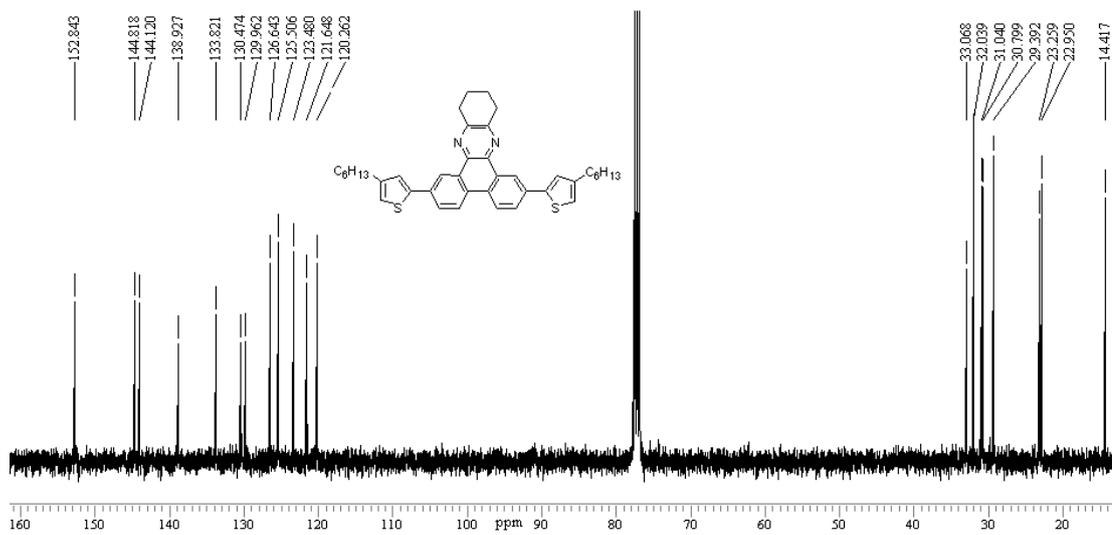
Figure 66 ^{13}C-NMR spectrum of 2,7-bis(4-hexylthiophen-2-yl)-10,11,12,13-tetrahydrodibenzo[*a,c*] phenazine **35.**
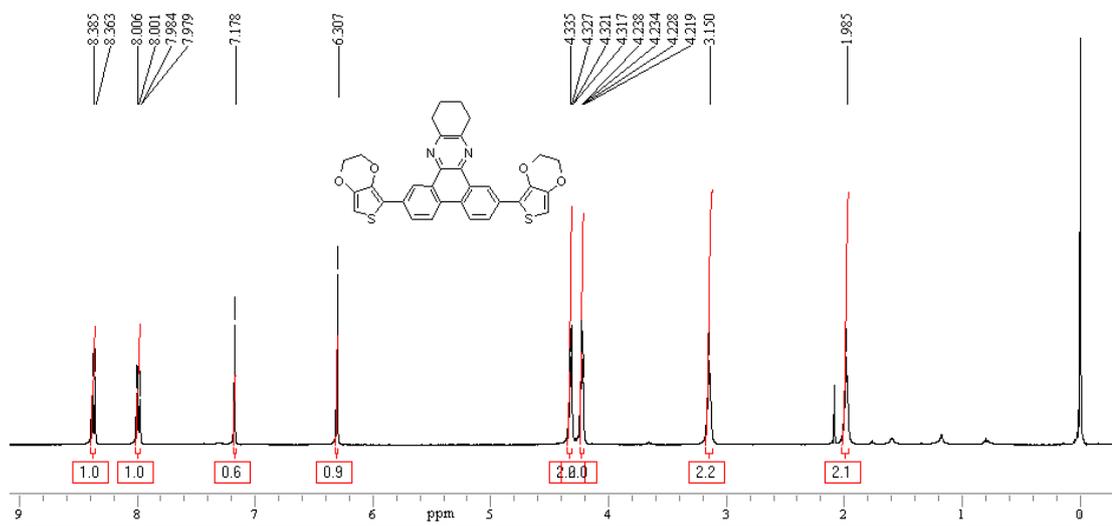

Figure 67 ^{1}H-NMR spectrum of 2,7-bis(2,3-dihydrothieno[3,4-*b*][1,4]dioxin-5-yl)-10,11,12,13-tetrahydrodibenzo [*a,c*]phenazine **36.**
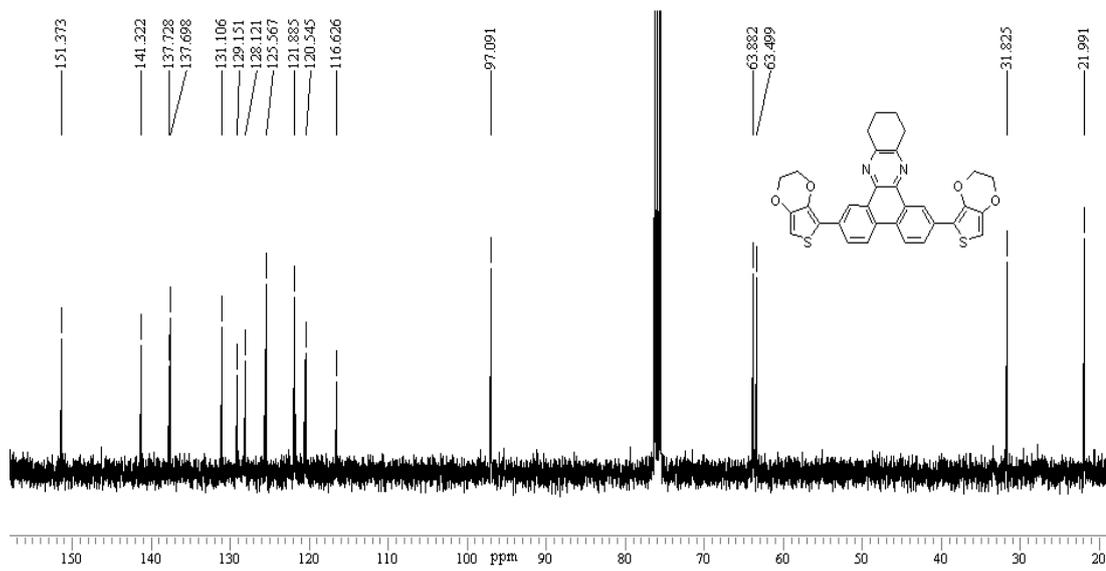
Figure 68 ^{13}C-NMR spectrum of 2,7-bis(2,3-dihydrothieno[3,4-*b*][1,4]dioxin-5-yl)-10,11,12,13-tetrahydrodibenzo [*a,c*]phenazine **36.**
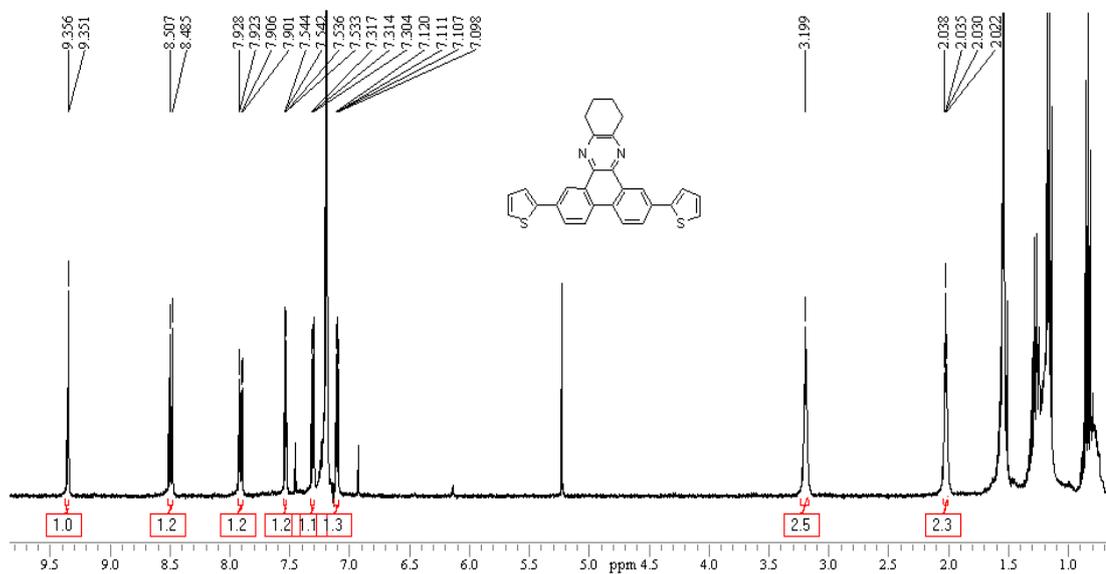

Figure 69 ^{1}H-NMR spectrum of 2,7-di(thiophen-2-yl)-10,11,12,13-tetrahydrodibenzo[*a,c*]phenazine **37.**

137

Figure 70 ^{1}H-NMR spectrum of 4,7-bis(4-hexylthiophen-2-yl)-5,6-dinitrobenzo[*c*][1,2,5]thiadiazole **40.**

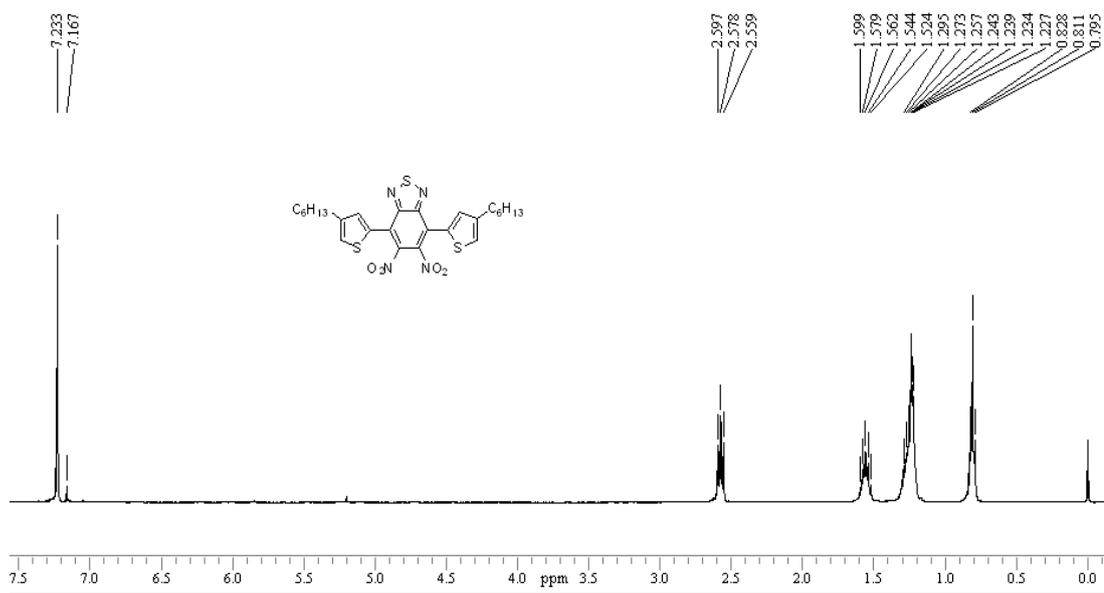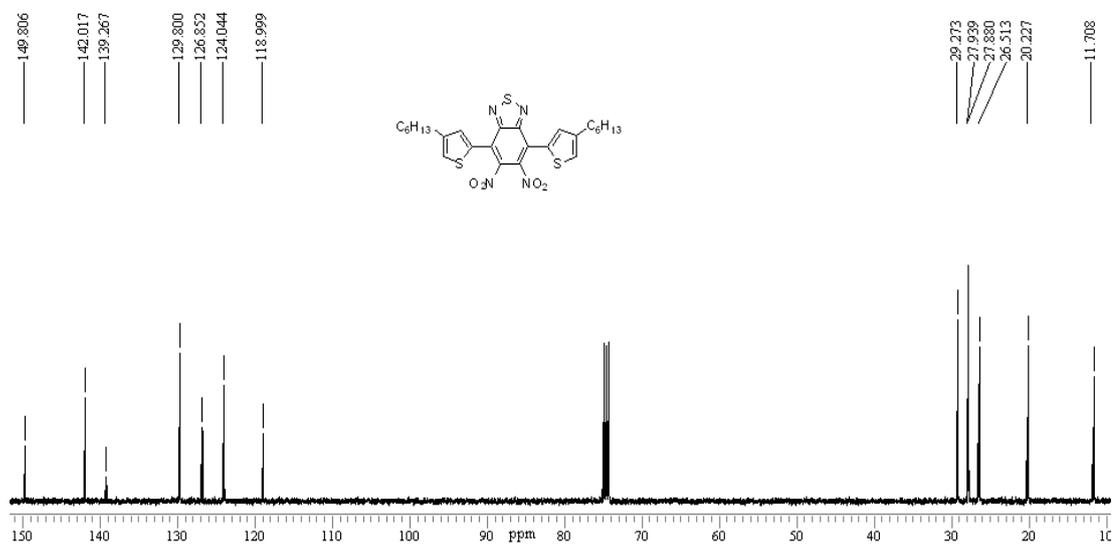**Figure 71** ^{13}C-NMR spectrum of 4,7-bis(4-hexylthiophen-2-yl)-5,6-dinitrobenzo[*c*][1,2,5]thiadiazole **40.**

138
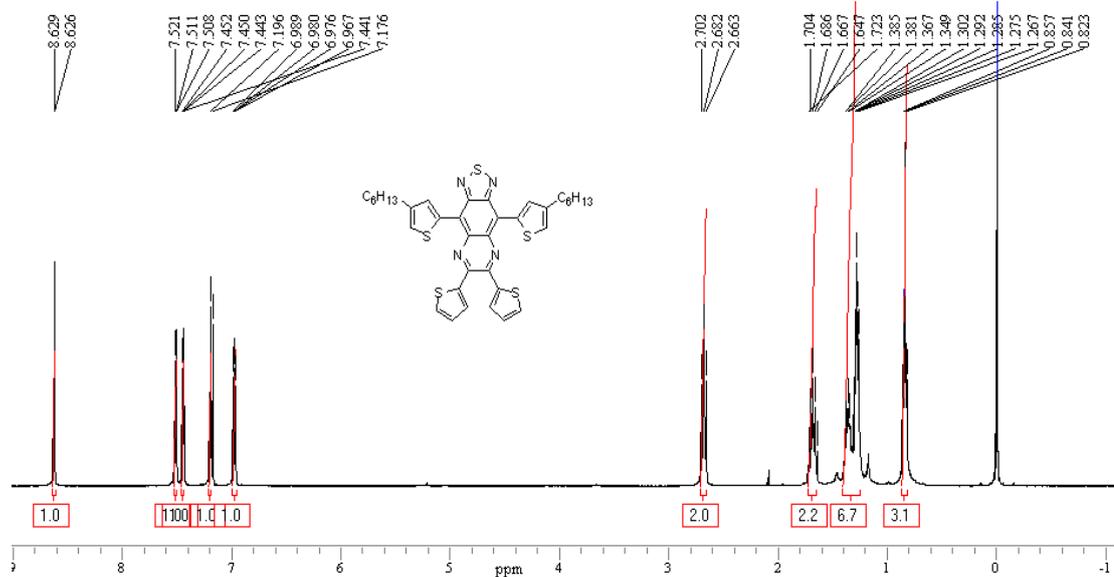
Figure 72 ^{1}H-NMR spectrum of 4,9-bis(4-hexylthiophen-2-yl)-6,7-di(thiophen-2-yl)-[1,2,5]thiadiazolo[3,4-*g*] quinoxaline **43.**
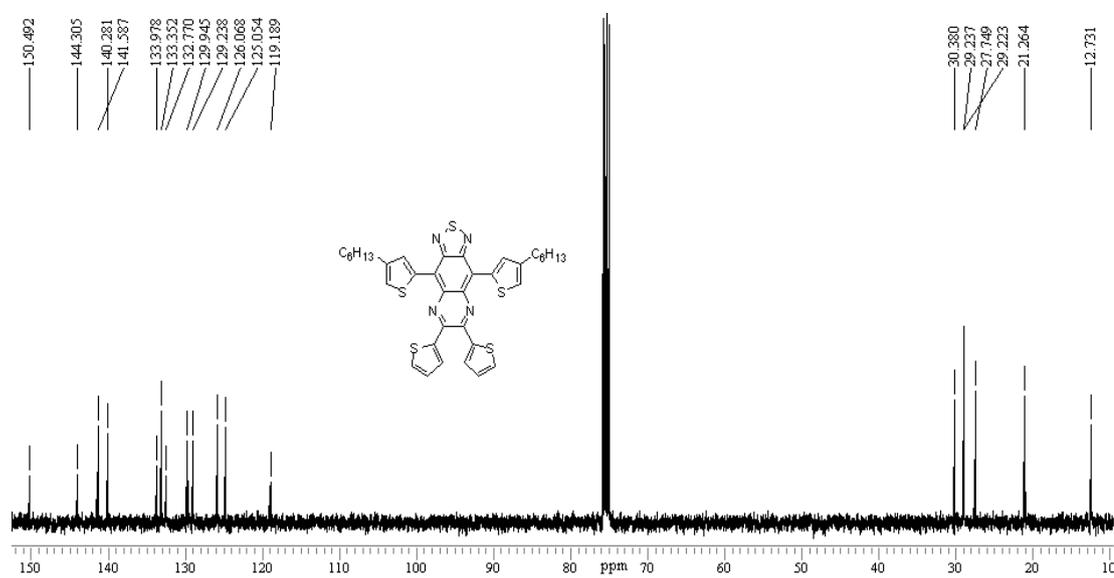
Figure 73 ^{13}C-NMR spectrum of 4,9-bis(4-hexylthiophen-2-yl)-6,7-di(thiophen-2-yl)-[1,2,5]thiadiazolo[3,4-*g*] quinoxaline **43.**
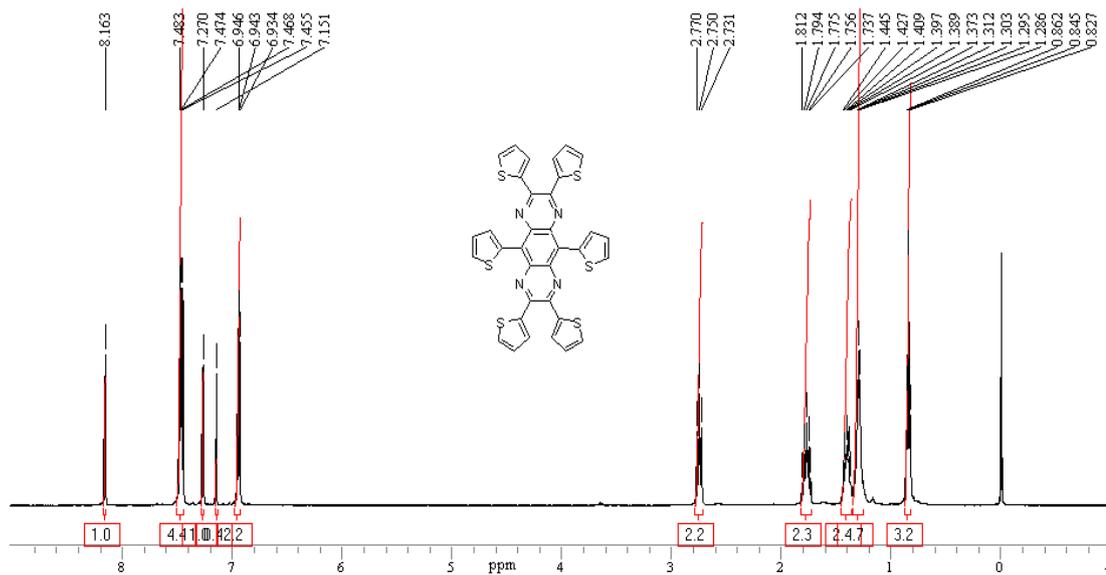
Figure 74 ^{1}H-NMR spectrum of 5,10-bis(4-hexylthiophen-2-yl)-2,3,7,8-tetra(thiophen-2-yl)pyrazino[2,3-*g*] quinoxaline **44.**
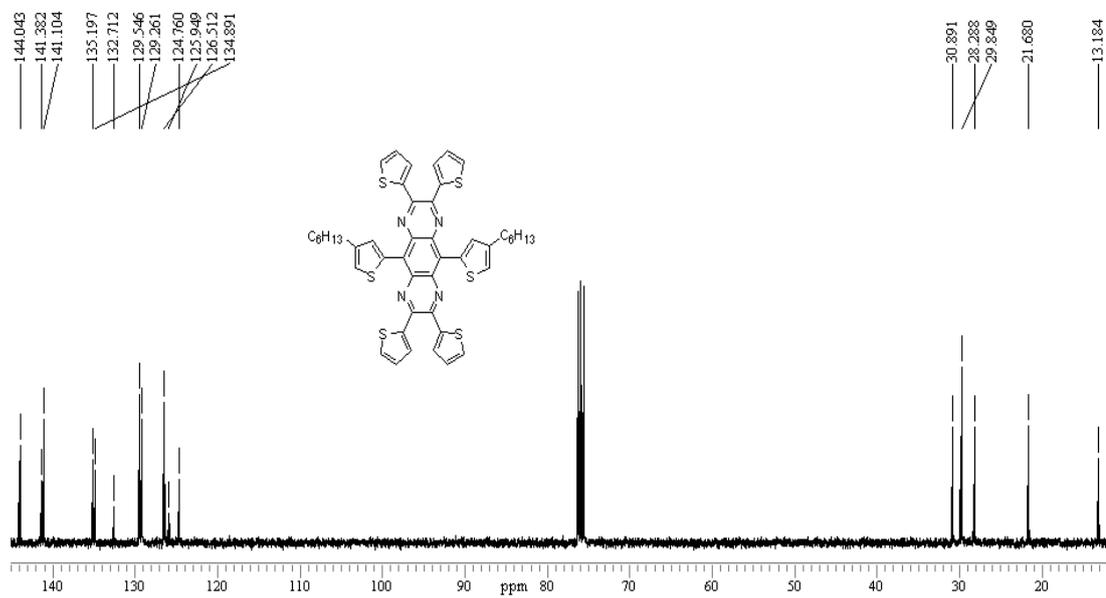
Figure 75 ^{13}C-NMR spectrum of 5,10-bis(4-hexylthiophen-2-yl)-2,3,7,8-tetra(thiophen-2-yl)pyrazino[2,3-*g*] quinoxaline **44.**
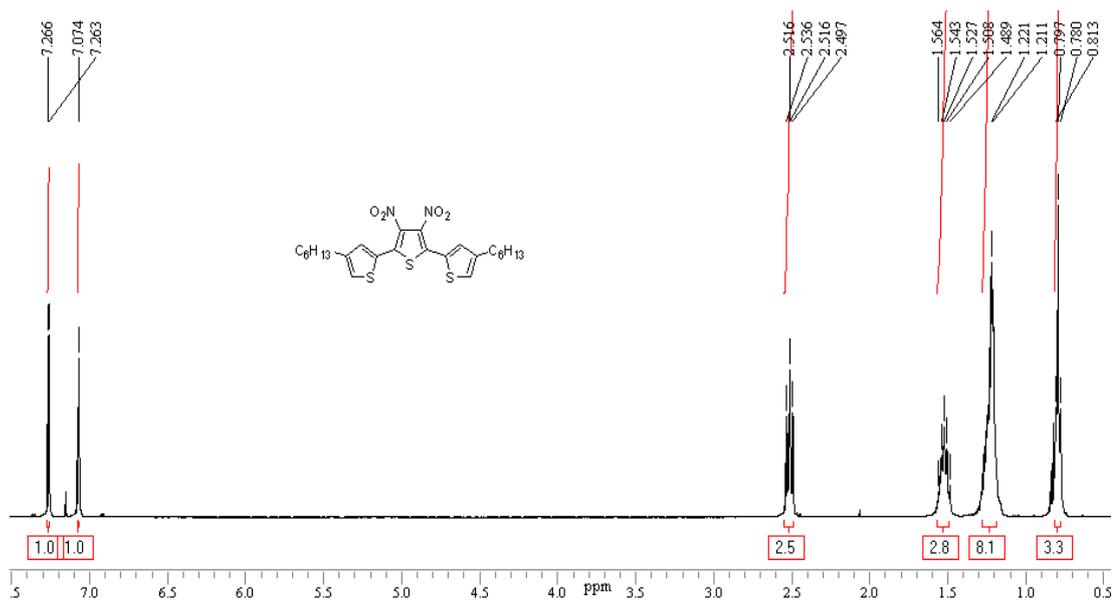
Figure 76 ^{1}H-NMR spectrum of 5-5'-bis(4-hexylthiophen-2-yl)-3,4-dinitrothiophene **46.**
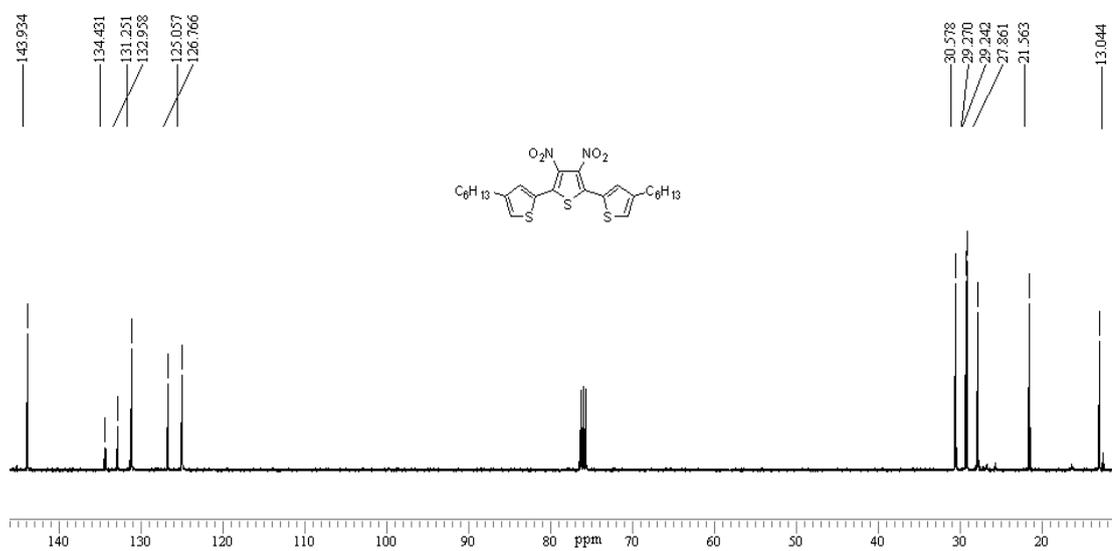
Figure 77 ^{13}C-NMR spectrum of 5-5'-bis(4-hexylthiophen-2-yl)-3,4-dinitrothiophene **46.**
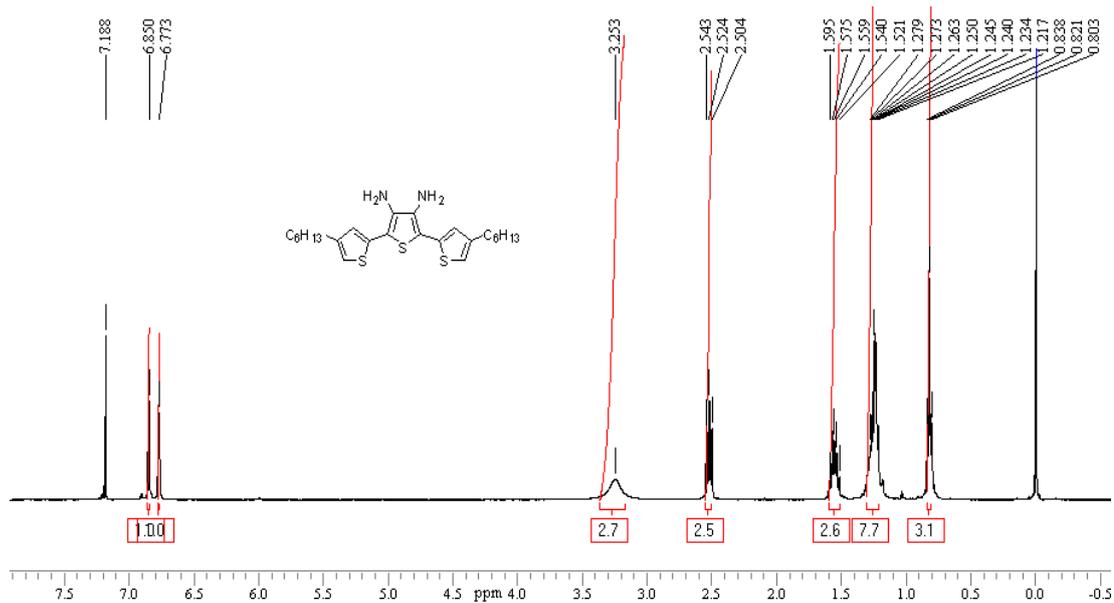
Figure 78 ¹H-NMR spectrum of 5-5'-bis(4-hexylthiophen-2-yl)-3,4-diaminothiophene **47.**
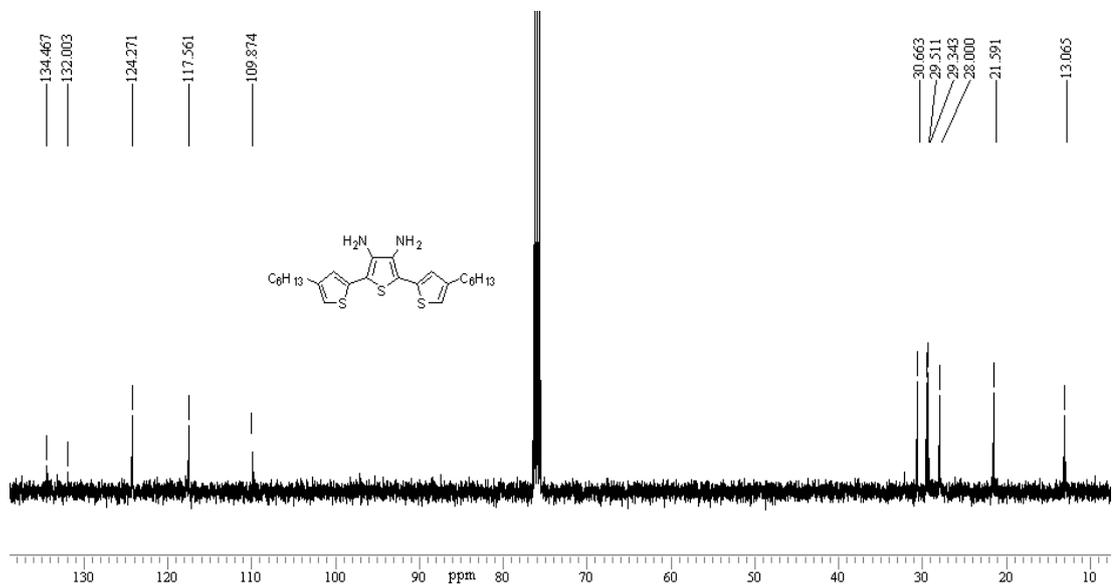
Figure 79 ¹³C-NMR spectrum of 5-5'-bis(4-hexylthiophen-2-yl)-3,4-diaminothiophene **47.**
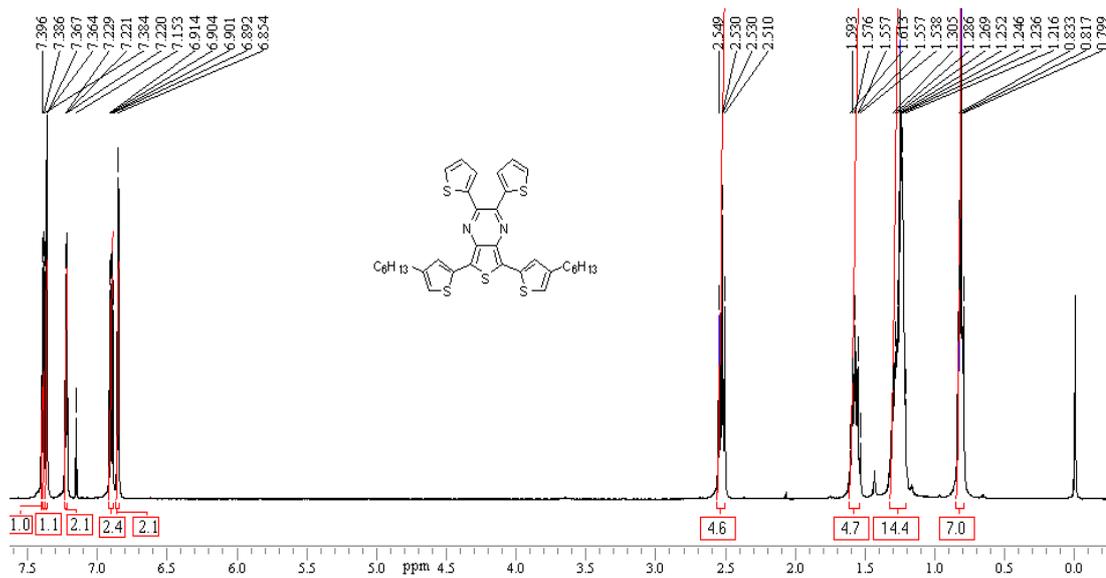
Figure 80 ^{1}H-NMR spectrum of 5,7-bis(4-hexylthiophen-2-yl)-2,3-di(thiophen-2-yl)thieno[3,4-*b*]pyrazine **48.**
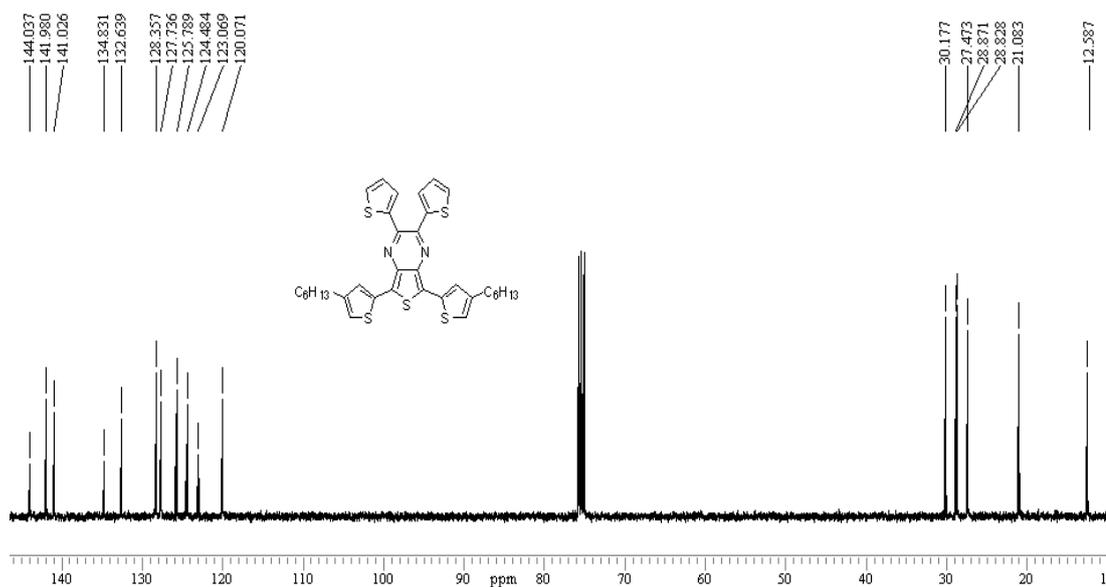
Figure 81 ^{13}C-NMR spectrum of 5,7-bis(4-hexylthiophen-2-yl)-2,3-di(thiophen-2-yl)thieno[3,4-*b*]pyrazine **48.**

143
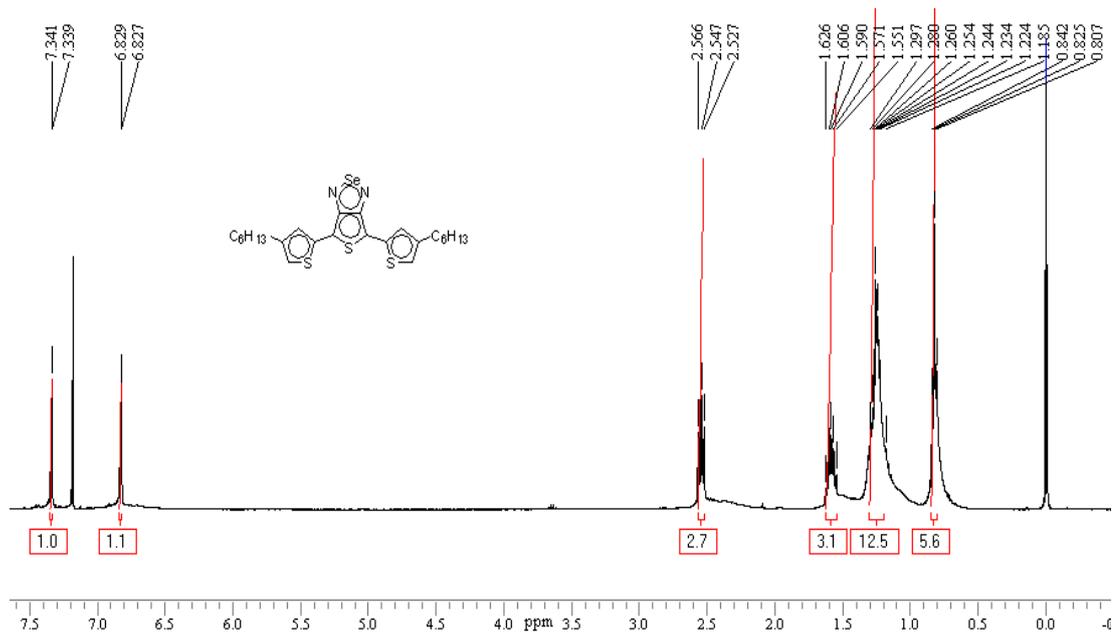
Figure 82 ¹H-NMR spectrum of 4,6-bis(4-hexylthiophen-2-yl)-4,6-dihydrothieno[3,4-*c*][1,2,5] selenadiazole **49.**
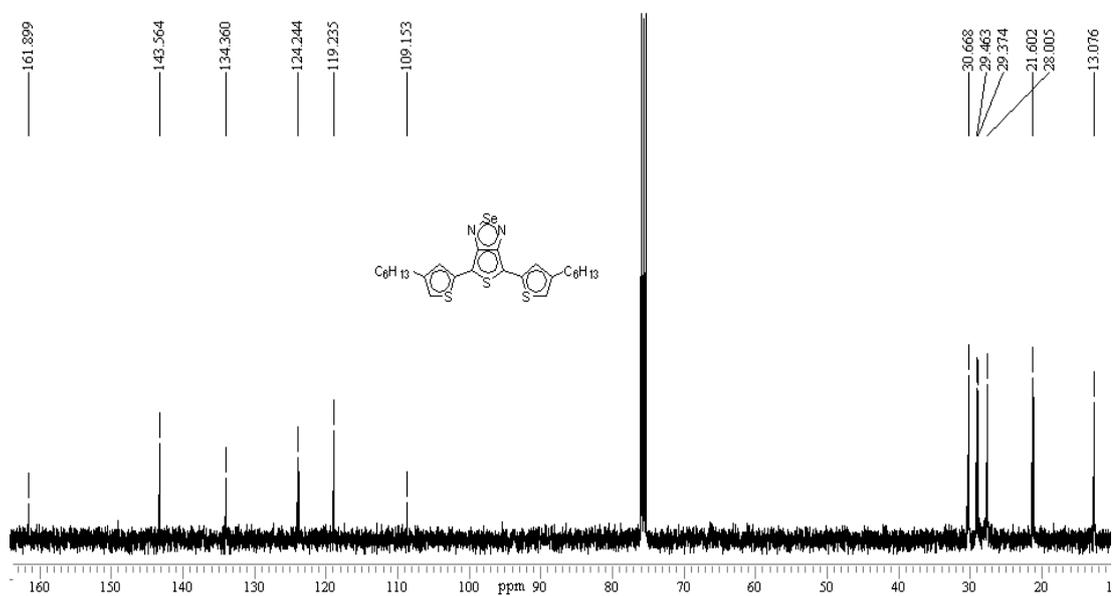
Figure 83 ¹³C-NMR spectrum of 4,6-bis(4-hexylthiophen-2-yl)-4,6-dihydrothieno[3,4-*c*][1,2,5] selenadiazole **49.**
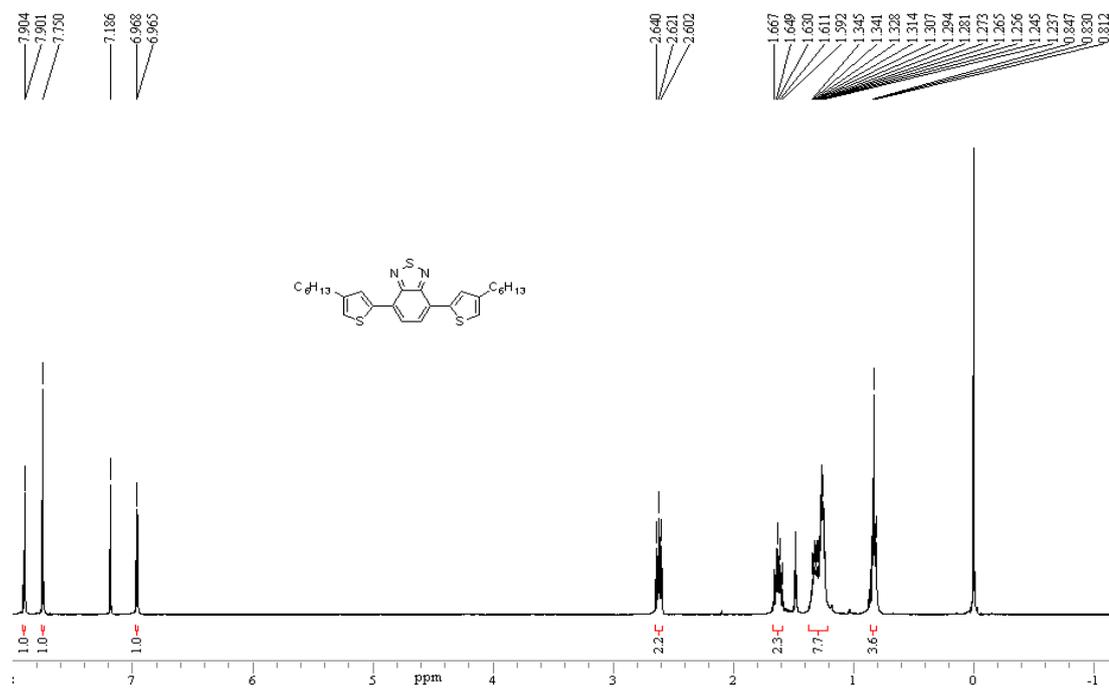
Figure 84 ^{1}H-NMR spectrum of 4,7-bis(4-hexylthiophen-2-yl)benzo[*c*][1,2,5]thiadiazole **51.**
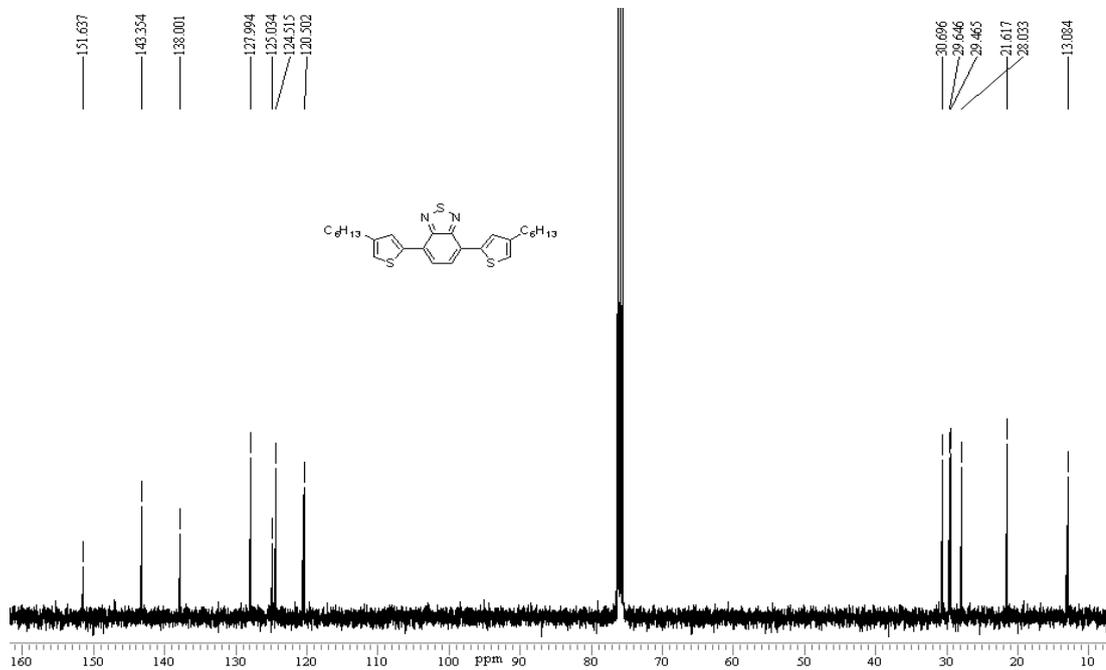
Figure 85 ^{13}C-NMR spectrum of 4,7-bis(4-hexylthiophen-2-yl)benzo[*c*][1,2,5]thiadiazole **51.**
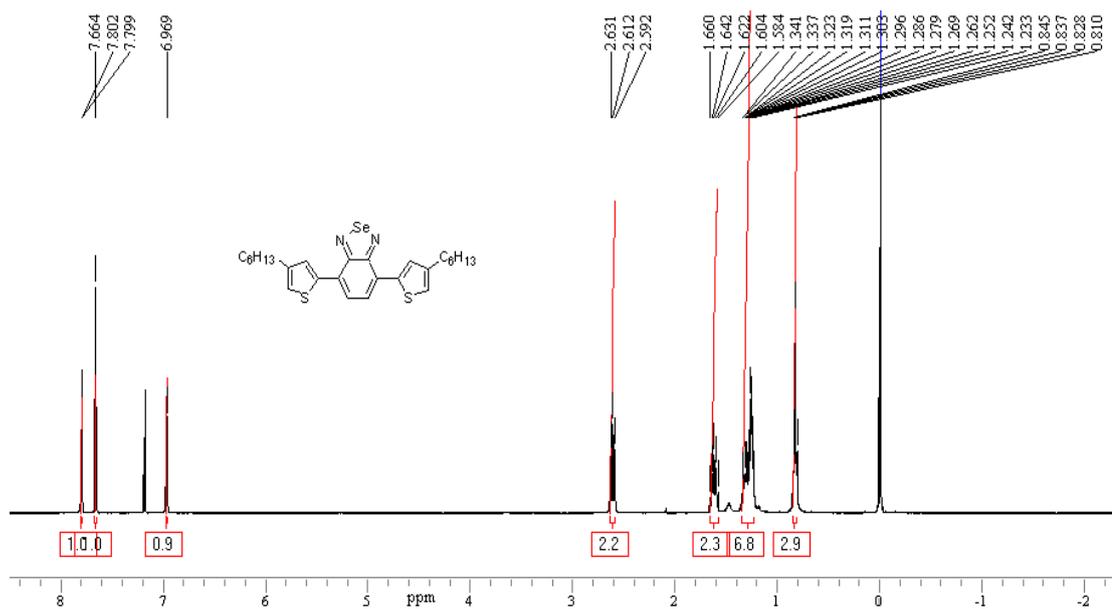
Figure   86   1H-NMR   spectrum   of   4,7-bis(4-hexylthiophen-2-yl)benzo[*c*][1,2,5]selenadiazole **53.**
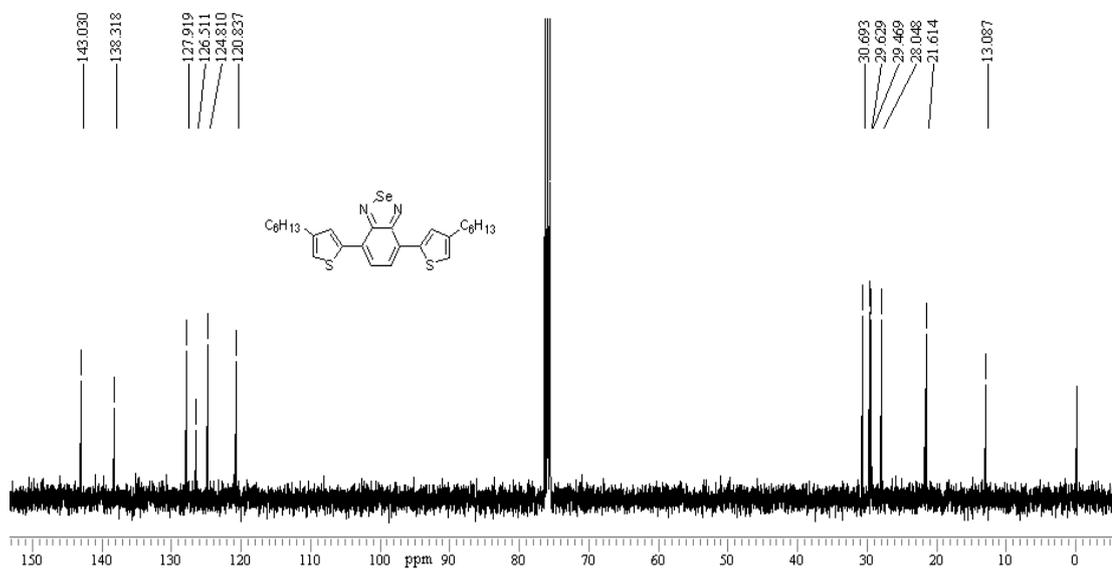
Figure   87 13C-NMR   spectrum   of   4,7-bis(4-hexylthiophen-2-yl)benzo[*c*][1,2,5] selenadiazole **53.**

REFERENCES

1. Scrosati, B., *Application of Electroactive Polymers, 1ˢᵗ Ed.*, Chapmen and Hall, London, 1993.

2. Letheby, H., J. Chem. Soc., 15, (1862) 161.

3. Monk, P.M.S, Mortimer, R.J., Rosseinsky, D.R., *Electrochromism and Electrochromic Devices*, Cambridge University Press, 2007.

4. Burroughes, J.H.; Bradley, D.D.C.; Brown, A.R.; Marks, R.N.; Mackay, K.; Friend, R.H.; Burns, P.L.; Holmes, A.B. Nature (London), 347, (1990) 539.

5. Kraft, A.; Grimsdale, A.C.; Holmes, A.B. Angew, Chem., Int.Ed. 37, (1998) 403.

6. Brabec, C.J.; Sariciftci, N.S.; Hummelen, J.C. Adv. Funct. Mater., 1, (2001) 15.

7. McQuade, D. T.; Pullen, A.E.; Swager, T.M. Chem. Rev., 100, (2000) 2537.

8. Knobloch, A.; Manuelli, A.; Bernds, A.; Clemens, W.J. Appl. Phys., 96, (2004) 2286.

9. Bredas, J.L.; Street, G.B. Acc. Chem. Res., 18, (1985) 309.

10. Chiang, C.K.; Fincher, C.R.; Park, Y.W.; Heeger, A.J.; Shirakawa, H.; Louis, E.J.; Gau, S.C.; McDiarmid, A.G. Phys. Reo. Lett. 39, (1977) 1098.

11. Türkaslan, Ö. *Sythesis and Characterization and Electrochromic Properties of Conducting Polymers of Terephlatic Acid Bis-(thiophene-3-ylmethyl)thiester Thiophene and Pyrrole and Conducting Polymer of 1-(4-Fluorophenyl)-2,5-di(thiophene-2yl)-1H-pyrrole,*Msc Thesis, METU, 2006.

12. Ikehata, S.; Kaufer, J.; Woerner, T.; Pron, A.; Druy, M.A.; Sivak, A.; Heeger, A.J.; McDiarmid, A.G. Phys. Reo. Lett., 45, (1980) 423.

13. Peo, M.; Roth, S.; Dransfeld, K.; Tieke, B.,; Hocker, J.; Gross, H.; Grupp, A.; Sixl, H. Solid State Commun., 35, (1980) 119.

14. Scott, J.C.; Krounbi, M.; Pfluger, P.; Street, G.B. Phys. Reu. B: Condens. Matter, 28, (1983) 2140.

15. Scott, J.C.; Bredas, J.L.; Pfluger, P.; Yakushi, K.; Street, G.B. Synth. Met., 9, (1984) 165.

16. Scott, J.C.; Bredas, J.L.; Kaufman, J.H.; Pfluger, P.; Street, G.B.; Yakushi, K. Mol. Cryst. Liq. Cryst., 118, (1985) 163.

17. Xu, Z.; Horowitz, G.; Gamier, F.J. Electroanul. Chem., 246, (1988) 467.

18. Roncali, J. Chem. Rev., 92, (1992) 711.

19. Sotzing, G.A. *Tuning The Electrochemical Properties of Electrochemically Synthesized Conducting Polyheterocycles*, MSc Thesis, University of Florida, 1997.

20. Somani, P.R.; Radhakrishnan, S. Materials Chemistry and Physics, 77 (2002) 117.

21. Buckley, D.N.; Burke, L.D. J. Chem Soc. Faraday 72 (1) (1975) 1447.

22.   Buckley, D.N.; Burke, L.D.; Mukahy, J.K. J. Chem. Soc. Faraday 72 (1) (1976) 1896.

23.   Burke, L.D.; O'Sakan, E.J.M. J. Electroanal. Chem. 93 (1978) 11.

24.   Burke, L.D.; Whelan, D.P. J. Electroanal. Chem. 103 (1979) 179.

25.   Burke, L.D.; Thomey, T.A.M.; Whelan, D.P. J. Electroanal. Chem., 107 (1980) 201.

26.   Burke, L.D.; Murphy, O.J. J. Electroanal. Chem. 109 (1980) 373.

27.   Haddon, R.C. Acc. Chem. Res. 25 (1992) 127.

28.   Cordoba de Torresi, S.I.; Torresi, R.M.; Ciampi, G.; Luengo, C.A. J. Electroanal. Chem. 377 (1994) 283.

29.   Rosseinsky, D.R.; Monk, P.M.S. J. Appl. Electrochem., 24, (1994) 1213.

30.   Sonmez, G.; Schwendeman, I.; Schottland, P.; Zong, K.; Reynolds, J.R. Macromolecules, 36, (2003) 639.

31.   Ho, K.-C.; Rukavina, T.G.; Greenberg, C.B., in *Electrochromic Materials ZI,* ed. Ho, K.-C. and MacArthur, D.A., PV 94-2, pp. 252, Electrochem. SOC. Proc. Ser., Pennington, New Jersey, 1994.

32.   Mortimer, R.J. Chemical Society Reviews, 26, (1997) 147.

33.   Fesser, K.; Bishop, A.R.; Campbell, D. K. Phys. Rev. B, 27, (1983) 4804.

34. Çamurlu, P., *Synthesis of Conducting Polymers of 3-Ester Subsituted Thiophenes and Characterization of Their Electrochromic Properties,* Phd Thesis, METU, 2006.

35. Fawcett, A.H., *High Value Polymers*, The Royal Society of Chemistry, Cambridge, 1996.

36. Kiss, H.G., *Conjugated Conducting Polymers,* Springer Series in Solid State Physics, Springer, Berlin, 1992.

37. Cotts, D.B.; Reyes, Z., *Electrically Conductive Organic Polymers for Advanced Applications*, Noyes Data Corporation, USA, 1986.

38. Siddle, J.; Pilkington PLC, *Personal Communication*, 1991.

39. Monk, P.M.S., Mortimer, R.J. and Rosseinsky, D.R., *Electrochromism: Fundamentals and Applications,* VCH, Weinheim, 1995.

40. Sonmez, G. Chem. Commun., (2005) 5251.

41. Sonmez, G.; Meng, H.; Wudl, F. Chem. Mater., 16, (2004) 574.

42. Thompson, K.G.; Benicewicz, B.C. Polymer Preprints, 41, (2), (2000) 1731.

43. Kupniewska A.; Biallozor, S. Advances in Engineering Science Sect. A (1), (2007) 33.

44. Wang, X.H.; Lu, J.L.; Chen, Y.; Li, J.; Wang, F.S. Advances in Engineering Science Sect. A (1), (2007) 45.

45. Baur, J.W., *Nanostructured Organic Photovoltaic Devices Via Electronic Self-Assembly Of Electroactive Polymers and Molecules*, 2000.

46. Tao, X., *Smart fibres, fabrics and clothing: Fundamentals and applications,* Woodhead Publishing Limited, 2001.

47. Friend, R.H.; Gymer, R.W.; Holmes, A.B.; Burroughes, J.H.; Marks, R.N.; Taliani, C.; Bradley, D.D.C.; Dos Santos, D.A.; Brédas, J.L.; Lögdlund M.; Salaneck, W.R. Nature, 397, (1999) 121.

48. Margolis, J. *Conductive Polymers and Plastics*, Chapman and Hall, 1989.

49. Guiseppi-Elie, A.; Wallace, G.G.; Matsue, T. *In Handbook of Conducting Polymers*, Editors: Skotheim, T.A., Elsenbaumer, R.L., Reynolds, J.R., pp. 963-992, 2nd Ed., Marcel Dekker Inc., 1998.

50. Hirai, T.; Zheng, J.; Watanabe, M.; Shirai, H. *In Smart fibres, fabrics and clothing: Fundamentals and applications,* Editor: Tao, X., pp. 7-30, Woodhead Publishing Limited, 2001.

51. Salaneck, W.R.; Clark, D.T.; Samuelsen, E.J. *Science and Application of Conducting Polymers*, IOP Publishing, 1991.

52. Sonmez, G.; Shen, C.K.F.; Rubin, Y.; Wudl, F. Angew. Chem. Int. Ed. 43 (2004) 498.

53. Huang, H.; Pickup, P.G. Chem. Mater., 10, (1998) 2212.

54. Kitamura, C.; Tanaka, S.; Yamashita, Y. Chem. Mater., 8, (1996) 570.

55. Brocks, G.; Tol, A., J. Phys. Chem., 100, (1996) 1838.

56. Chen, W.C.; Jenekhe, S.A. Macromolecules, 28, (1995) 465.

57.   Jenekhe, S.A.; Lu, L.; Alam, M.M. Macromolecules, 34, (2001) 7315.

58.   Mullekom, H.A.M.; Vekemans, J.A.J.M.; Havinga, E.E.; Meijer, E.W. Mater. Sci. Eng., 32, (2001) 1.

59.   Zhu, Y.; Yen, C.-T.; Jenekhe, S.A.; Chen, W.-C. Macromol. Rapid Commun., 25, (2004) 1829.

60.   Admassie, S.; Inganäs, O.; Mammo, W.; Perzon, E.; Andersson, M.R. Synth. Met. 156, (2006) 614.

61.   Champion, R.D.; Cheng, K.-F.; Pai, C.-L.; Chen, W.-C.; Jenekhe, S.A., Macromol. Rapid Commun., 26, (2005) 1835.

62.   Roncali, J. Chem. Rev. 97, (1997) 173.

63.   Hou, J.H.; Chen, H.-Y.; Zhang, S.Q.; Li, G.; Yang, Y.J. Am. Chem. Soc., 130, (2008) 16144.

64.   Wu, P.-T.; Bull, T.; Kim, F.S.; Luscombe, C.K.; Jenekhe, S.A., Macromolecules, 42, (2009) 671.

65.   Mei, J.G.; Heston, N.C.; Vasilyeva, S.V.; Reynolds, J.R. Macromolecules, 42, (2009) 1482.

66.   Wienk, M.M.; Turbiez, M.; Gilot, J.; Janssen, R.A.J. Adv. Mater., 20, (2008) 2556.

67.   Yue, W.; Zhao, Y.; Tian, H.; Song, D.; Xie, Z.; Yan, D.; Geng, Y.; Wang, F. Macromolecules, 42, (2009) 6510.

68.   Alam, M.M.; Jeneche, S. A. Chem Mater., 16, (2004) 4647.

69. Shang, Y.; Wen, Y.; Li, S.; Du, S.; He, X.; Cai, L.; Li, Y.; Yang, L.; Gao, H.; Song, Y. J. Am. Chem. Soc., 129, (2007) 11674.

70. Chu, C.W.; Ouyang, J.Y.; Tseng, J.H.; Yang, Y. Adv. Mater., 17, (2005) 1440.

71. Wu, H.M.; Song, Y.L.; Du, S.X.; Liu, H.W.; Gao, H.J.; Jiang, L.; Zhu, D.B. Adv. Mater., 15, (2003) 1925.

72. Brocks, G.; Tol, A. J. Phys. Chem., 100, (1996) 1838.

73. Ahonen, H.J.; Lukkari, J.; Kankare, J. Macromolecules, 33, (2000) 6787.

74. Gorman, C.B.; West, R.C.; Palovich, T.U.; Serron, S. Macromolecules, 32, (1996) 4157.

75. Thomas, C.A., PhD Thesis, University of Florida, 2002.

76. Durmuş, A., *Realization of Neutral State Green Polymeric Materials*, METU, 2009.

77. Kosugi, M.; Shimizu, Y.; Migita, T. Chem. Lett. (1977) 1423.

78. Kosugi, M.; Shimizu, Y.; Migita, T. J. Organomet. Chem. (1977) 129.

79. Kosugi, M.; Sasazawa. K., Shimizu, Y.; Migita, T. Cemm. Lett. (1977) 301.

80. Milstein, D.; Stille, J. K. J. Am. Chem. Soc. 100, (1978) 3636.

81. Beletskaya, I. P. J. Organomet. Chem. 250, (1983) 551.

82. Stille J. K. Angew. Chem., Int. Ed. Engl. 25, (1986) 508.

83. Farina, V.; Krishnamurty, V.; Scott, W. J. *The Stille Reaction*, Wiley, 1998.

84. a). Meijere, A.; Diederich, F. *Metal-catalyzed Cross-coupling Reactions*, Second Eddition Wiley-Vch, 2004 b). Sadki, S.; Schottland, P.; Brodie, N.; Sabouraud, G. Chem. Soc. ReV. 29, (2000) 283.

85. Sadki, S., Schottland, P., Brodie, N., Sabouraud, G., Chem. Soc. Rev. 29, (2000) 283.

86. Roncali, J. Chem. Rev. 92, (1992) 711.

87. Waltman, R. J.; Bargon, J. Can. J. Chem. 64, (1986) 76.

88. Toshima, N.; Hara, S. Prog. Polym. Sci. 20, (1995) 155.

89. Cheng, Y.-J.; Luh, T.-Y. J. Organomet. Chem. 689, (2004) 4137.

90. Tamao, K.; Sumitani, K.; Kumda, M. J. Am. Chem. Soc. 94, (1972) 4374.

91. Stille, J. K. Angew. Chem., Int. Ed. 25, (1986) 508.

92. Miyaura, N.; Suzuki, A. Chem. ReV. 95, (1995) 2457.

93. Sonogashira, K. J. Organomet. Chem. 653, (2002) 46.

94. Bao, Z.; Chan, W. K.; Yu, L. J. Am. Chem. Soc. 117, (1995) 12426.

95. Cheng, Y.J.; Yang, S.H.; Hsu, C.S. Chem. Rev. 109, (2009) 5868.

96. Hou, J.; Tan, Z.; Yan, Y.; He, Y.; Yang, C.; Li, Y. J. Am. Chem. Soc. 128, (2006) 4911.

97. Li, Y.; Zou, Y. AdV. Mater. 20, (2008) 2952.

98. Zhu, Z.; Waller, D.; Gaudiana, R.; Morana, M.; Mu¨hlbacher, D.; Scharber, M.; Brabec, C. Macromolecules 40, (2007) 1981.

99. Zhang, M.; Tsao, H. N.; Pisula, W.; Yang, C.; Mishra, A. K.; Müllen, K. J. Am. Chem. Soc. 129, (2007) 3472.

100. Yamaguchi, S.; Tamao, K. Bull. Chem. Soc. Jpn. 69, (1996) 2327.

101. Tamao, K.; Uchida, M.; Izumizawa, T.; Furukawa, K.; Yamaguchi, S. J. Am. Chem. Soc. 118, (1996) 11974.

102. Liu, M. S.; Luo, J.; Jen, A. K.-Y. Chem. Mater. 15, (2003) 3496.

103. Luo, J.; Xie, Z.; Lam, J. W. Y.; Cheng, L.; Chen, H.; Qiu, C.; Kwok, H. S.; Zhan, X.; Liu, Y.; Zhu, D.; Tang, B. Z. Chem. Commun. 2001, 1740.

104. Chen, J.; Cao, Y. Macromol. Rapid Commun. 28, (2007) 1714.

105. Hou, J.; Chen, H. Y.; Zhang, S.; Li, G.; Yang, Y. J. Am. Chem. Soc. 130, (2008) 16144.

106. Ono, K.; Tanaka, S.; Yamashita, Y. Angew. Chem., Ind. Ed. Engl. 33, (1994) 1977.

107. Karikomi, M.; Kitamura, C.; Tanaka, S.; Yamashita, Y. J. Am. Chem. Soc. 117, (1995) 6791.

108. Bundgaard, E.; Krebs, F. C. Macromolecules 39, (2006) 2823.

109. Durmus, A.; Gunbas, E. G., Camurlu, P., Toppare, L. Chem. Commun. (2007) 3246.

110. Balan, A.; Baran, D.; Gunbas, G.; Durmus, A.; Ozyurt, F.; Toppare, L. Chem. Commun. (2009) 6768.

111. Yamamoto, T.; Okuda, T. J. Electroanal. Chem. 460, (1999) 242.

112. Izumi, A.; Nomura, R.; Masuda, T. Macromolecules 33, (2000), 8918.

113. Puskas, Z.; Inzelt, G. Electrochim Acta 50, (2005) 1481.

114. Zhu, Y.; Gibbons, K. M.; Kulkarni, A. P.; Jenekhe S. A. Macromolecules 40, (2007), 804.

115. He, B.; Tian, H.; Geng, Y.; Wang, F.; Mullen, K. Org. Lett. 10, (5) (2008), 773.

116. Hanif, M.; Lu, P.; Li, M.; Zheng, Y.; Xie, Z.; Ma, Y.; Li, D.; Li, J. Polym. Int. 56, (2007) 1507.

117. Dewhurst, F.; Shah, P. K. J. J. Chem. Soc. (1969) 1503.

118. Gautrot, J. E.; Hodge, P.; Helliwell, M.; Rafrey, J.; Cupertino, D.; Journal of Materials Chemistry, 19, 4148.

119. Putala, M.; Pustet, N. K.; Mannschreck, A. Tetrahedron: Asymmetry 12 (2001) 3333.

120. Pinhey, J. T.; Roche, E. G. J. Chem. Soc. Perkin Trans. I (1988) 2415.

121. Bundgaard, E.; Kreb, F. C. Polymer Bulletin 55, (2005) 157.

122. Kim, E.; Kim, M.; Kim, K. Tetrahedron 62 (2006) 6814.

123. Brenno A. DaSilveira Neto,a Aline Sant'Ana Lopes,a Gunter Ebeling,a Reinaldo S. Gonc¸alves,a Valentim E. U. Costa,a Frank H. Quinab and Jairton Dupon Tetrahedron 61, (2005) 10975.

124. Wen, L.; Rasmussen, S. C. Journal of Chemical Crystallography, 37 (6) (2007).

125. Karsten, B. P.; Janssen, R. A. J. Org. Lett., 10, (16) (2008) 3513.

126. Tsubata, Y.; Suzuki, T.; Myashi, T. J. Org. Chem. 57, (1992) 6749.

127. Beaujuge, P. M.; Ellinger, S.; Reynolds, J. R. Nat. Mater. 7, (2008) 795.

128. McDonagh, A. M.; Bayly, S. R.; Riley, D. J.; Ward, M. D.; McCleverty, J. A.; Cowin, M. A.; Morgan, C. N.; Varrazza, R.; Penty, R. V.; White, I. H. Chem. Mater.12, (2000) 2523.

129. Meng, H., Tucker, D., Chaffins, S., Chen, Y., Helgeson, R., Dunn, B., Wudl, F. Adv. Mater. 15, (2003) 146.

CURRICULUM VITAE

PERSONAL INFORMATION

Surname, Name: Ünver, Elif
Nationality: Turkish (T.C.)
Date and Place of Birth: 15 October 1979, Balıkesir
Marital Status: Married
Phone: +90 312 229 78 99
E-mail: elfkose79@hotmail.com

EDUCATION

Degree	Institution	Year of Graduation
MS	METU Chemistry Department	2004
BS	ANADOLU UNIVERSITY Chemistry Department	2000
High School	Şehit Mehmet Gönenç High School, Bandırma	1996

WORK EXPERIENCE

Year	Place	Enrollment
2003-2008	METU Department of Chemistry	Research Assistant
1999-July	ETI BOR	Intern Research Student

FOREIGN LANGUAGES

Advanced English

PUBLICATIONS

1. Demir A.S.; Fındık, H.; Köse, E. "A new and efficient chemoenzymatic route to both enantiomers of α'-acetoxy-α-methyl and γ-hydroxy-α-methyl cyclic enones"; Tetrahedron: Asymmetry, Volume 15, Issue 5, 777-781.

HOBBIES

Riding horse, sailing, handcrafts.